Quantum Theory of Electron Transport in Molecular Nanostructures

Jehan Saeed Alqahtani

B.Sc., King Khalid University
M.A., Kent state University
P.h.D., Lancaster University

Department of Physics, Lancaster University, UK
Ph.D. Thesis

Declaration

Except where stated otherwise, this thesis is a result of the author's original work and has not been submitted in whole or in part for the award of a higher degree elsewhere. This thesis documents work carried out between July 2016 and March 2020 at Lancaster University, UK, under the supervision of Prof. Colin J. Lambert and funded by King Khalid University, Saudi Arabia.

Jehan

Dedication

To the soul of my father who raised me to be persistent, confident and ambitious.

Abstract

This thesis addresses the fundamental aspects of controlling transport through organic molecules by presenting a series of studies in the electronic properties of molecular junctions. The exploration and understanding of the electronic characteristics of single molecules connected to electrodes is an essential part in the application of electronics. Here, I implemented transport calculations based on the Landauer formula combined with Kohn–Sham orbitals extracted from density functional theory (DFT). Chapter 4 elucidates the validity of a 'curly arrow rule', which has been used widely by chemists and physicists to predict the electronic properties of molecular junctions. Anthraquinone is found to break this rule in the case of meta connectivity to electrodes. This is significant, because changing the redox state of meta-connected dihydroxyanthracene to meta-connected anthraquinone, increases the conductance by a couple of orders of magnitude, due to the transition from constructive to destructive QI, which can help in the design of the QI based single-molecule switches such as data storage elements. Finally, chapter 5 presents a theoretical investigation of electron transport through dimethyldihydropyrene (DHP) and *cyclophanediene* (CPD) systems focusses on changes in the conductance as a consequence of photochemical stimuli. These molecules could be exploited in the function of electronic devices, when responding to external stimuli.

Acknowledgments

As a PhD student, it is really hard to find the appropriate words to thank all of those who helped me along the way. I was privileged to be surrounded by supporting family members, friends, and mentors. It is truly overwhelming to try to thank all of them in few pages.

I would like to start by thanking my supervisor, Professor Colin J.Lambert who always put his students interests first. His kindness, patience and support are indescribable. I am so grateful to have worked with such great physicist and human being.

Next, I would like to thank Dr. Hatef Sadeghi; none of this work would have been accomplished without his dedicated time, guidance and patience. I am sure that I caused him a lot of headaches along the way with my naive questions and repetitive mistakes, but he with his big heart would take the pen and explain everything step by step. I am also grateful for Dr. Sara Sangtarash who helped and guided me during my thesis.

In addition, I would like to thank all the co-supervisors in our group (Dr.Iain, Dr. Ali, Dr. Michael, Dr. qingqing, Dr.songjun. Everyone has helped me learn something and added a positive impact during my studying. I would like also to thank all my friends and colleagues in Colin's group. My thanks also go out to the support I received during my PhD from the ministry of higher education in Saudi Arabia and King Khalid University.

Finally, I owe thanks to a very special person, my husband, Saeed for his continued and unfailing love, support and understanding during my pursuit of Ph.D degree that made the completion of thesis possible. My thesis acknowledgement would be incomplete without thanking my children (Mohammad and Serene), their smiling faces always made me happy and inspired me. I cannot begin to express my gratitude to my family for all of the love, support, encouragement and prayers they have sent my way along this journey. To my Mother, thank you for being my champions throughout the past years. Your unconditional love and support has meant the world to me, I hope that I have made you proud.

List of Publications

During my PhD studies I published the following journal articles:

Alqahtani, Jehan, et al. "Breakdown of Curly Arrow Rules in Anthraquinone." *Angewandte Chemie* 130.46 (2018): 15285-15289.

Table of Contents

Chapter 1

"Ambition is the path to success. Persistence is the vehicle you arrive in."

1.1 Introduction

Molecular electronics involves using single molecules as active components in the electronic circuits such as transistors[1], rectifiers[2], [3], sensors[4], [5] and switches[6]. In 1965, Gordon Moore noted that the number of transistors per chip doubles every two years, which is known as Moore's law. He expected this trend to continue for ten years, but due to the rapid developments, it lasted a half century later. Due to the limits of Moore's law [7] as component approach the sub-10nm length scale, scientists are eager to find substitutes for silicon-based devices to enable the creation of electronic components at the molecular scale. Therefore, the field of single molecule electronics has the potential to offer an alternative to silicon-based devices by replacing the traditional semiconductor with a single molecule. Molecular electronic devices have attracted scientific interest due to their unique properties, such as the size of a single molecule, which is typically only a few nanometres. They also allow self-assembly when the molecular units spontaneously organise themselves into ordered structures by non-covalent interactions. The first molecular device was proposed by Avriam and Ratner the 1970s as a molecular rectifier to make a single molecule switch. More recently, the field of molecular electronics has paved the way to understanding sub-10nm electron transport and associated properties, in order to validate theoretical models, and open a window to the exploration of new electronic applications at the nanometre scale. Experimentally, many techniques have been developed in order to study these junctions intensively such as Scanning Tunnelling Microscopy Break Junctions (STM-BJ)[8], [9] and Mechanically Controllable Break Junctions MCBJ [10][11].This has enabled connections between the theory and the experiment, which together have led to recent many advances in this field. The key question

4

is what are the fundamental processes in molecular junctions composed of a single molecule in contact with one or more electrodes? One such process is the alignment of the molecular spectrum when it interacts with the electrode surface and the broadening of molecular orbitals due to the coupling to the electrode. This results in a charge transfer from the electrodes to the molecule and thereby shifts the molecular orbital with respect the Fermi energy of the electrode. Eventually, during this process many effects can impact the electron transport of the junction such as the conformation and orientation of the molecule, the gap between the highest occupied molecule orbital (HOMO) and the lowest occupied molecule orbital (LUMO), the alignment of this gap relative to the Fermi level of the electrode and the metal molecule interface.

In spite of these challenges and limitations to both theory and experiment, much progress in the development of the molecular electronics has been made, which provides a valuable to roadmap for the future electronics applications. This thesis covers key concepts in the quantum transport theory needed to describe fundamental aspects of molecular junctions in the nanoscale, including an introduction to two theoretical approaches; density functional theory, which is implemented in the SIESTA code, and the Green's function formalism of electron transport which is implemented in the Gollum code.

1.2 Switch Mechanism in single molecules

Molecular switch devices have been studied intensively in the last decades, and have had a vital impact in order to improve the functionality of the electronics devices and its applications. Molecular switches based on single molecule are of interest due to their key features such as size, speed (conductance switching) and stability (large energy barrier between the two molecular states). This chapter will discuss briefly about the switching mechanism. To clarify the switching process, I will mainly highlight two kinds of switching mechanism based on the factor to induce the switch. One example is a switch based on conformation, when the chemical bond is formed or cleavage by the light or bias voltage. Another is based on redox

switching[12], where the electron typically transfers between two states as shown in chapter (5).These changes in geometry of the molecules in turn make a difference in their electronic structure, their electronic transport characteristics and their electrical conductance. In what follows, my theoretical calculations will be supported by experimental observations in chapter (5), which highlight the unique characteristics of DHP and its derivatives. The challenge in creating a useful switch is to achieve a significant difference in the conductance between the two states. An opening and closing cycle of these switches can be realised by associating the excited state with the open state and then letting it relax to achieve the closed state and then stimulating the molecule in a closed state by heat or light or electric field to move over the energy barrier separating the two states[13].

1.2.1. Switch induced by light (configuration)

Light has been widely used as a switching mechanism in various molecules[14] [15][16][17], because photochromic molecules have the attractive features that they undergo two reversible, processes between closed and open states, stimulated by visible and UV light . He et al investigated the switching behaviour that is induced by the light and its effect on electronic structure[18]. Previous work demonstrated an accurate picture of switching behaviour for diarylethene in single molecule junctions. This study attributed the difference in conductance due to the impact of the change in molecular geometry between the on and off state emphasising that π-system electrons play a crucial role either in the formation of the closed state or in deformation for the open one. A difference in conductance of two orders of magnitude is reached[18][19][20]. Other experimental and theoretical frameworks explained different photo-isomers of single molecules, such as azobenzene[21][22] and [15]dimethyldihydropyrene (DHP)cyclophanediene (CPD) [23].

1.2.2. Switch induced by charge transfer:

Obviously, charge transfer in the molecular electronics is a crucial factor that can change the electronics properties of the molecules. Electronic transport based on oxidation and reduction is called redox reaction, in which usually the HOMO-LUMO gap can be altered. The key point is how to design a single molecule switch that can change significantly their conductance between the on and off states. Tetrathiafulvalene(TTF) is a candidate that has been used in a redox-based switch . Liao et al demonstrated that the change in the oxidation states of TTF can cause a rearrangement of the TTFdT molecular orbitals, which change the conductance by about one order of magnitude [24]. Furthermore, anthraquinone has also been used successfully as switch for molecular junctions that can be reversibly switched.

This molecule is reported to show a difference in conductance when switching between cross-conjugated anthraquinone and linear conjugated reduced hydroanthraquinone[25].

1.4 Thesis outline

This thesis will report theoretical simulations of the molecular electronics and electron transport at the nanoscale. To begin with, chapter 2 gives a brief overview of density functional theory (DFT), which is used in this thesis to study and understand the electronic properties of single-molecule junctions. Chapter 3 describes the single particle Green's function based scattering theory, and related topics such as the Landauer formula and some concepts in quantum transport. Chapter 4 introduces a theoretical study of anthraquinone and it derivatives between gold and graphene electrodes and tests the validity of the curly arrow rule on these derivatives. Chapter 5 presents a study of charge transport in a photo switchable dimethyldihydropyrene and it derivatives. It also discusses how perturbation theory can be used to elucidate fundamentals of the switch mechanism in these molecules.

The final chapter presents the conclusions of my thesis and suggestions for future work.

Bibliography:

[1] E. Burzurí *et al.*, "Single-molecule transistors," *Nano Lett.*, vol. 8, no. 4, pp. 1–10, 2016.

[2] A. Batra *et al.*, "Tuning Recti fi cation in Single-Molecular Diodes," vol. 22, 2013.

[3] J. Zhao *et al.*, "Single C 59 N Molecule as a Molecular Rectifier," vol. 045502, no. July, pp. 1–4, 2005.

[4] H. Sadeghi *et al.*, "Graphene Sculpturene Nanopores for DNA Nucleobase Sensing," 2014.

[5] A. Phys, "Silicene-based DNA nucleobase sensing," vol. 103104, no. November 2013, 2014.

[6] S. Jan Van Der Molen and P. Liljeroth, "Charge transport through molecular switches," *J. Phys. Condens. Matter*, vol. 22, no. 13, 2010.

[7]B. G. E. Moore, "Cramming more components onto integrated circuits," vol. 38, no. 8, 1975.

[8] C. Li, I. Pobelov, T. Wandlowski, A. Bagrets, A. Arnold, and F. Evers, "Charge Transport in Single Au | Alkanedithiol | Au Junctions : Coordination Geometries and Conformational Degrees of Freedom," no. 17, pp. 318–326, 2008.

[9] B. Xu and N. J. Tao, "Measurement of Single-Molecule Resistance by Repeated Formation of Molecular Junctions," vol. 301, no. August, pp. 1221–1224, 2003.

[10] M. T. Gonza, S. Wu, R. Huber, S. J. Van Der Molen, and M. Calame, "Electrical Conductance of Molecular Junctions by a Robust Statistical Analysis," 2006.

[11] M. A. Reed, C. Zhou, C. J. Muller, T. P. Burgin, and J. M. Tour, "Conductance of a Molecular Junction," vol. 278, no. October, pp. 252–255, 1997.

[12] S. Jan Van Der Molen and P. Liljeroth, "Charge transport through molecular switches," J. Phys. Condens. Matter, vol. 22, no. 13, 2010.

[13] L. Sun, Y. A. Diaz-Fernandez, T. A. Gschneidtner, F. Westerlund, S. Lara-Avila, and K.

Moth-Poulsen, "Single-molecule electronics: From chemical design to functional devices," Chem. Soc. Rev., vol. 43, no. 21, pp. 7378–7411, 2014.

[14] Y. Kim *et al.*, "Charge transport characteristics of diarylethene photoswitching single-molecule junctions," *Nano Lett.*, vol. 12, no. 7, pp. 3736–3742, 2012.

[15] X. Zhang, L. Hou, and P. Samorì, "Coupling carbon nanomaterials with photochromic molecules for the generation of optically responsive materials," *Nat. Commun.*, vol. 7, 2016.

[16] T. Sendler *et al.*, "Light-Induced Switching of Tunable Single-Molecule Junctions," *Adv. Sci.*, vol. 2, no. 5, pp. 1–7, 2015.

[17] Y. Tsuji and R. Hoffmann, "Frontier orbital control of molecular conductance and its switching," *Angew. Chemie - Int. Ed.*, vol. 53, no. 16, pp. 4093–4097, 2014.

[18] J. He *et al.*, "Switching of a photochromic molecule on gold electrodes: Single-molecule measurements," *Nanotechnology*, vol. 16, no. 6, pp. 695–702, 2005.

[19] A. C. Whalley, M. L. Steigerwald, X. Guo, and C. Nuckolls, "Reversible switching in molecular electronic devices," *J. Am. Chem. Soc.*, vol. 129, no. 42, pp. 12590–12591, 2007.

[20] N. Katsonis, T. Kudernac, M. Walko, S. J. Van Der Molen, B. J. Van Wees, and B. L. Feringa, "Reversible conductance switching of single diarylethenes on a gold surface," *Adv. Mater.*, vol. 18, no. 11, pp. 1397–1400, 2006.

[21] M. Alemani, M. V. Peters, S. Hecht, K. H. Rieder, F. Moresco, and L. Grill, "Electric field-induced isomerization of azobenzene by STM," J. Am. Chem. Soc., vol. 128, no. 45, pp. 14446–14447, 2006.

[22] M. Del Valle, R. Gutiérrez, C. Tejedor, and G. Cuniberti, "Tuning the conductance of a molecular switch," *Nat. Nanotechnol.*, vol. 2, no. 3, pp. 176–179, 2007.

[23] D. Roldan *et al.*, "Charge transport in photoswitchable dimethyldihydropyrene-type single-molecule junctions," *J. Am. Chem. Soc.*, vol. 135, no. 16, pp. 5974–5977, 2013.

[24] J. Liao *et al.*, "Cyclic conductance switching in networks of redox-active molecular junctions," *Nano Lett.*, vol. 10, no. 3, pp. 759–764, 2010.

[25] E. H. Van Dijk, D. J. T. Myles, M. H. Van Der Veen, and J. C. Hummelen, "Synthesis and properties of an anthraquinone-based redox switch for molecular electronics," *Org. Lett.*, vol. 8, no. 11, pp. 2333–2336, 2006.

Chapter 2

Density functional theory

2.1 Introduction

During the last decades, the field of molecular electronics has grown tremendously in understanding the electronic properties. DFT and its implementation in the SIESTA code[1] is one of the most widely used theoretical tools by physicists and chemists to gain understanding in the electronic structure[2][3][4][5][6][7][8]. This theory calculates the ground state of the organic molecules based on the Khan-Sham formalism. [4][3] This approach is powerful when considering the electron density and using a variety of approximations to explore the structural and electronic information in the field

of nano-scale molecular junction and predicting experimental results.

These works fall primarily into two sections. The first section is to introduce the basic concept of the density functional theory(DFT) from the starting point of solving the Schrodinger equation, which was a major motivation for the development of DFT. Coupled with the Born and Oppenheimer approximation of the nuclei and the two Hohenberg-kohn theorems and finally to Khan-Sham formalism. These approximations have been necessarily used to turn DFT to a computational code(Siesta)[1]. The next section is devoted to Siesta which has been already used extensively in my thesis calculations. Therefore, in the second section I illustrate the idea of pseudo-potentials and the basis set to simplify the task of constructing electronic wave-functions. All of the previous efforts have been done to reduce the expense of the DFT, meanwhile providing adequate accuracy. Finally, I look at the schematic process of self-consistency within SIESTA.

2.2 The Schrodinger equation

Finding the solution of Schrodinger equation is possible when only a few numbers of electrons are calculated. However for larger systems, solving the many body Schrodinger equations is challenging, insoluble and has been a goal for physicists and chemists to achieve. In general, the Hamiltonian of many body system is divided to five parts and could be written as:

$$\hat{H} = \hat{T}_n + \hat{T}_e + \hat{V}_n + \hat{V}_e + \hat{V}_{en} \tag{2.1}$$

Particularly, the atomic system contains electrons and nuclei, the Hamiltonian is described as:

$$\hat{H} = -\underbrace{\sum_n^N \frac{\hbar^2}{2M}\nabla_n^2}_{\hat{T}_n} - \underbrace{\sum_i \frac{\hbar^2}{2m}\nabla_i^2}_{\hat{T}_e} + \underbrace{\frac{1}{4\pi\epsilon_0}\frac{1}{2}\sum_{n\neq m}\frac{Z_n Z_m e^2}{|R_n - R_m|}}_{\hat{V}_n} + \underbrace{\frac{1}{4\pi\epsilon_0}\frac{1}{2}\sum_{i\neq j}\frac{e^2}{|r_i - r_j|}}_{\hat{V}_e}$$

$$+ \underbrace{\frac{1}{4\pi\epsilon_0}\frac{1}{2}\sum_{i,j}\frac{Z_n e^2}{|r_i - R_n|}}_{\hat{V}_{en}} \tag{2.2}$$

where $\hat{T}_e$ is the kinetic energy of the electron, $\hat{T}_n$ is the kinetic energy of nuclei and $\hat{V}_n$, $\hat{V}_e$ are the potential energy of electron and nuclei respectively. Clearly, solving the Schrodinger equation for a simple system such as the Hydrogen atom is obtainable in order to get the wave function of

this system. It is impossible to find the exact solution of Schrodinger equations for many-body system with more than a few electrons, unless some approximations are made to tackle this problem. Due to the fact that the nuclear masses are large, the nuclear kinetic energy could be neglected to yield Born-Oppenheimer approximation.[9]

2.3   Born-Oppenheimer approximation

We can simplify the Schrodinger equation by using the Born Oppenheimer approximation, which considers the electronic part of the equation, and neglects the nuclei parts as a result of the massive mass of the nuclei which is at least three order of magnitude larger than the mass of electron[9][10]which make it move slower than the electrons[9].
Thus,

$$\hat{H}_e = \underbrace{\sum_{i=1}^{N} \frac{\hbar^2}{2m} \nabla_i^2}_{\hat{T}_e} + \underbrace{\frac{1}{4\pi\epsilon_0} \frac{1}{2} \sum_{i \neq j}^{N} \frac{e^2}{|r_i - r_j|}}_{\hat{V}_e} + \underbrace{\frac{1}{4\pi\epsilon_0} \frac{1}{2} \sum_{i,j}^{N} \frac{e^2}{|r_i - R_n|}}_{\hat{V}_{en}} \qquad (2.3)$$

$$\{\underbrace{\sum_{i=1}^{N} \frac{\hbar^2}{2m} \nabla_i^2}_{\hat{T}_e} + \underbrace{\frac{1}{4\pi\epsilon_0} \frac{1}{2} \sum_{i \neq j}^{N} \frac{e^2}{|r_i - r_j|}}_{\hat{v}_e} + \sum_{i,j}^{N} V_{ext}(r_i)\}\Psi_e = E_e\Psi_e \qquad (2.4)$$

13

where V_{ext} represent the external potential due to nuclei and electron interaction.

Moreover, this was the first simplification to obtain the goal. Further steps are needed, and this based on the spatial coordinates(x, y, z) instead of $3N$ coordinates.

$$\Psi_i H(r, R) = E \Psi_i(r, R) \qquad (2.5)$$

Where (r) is the electron coordinate, (R) is the nuclei coordinate and (H) is the Hamiltonian of the system. The Hohenberg-kohn theorems was the first step to form the density functional theory that determines all the electronic properties by the ground state density$\rho_0(\mathbf{r})$[11][12], which switches the attention from the wave-function to the ground state density.

2.4 Hohenberg-kohn theorem approximation

The Hohenberg-Kohn theorem is a remarkable theorem which is considered to be the foundation of DFT due to its ability to determine the ground state properties of a system and can be applied to any system of electrons moving in a external potential.

$$\hat{H} = \hat{T}_e + \hat{v}_e + \sum_{i,j} V_{ext}(r_i) \qquad (2.6)$$

Writing the total electronic energy as functional of density :

$$E_{HK}[\rho] = F_{HK}[\rho] + \int dr v_{ext}(r)\rho(\vec{r}) \qquad (2.7)$$

Where F_{HK} is the the kinetic and internal energy of the electrons $T[\rho] + E_{[}\rho]$.

[7] [12] This approximation formally relies on two key theorems. The first theorem: states that the ground state electronic density is uniquely determined by only one external potential which means that there cannot be two external potentials where $v_{ext2}(\vec{r}) \neq V_{ext1}(\vec{r}) + constant$ leading to same ground state density. If we assume that there are two Hamiltonians and different external potentials where $v_{ext_2}(\vec{r}) \neq v_{ext_1}(\vec{r}) + constant$ cannot give rise to same ground state density.

The second theorem: The global minimum of the total energy functional is obtained when the density ground state minimizes the functional or in other words: There exists a universal functional of the density $F_{HK}[\rho]$ such that the ground state energy E is minimized at the true ground state density.$F_{HK}[\rho]$ is only dependent on $\rho(\vec{r})$ and independent from any external potential v(r). Thus, $F_{HK}[\rho]$ is a universal functional of $\rho(\vec{r})$.

15

2.5 Kohn-sham approach

The Khon-sham method[4] [13][14] involves working with a fictitious non-interacting system which mimics the interacting electrons in such a way that the density of this system is same as the interacting one and removing the electron-electron interactions. This picture can be formally [4]introduced by replacing the original Hamiltonian of interacting system with an effective Hamiltonian of non-interacting particles in effective external potential. Replacing the direct interaction in equation(2.4) to one electron potential that describe the average effect of the interaction

$$\hat{H}_{eff} = \sum_{i=1}^{N_e} \frac{\hbar^2}{2m}\nabla_i^2 + \sum_{i=1}^{N_e} V_{ext}(r_i) + \sum_{i=1}^{N_e} V_{ave}(r_i) \qquad (2.8)$$

Thereby:

$$\hat{H}_{eff} = \sum_{i=1}^{N_e} \frac{\hbar^2}{2m}\nabla_i^2 + \sum_{i=1}^{N} V_{eff}(\vec{r_i}) \qquad (2.9)$$

$$\hat{H}_{eff} = \sum_{i=1}^{N} \hat{h}_{eff}(\vec{r_i}) \qquad (2.10)$$

The ground state energy functional can be written as based on the Hohenberg-Kohn variational principle:

$$E_{KS}[\rho(r)] = \int V_{ext(r)}\rho(r)dr + T_s[\rho(r)] + \frac{1}{2}\int \frac{\rho(r)\rho(\vec{r'})}{|r-r'|}drdr' + E_{xc}[\rho(r) \geq E$$

$$(2.11)$$

16

The variational problem for the Hohenberg-Kohn density-functional introduces a Lagrange multiplier μ to constrain the number of electrons to be N:

$$\delta[F(\rho)] + \int dr V_{ext}(\vec{r})\rho(\vec{r}) - \mu(\int dr\rho(\vec{r}) - N) = 0 \qquad (2.12)$$

Where $F(\rho)$ is separated to three part which are:

$$F[\rho] = T_s(\rho) + \frac{1}{2}\int\int drdr'\frac{\rho(\vec{r})\rho(\vec{r'})}{|\vec{r} - \vec{r'}|} + E_{xc}(\rho) \qquad (2.13)$$

Where the first term is the kinetic energy of a non-interacting system and the second term is the classical electrostatic energy (describing the electron electron interaction of the classical charge distribution) which is called the Hartree energy and the last term is the exchange correlation energy which is the difference between the kinetic energy for interacting and non- interacting systems and non classical electrostatic interaction energy. Applying this to equation (2.12) which can then be written as:

$$\mu = V_{KS}(\vec{r}) + \frac{\delta T_s(\rho)}{\delta\rho(\vec{r})} \qquad (2.14)$$

V_{KS} is the Khon-Sham potential and it is separated into three terms which are:

$$V_{KS} = \int dr'\frac{\rho(\vec{r'})}{|\vec{r} - \vec{r'}|} + V_{xc} + V_{ext}(\vec{r}) \qquad (2.15)$$

17

Where the first term is the Hartree potential and second is the exchange correlation potential which is given as:

$$V_{xc} = \frac{\delta E_{xc}(\rho)}{\delta \rho(\vec{r})} \tag{2.16}$$

$$V_H = \frac{\delta E_H[\rho(\vec{r})]}{\delta \rho(\vec{r})} \tag{2.17}$$

The Euler-Lagrange equation(2.14) is now the same as the equation obtained in the non-interacting system moving in an external potential(one-electron Schrodinger equations)$V_{KS}(\vec{r})$

Solving the one-electron Schrodinger equations to find the ground state density of non-interacting system :

$$[-\frac{1}{2}\nabla^2 + V_{KS}(\vec{r})]\psi_i(\vec{r}) = \varepsilon_i \psi_i(\vec{r}) \tag{2.18}$$

Finally, Kohn-Sham one-electron orbitals and the electron density for each spin is defined as,

$$\rho(\vec{r}) = \sum_{i=1}^{N} |\psi_i(\vec{r})|^2 \tag{2.19}$$

Where equation (2.19)and (2.20)are called the Kohn-Sham Equations. The ground state energy for a many-body system(DFT total energy)is:

$$E_{KS} = \sum_N \varepsilon_N - \frac{1}{2}\int dr dr' \frac{\rho(\vec{r})\rho(\vec{r})}{|\vec{r} - \vec{r'}|} - \int dr v_{xc}(\vec{r})\rho(\vec{r}) + E_{xc}\rho(\vec{r}) \tag{2.20}$$

[12]

2.5.1 The Exchange correlation functional

Remarkably, as a result of using the Kohn-sham approach, the reduced ground state density of a many-body system to one single body problem is solved. However, the only issue is determining the actual form of the exchange-correlation energy which is unknown. To overcome this issue an approximation has been made.

2.5.1.1 Local Density Approximation

There have been hundreds of approximations to the exchange correlation formed over the past decades[14,15], one of the simplest is the Local Density Approximation (LDA). LDA is written as[15]

$$E^{xc}_{LDA}[\rho(\mathbf{r})] = \int \rho(\mathbf{r}) E^{xc}_{HGE}[\rho(\mathbf{r})] d(\mathbf{r}) \qquad (2.21)$$

Where E^{xc}_{HGE} is the exchange correlation energy of the homogeneous gas with density of $\rho(\vec{r})$ LDA is accurate and performs very well when the electron density varies slowly. So, this kind of functional favours the homogeneous systems with (sp) bond like graphene and carbon nanotubes. In order to obtain the term E^{xc}_{HGE} it is separated into the sum of two contributions as:

$$E^{LDA}_{xc} = \int d(\vec{r}) \rho(\vec{r}) E^{HGE}_{c}[\rho(\vec{r})] + E^{HGE}_{x}[\rho(\vec{r})] \qquad (2.22)$$

19

2.5.1.2 Generalized Gradient Approximation

LDA has been improved in the case where the charge density undergoes a rapidly varying function of position(**r**). A further step is taken by getting all the information not only about the density at that point but including the gradient of electron density which is known as Generalized Gradient Approximation:

$$E_{xc}^{GGA}[\rho(\vec{r})] = \int \rho(\vec{r}) \varepsilon_{xc}^{GGA}[\rho(\vec{r}), |\nabla \rho(\vec{r})|] d(\vec{r}) \qquad (2.23)$$

2.6 SIESTA

Is a full software package that performs DFT calculation to enable solving the Khon-Sham equations and uses a linear combination of atomic orbitals(LCAO) to carry out calculations[1]. Siesta investigates the electronic structures of molecules to provide a complete picture about the electronic properties, such as the charge density, binding energy and many other features. Moreover, Siesta plays a major role for the development and use of density functional theory. In order to provide feasible calculations, there are many approximations required to make it efficient and reliable. These approximations will be primary discussed in the next section.

2.6.1 Pseudopotential Approximation

The pseudopotential approximation is another approximation that is made in order to solve the many-body schrodenger equation. This approximation can be reached by splitting the electrons into two types. The core electrons in which the electrons occupy the filled shells of the atomic orbitals and the valence electrons which lie in the partially filled shells. A pseudopotential is constructed by replacing core electrons such that they approximate the potential in such a way that these core electron are felt by the valence electrons. The core electrons in most molecules do not contribute in the formation of the molecular orbitals. Moreover,this was first suggested by Fermi in 1934 and in our work a special kind of pseudopotential is used. Chemically, only valance electrons play a vital role to determine most of the chemical properties compared to the core electrons. In this regard, approximation is allowed to get rid of the core electrons due to the rapid interaction with the atomic nucleus and take advantage of treating only the valence ones. In fact, It is generally necessary to include the valence electrons because their states overlap with the other valence electrons states from neighbouring atoms to form the molecular orbital.

2.7 Calculation in Practice

The transport calculations in this thesis are performed by using SIESTA method[1], starting with constructing the atomic configuration of the desired system and choosing appropriate pseudopotentials for each element, which can be different for every exchange-correlation functional. Moreover, choosing a suitable basis set for each element present in the calculation is a tradeoff between the speed of the calculation and the accuracy which can be decided by the user. In order to ensure that the calculation is accurate , another input parameters in need such as the grid fineness and density or energy convergence tolerances. Another type of parameters is the convergence controlling parameters, such as the Pulay parameter, which accelerate or maintains the stability of the convergence of the charge density in Siesta. Next stage, generating the initial charge density for non-interacting systems from the pseudopotential as shown in figure(2.7.1).

The first stage of the calculation begins when a self-consistent calculation is set up to calculate the Hartree potential and the exchange correlation potential. A new charge density is obtained by solving the Kohn-Sham equations. Then the next iteration is started and repeated many times until the convergence criteria is reached. Thereby, obtaining the ground state Kohn-
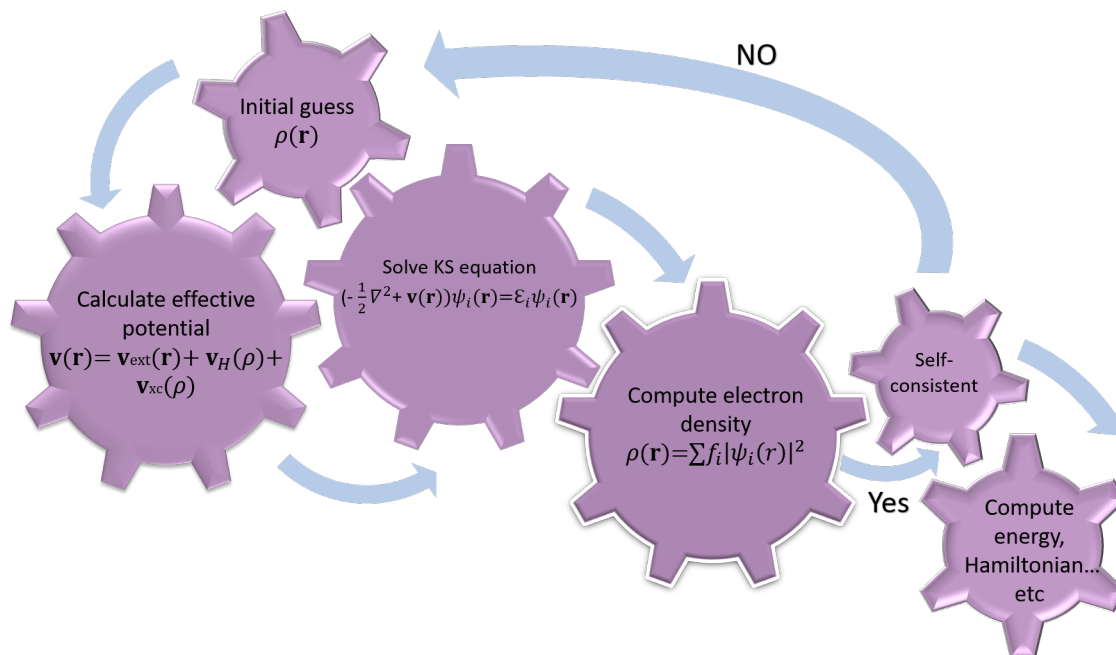
Figure 2.7.1: Schematic of the self-consistency process within SIESTA

Sham orbitals and the ground state energy for a particular structure. For optimisation purposes the process described before is in another cycle, which is controlled by the a conjugate gradient method to find the minimum ground state energy and atomic configuration. Finally, when the self-consistency is performed the Hamiltonian and density matrix are obtained.

Chapter 3

Transport Theory

3.1 Introduction

This chapter is meant to give an insight about the feild of molecular electronics. Recently, many investigations have been performed and study a broad range of applications. When a molecule is connected between two electrodes, charge flows from one side to the other. Moreover, interesting features appear due to the quantum effects that are involved in the electron wave function which will be discussed here. The phase coherent length scale is a fundamental concept in ballistic transport, because the mean free path of an electron $\ell > L$ where L is the length of the sample. In this chapter

the goal is to give an introduction to scattering problems and relate these problems to the conductance. Moreover, I will discuss scattering theory and Green's functions for different transport regimes such as a one dimensional structure with an arbitrarily scattering region. Then describe the general methodology to calculate the transmission coefficient $T(E)$ in a molecular junction for electrons passing from one electrode to the other.

3.2 Fundamental concepts in transport curves

At room temperature, electron transport through multiple paths in a single molecular junction is mainly affected by the signature of quantum interference. These interference effects lead to resonances or antiresonances, although experiments can only measure the conductance. This section focuses on studying these signatures in order to have a broad understanding of electronic devices and several fundamental concepts will be discussed including the Breit-Wigner resonance[16], antiresonances [17] [18] and Fano resonances[19][20]

3.2.1 Breit-Wigner resonance

The Transmission coefficient $T(E)$ has a peak and can be obtained from the Breit-Wigner formula and it applies when the energy of an incident electron resonates with an energy level of the isolated system.

$$T(E) = \frac{4\Gamma_1\Gamma_2}{(E - \varepsilon_n)^2 + (\Gamma_1 + \Gamma_2)^2} \tag{3.1}$$

Where Γ_1 and Γ_2 is the coupling of the molecular orbital to the electrode and $\varepsilon_n = \lambda - \sigma_L - \sigma_R$. Where λ is the eigenenergy of the molecular orbital shifted slightly by the amount of $\sigma = \sigma_L - \sigma_R$ due to the coupling of the orbitals to the electrodes.

This transmission coefficient is affected by many ingredients. When the coupling to electrode is weak the resonance is sharp. If the electrodes are symmetric $\Gamma_1 = \Gamma_2$ transmission coefficient can reach its maximum. This formula is vaild in the case that the level spacing of the isolated molecule is larger than the width of the resonance.

3.2.2 Antiresonance

The antiresonance phenomena can occur when the energy of the incoming electron E coincides with the eigenenergy E_n of one of the two branches as
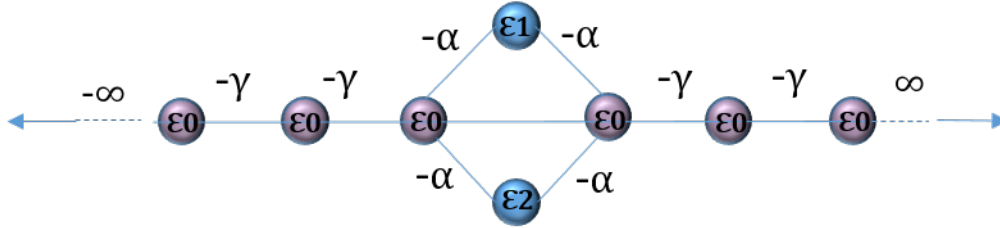
Figure 3.2.1: Tight binding model of antiresonance. When two semi-finite one-dimenstional chains connected to scattering region

shown in figure(3.2.1). A destructive interference occurs between propagating waves at the nodal point.

3.2.3 Fano-resonance

The appearance for this phenomena is due to the interference between a discrete state which is weakly coupled with the continuum state, and gives this asymmetric peak. This kind of phenomena is present because of the additional site which comes from the side group as shown in figure(3.2.2). When the pendant group is connected to a central backbone by the coupling of (α) which I consider to be more weakly coupled than the coupling to the open system.

$$T(E) = \frac{4\Gamma_1\Gamma_2}{(E - \varepsilon)^2 + (\Gamma_1 + \Gamma_2)^2} \tag{3.2}$$

28
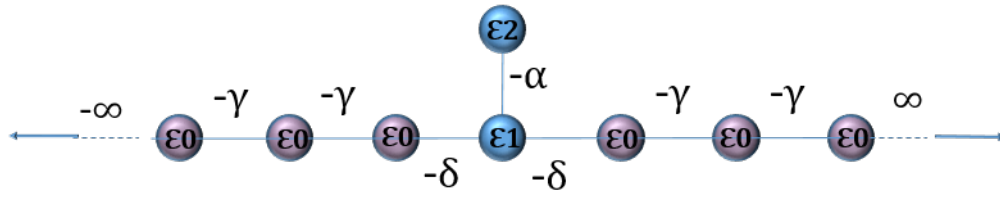
Figure 3.2.2: Tight binding model of fanoresonance. when two semi-finite one-dimensional chains connected to scattering region

Where $\varepsilon = \frac{\varepsilon_1 + \alpha^2}{(E - \varepsilon_2)}$, when $E - \varepsilon = 0$ this gives two cases, when $E = \varepsilon_1$ the Breit-Wigner resonance occurs, but if $E = \varepsilon_2$ this generates a resonance close to an antiresonance and by the superposition of quantum mechanics when two states are combined to give the new feature of a Fano resonance[20] [21].
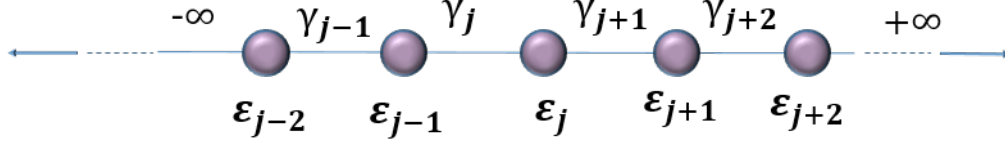
Figure 3.3.1: Tight binding model of infinite chain. (ε_j) **represent the site energy while** (γ_j) **represents the coupling**

3.3   Bond current

Suppose an infinite chain with on-site energy(ε_j) with coupling of $(-\gamma_j)$ The time independent Schrodinger equation for the system is:

$$\varepsilon_j\psi_j - \gamma_{j-1}\psi_{j-1} - \gamma_{j+1}\psi_{j+1} = E\psi_j \tag{3.3}$$

$$\Sigma_i H\psi_j = E\psi_j \tag{3.4}$$

$$i\hbar\frac{\partial|\psi_j(t)\rangle}{\partial t} = H|\psi(t)\rangle \tag{3.5}$$

$$i\hbar\frac{\partial|\psi(t)\rangle}{\partial t} = \Sigma_{i=1}H_{ji}|\psi_j(t)\rangle \tag{3.6}$$

$$\varepsilon_j\psi_j - \gamma_{j-1}\psi_{j-1} - \gamma_{j+1}\psi_{j+1} = E\psi_j \tag{3.7}$$

Picking a particular atom(j) from this system, then the probability of finding an electron on this atom (j) in time (t) after making many measurements is

:

$$|\psi_j(t)|^2 = n_j(t) \tag{3.8}$$

where (n_j) is the average number of electrons on that atom.

$$\frac{\partial n_j(t)}{\partial t} = I_{j-1} \rightarrow I_j - I_j \rightarrow I_{j+1} \tag{3.9}$$

Solving the time dependant Schrodinger equation for the rate of change of time:

$$\frac{\partial n_j(t)}{\partial t} = \frac{\partial |\psi_j(t)|^2}{\partial t} = \frac{\partial}{\partial t}\left(\psi_j^*(t)\psi_j(t)\right) \tag{3.10}$$

$$= \psi_j^*\frac{\partial \psi_j(t)}{\partial t} + \psi_j\frac{\partial \psi_j^*(t)}{\partial t} \tag{3.11}$$

$$= \frac{1}{i\hbar}\left\{\underbrace{\gamma_j\left(\psi_j(t)\psi_{j+1}^*(t) - \psi_j^*(t)\psi_{j+1}(t)\right)}_{I_{j\rightarrow j+1}} - \underbrace{\gamma_{j-1}\left(\psi_{j-1}(t)\psi_j^*(t) - \psi_{j-1}^*(t)\psi_j(t)\right)}_{I_{j_1\rightarrow j}}\right\}$$

$$\tag{3.12}$$

where $I_j \longrightarrow I_{j+1}$ is the bond current from (j) to (j+1) and $I_{j-1} \longrightarrow I_j$ is the bond current from (j-1) to (j)

$$I_j \longrightarrow I_{j+1} = \frac{2\gamma_j}{\hbar}Im[\psi j^*(t)\psi_{j+1}(t)] \tag{3.13}$$

If ψ_j is an eigenstate of H then: $I_j \longrightarrow I_{j+1}{=}I_{j-1} \longrightarrow I_j$ if $|\psi\rangle = A(t)|\phi\rangle$

31

3.4 Scattering-matrix

After finding the transmission and the reflection coefficients, it is therefore possible to calculate the scattering matrix. Solving the time independent Schrodinger for an electron approaching from the left electrode

$$\psi_j = \frac{A}{\sqrt{v_l}}e^{ik_l j} + \frac{B}{\sqrt{v_l}}e^{-ik_l j} \tag{3.14}$$

the current per unit energy that it carries is:

$$I_{left} = |A^2| - |B^2| \tag{3.15}$$

for the right electrode:

$$\psi_j = \frac{A}{\sqrt{v_r}}e^{ik_r j} + \frac{B}{\sqrt{v_r}}e^{-ik_r j} \tag{3.16}$$

$$I_{right} = |C^2| - |D^2| \tag{3.17}$$

since the bond current satisfies the relation $I_l = I_r$

$$|A^2| - |B^2| = |C^2| - |D^2| \tag{3.18}$$

And therefore:

$$|A^2| + |D^2| = |B^2| + |C^2| \tag{3.19}$$

which states that the incoming current is equal to outgoing current. The wave functions for the left electrode and right respectively are:

$$Ae^{ikj} + Be^{-ikj} \tag{3.20}$$

$$Ce^{ikj} + De^{-ikj} \tag{3.21}$$

To relate the outgoing with incoming coefficients I construct the s-matrix :

$$\begin{bmatrix} B \\ C \end{bmatrix} = \begin{bmatrix} S_{11} & S_{12} \\ S_{21} & S_{22} \end{bmatrix} \begin{bmatrix} A \\ D \end{bmatrix} \tag{3.22}$$

$$B = S_{11}A + S_{12}D \tag{3.23}$$

$$C = S_{21}A + S_{22}D \tag{3.24}$$

If A=1 and D=0:

then: B=r,C=t

$$\begin{bmatrix} B \\ C \end{bmatrix} = \begin{bmatrix} S_{11} & A \\ S_{21} & A \end{bmatrix} \tag{3.25}$$

By comparing with equations (3.23) and (3.24)

$$Ae^{ikj} + S_{11}A = S_{21}AC \tag{3.26}$$

S_{11} is (r) and S_{21} is (t) which is the reflection and transmission respectively.

If D=1 and A=0:

$$\begin{bmatrix} B \\ C \end{bmatrix} = \begin{bmatrix} D & S_{12} \\ D & S_{22} \end{bmatrix} \tag{3.27}$$

33

By comparing with equation (3.23) and (3.24):

$$De^{-ikj} + S_{22}D = S_{12}DB \tag{3.28}$$

Where S_{12} is (t') and S_{22} is (r') which is the reflection and transmission respectively.

Then :

$$S = \begin{pmatrix} S_{11} & S_{12} \\ S_{21} & S_{22} \end{pmatrix} = \begin{pmatrix} r & t' \\ t & r' \end{pmatrix} \tag{3.29}$$

Since the bond current satisfies the relation $I_l = I_r$

$$|A^2| - |B^2| = |C^2| - |D^2| \tag{3.30}$$

And thereby:

$$|A^2| + |D^2| = |B^2| + |C^2| \tag{3.31}$$

$$\begin{pmatrix} A^* & D^* \end{pmatrix} S^\dagger S \begin{pmatrix} A \\ D \end{pmatrix} = \begin{pmatrix} B^* & C^* \end{pmatrix} \begin{pmatrix} B \\ C \end{pmatrix} \tag{3.32}$$

34

Where $S^\dagger S$ is the unitary matrix and a consequence of charge conservation.

$$\begin{pmatrix} r^* & t^* \\ t^* & r^* \end{pmatrix} \begin{pmatrix} r & t' \\ t & r' \end{pmatrix} = \begin{pmatrix} 1 & 0 \\ 0 & 1 \end{pmatrix} \tag{3.33}$$

In terms of scattering theory :

$$|r^2| + |t^2| = 1 \Rightarrow R + T = 1 \tag{3.34}$$

$$|r'^2| + |t'^2| = 1 \Rightarrow R' + T' = 1 \tag{3.35}$$

Where T and R represent the transmission and reflection

In summary, the scattering-matrix is considered to be a powerful tool and is useful to provide insight about the transport properties in scattering theory.

3.5 The Landauer formula

Typically, in nano-structured devices the fundamental idea of a scattering problem in transport experiments is to make a connection between the probabilities of the transmission and reflection with the transport properties. This is extremely useful in nano-scale devices including single molecule electronics. In a molecular device, the Landauer formula[22][23] describes the transport of non interacting electrons for a scattering region in terms of a transmission

coefficient and a Fermi distribution of the connected electrodes. These electrodes supply the system with electrons and these reservoirs have a slightly different chemical potential $(\mu_L - \mu_R = E > 0)$ which leads to the passing of electrons from the left to the right[21]. To calculate the current for this system moving from left to right in a particular energy range and similarly from right to left:

The current generated by the chemical potential difference is :

$$\delta I = e \, \nu_g \, \frac{\partial n}{\partial E} \, \delta E = e \, \nu_g \, \frac{\partial n}{\partial E}(\mu_L - \mu_R) \tag{3.36}$$

Where the electron charge is e, the group velocity is ν_g , $\frac{\partial n}{\partial E}$ is the density of states per unit length and can be defined by the chemical potential of the contact.

$$\frac{\partial n}{\partial E} = \frac{\partial n}{\partial k}\frac{\partial k}{\partial E} = \frac{\partial n}{\partial k}\frac{1}{\nu_g \hbar} \tag{3.37}$$

In one-dimension, when having spin dependency $\frac{\partial n}{\partial k} = \frac{1}{2\pi}$, substituting into Eq. (3.37) gives:

$$\frac{\partial n}{\partial E} = \frac{1}{\upsilon_g h} \tag{3.38}$$

Equation (3.36) becomes:

$$\delta I = \frac{2e}{h}(\mu_L - \mu_R) \tag{3.39}$$
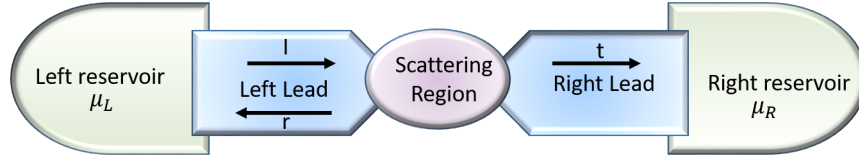
Figure 3.5.1: A scattering region connected to two electrodes. The electrodes are connected to a reservoir with chemical potential $\mu_{\mathbf{L}}$ and $\mu_{\mathbf{R}}$

$$\delta I = \frac{2e^2}{h}\delta V \tag{3.40}$$

where δV is the voltage in the reservoir generated by the difference in the potential. When considering a scattering region, the current passing through the scatterer to the right lead is written as:

$$\delta I = \frac{2e^2}{h}T\delta V \tag{3.41}$$

$$G = \frac{\delta I}{\delta V} = \frac{2e^2}{h}T \tag{3.42}$$

In the absence of a scattering region:

$$G = \frac{2e^2}{h} \tag{3.43}$$

$$G_0 = \frac{2e^2}{h} \tag{3.44}$$

G_0 is the quantum of conductance, equal to 77.5 μS.

In the presence of the scattering region the current will be:

$$G = \frac{2e^2}{h}T \tag{3.45}$$

$$G = G_0 T(E) \tag{3.46}$$

$$I = \frac{2e}{h}\int_{-\infty}^{\infty} dE T(E)[f_L(E) - f_R(E)] \tag{3.47}$$

Equation (3.46) is called the Landauer formula for a one-dimension system.

Where $e = -|e|$ and h is Plank's constant and T(E) is the transmission coefficient.

$$f_{L(R)}(E) = \frac{1}{e^{\frac{E-\mu_{L(R)}}{k_B T + 1}} + 1} \tag{3.48}$$

is the Fermi-Dirac distribution function and $\mu_L(R)$ is the chemical potential of the left (right) reservoir respectively. At zero temperature and finite voltage the current will be:

$$I = \frac{2e}{h}\int_{E_F - \frac{ev_b}{2}}^{E_F + \frac{ev_b}{2}} dE T(E) \tag{3.49}$$

The electrical conductance at zero voltage and finite temperature is:

$$G = \frac{I}{V} = G_0 \int_{-\infty}^{\infty} dE T(E)\left(-\frac{df(E)}{dE}\right)_{\mu=E_F} \tag{3.50}$$

38
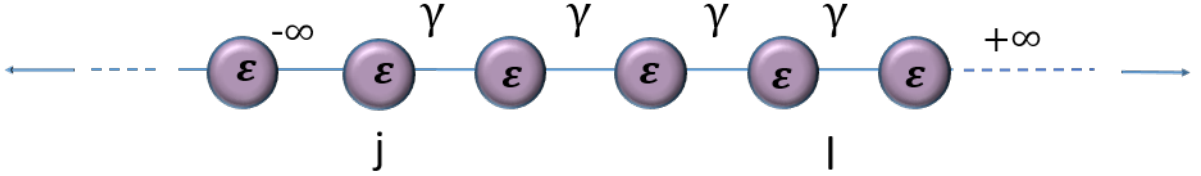
Figure 3.6.1: Tight binding model for a doubly infinite chain for the electrodes.

3.6 Green's Function

This section provides valuable insight about the concept of Green's functions and what sort of information this function contributes to the transport[24]. Moreover, I analyse the transport properties for different nano-scale systems by including several situations to show key results.

3.6.1 Green's function of a doubly infinite chain

This section, presents the Green's function of the doubly infinite chain for the electrodes, where the electrodes are a perfect chain as in figure(3.6.1). The time independent Schrodinger equation is:

$$(E - H)|\psi\rangle = 0 \tag{3.51}$$

The Green's function of a system described by a Hamiltonian (H) can be defined as the solution of

$$(E - H)G = I \qquad (3.52)$$

The formal solution to this equation would be given by:

$$G = (E - H)^{-1} \qquad (3.53)$$

Where G is the retarded Green's function(g_{jl})

$$(E - H)g_{j,l} = \delta_{j,l} \qquad (3.54)$$

Where δ is Kronecker delta, which is equal to 1 if j=l and zero otherwise. The green's function for infinite system

$$\varepsilon_0 g_{jl} - \gamma g_{j+1,l} - \gamma g_{j-1,l} + \delta_{jl} = E g_{jl} \qquad (3.55)$$

if the solutions is :

$$g_{jl} = \begin{cases} Ae^{ikj} & j \geq l \\ Be^{-ikj} & j \leq l \end{cases} \qquad (3.56)$$

Where A and B represent a wave coming from the right and left respectively.

Because a Green's function is continuous at j=l, I can write that :

$$g_{jl}\big|_{j=l} = \begin{cases} Ae^{ikj} & A = \alpha e^{-ikl} \\ Be^{-ikj} & B = \alpha e^{ikl} \end{cases} \qquad (3.57)$$

Therefore: $g_{ll} = \alpha$. Applying these results to Eq.(3.55) and considering the energy for the infinite system I obtain:

$$(\varepsilon_0 - E)\alpha - \gamma\alpha e^{ik} - \gamma\alpha e^{ik} = -1 \qquad (3.58)$$

$$\gamma\alpha(2cosk - 2e^{ik}) = -1 \qquad (3.59)$$

$$\alpha = \frac{1}{2i\gamma sink} \qquad (3.60)$$

$$\alpha = \frac{1}{i\hbar\nu} \qquad (3.61)$$

Where ν is the group velocity. The result of (3.61) and Eq(3.57) combines to get the Green's function for the double infinite chain[25][26]:

$$g_{jl}^{\infty} = \frac{e^{ik|j-l|}}{i\hbar\nu} \qquad (3.62)$$

Where g_{jl} is the retarded Green's function which describes the two outgoing waves from the source j=l

3.6.2 Green's function of semi-infinite one dimensional chain

To derive the Green's function of a semi-infinite chain consider the problem of a double infinite chain. Except, introducing a boundary condition to switch it

41
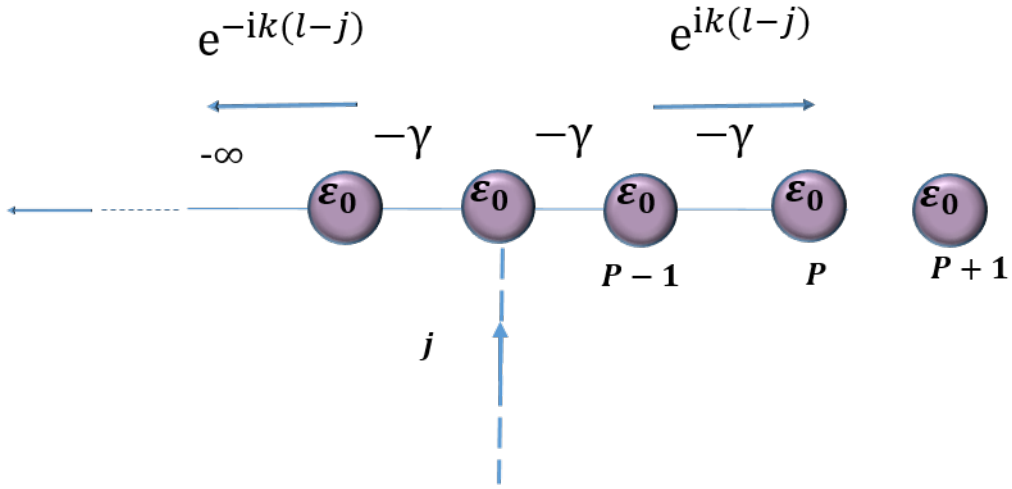
Figure 3.6.2: Tight binding model of a semi-infinite one dimensional chain.

to a semi-infinite chain in order to obtain the Green's function for this system. Let's consider a one dimensional infinite lead with site (ε_0) and coupling of ($-\gamma$)as shown in the figure(3.6.2). This infinite chain must terminate at a given point $P + 1$ which means the Green's function is eliminated at the site $P + 1$. This can be obtained by adding a wave function to a double infinite Green's function.

The general Green's function is written as:

$$g_{jl} = g_{jl}^\infty + \psi_{jl} \tag{3.63}$$

The appropriate wave function is simply:

$$\psi_{jl} = A e^{-ikl} \tag{3.64}$$

$$A = -\frac{e^{-ikj}}{i\hbar\upsilon} e^{2ik(p+1)} \tag{3.65}$$

The Green's function terminated at point (p) due to source at (l=j), is:

$$g_{p,j} = \frac{e^{ikp} \, e^{-ikj} - e^{-ikj} \, e^{2ik(p+1)} \, e^{-ikp}}{i\hbar\upsilon} \tag{3.66}$$

From the boundary condition where l=j=p, thereby:

$$g_{p,j} = \frac{-e^{ik}}{\gamma} e^{ik(p-j)} \tag{3.67}$$

The Green's function for site $j = p$ due to source at site $l = p$

$$g_{p,p} = -\frac{e^{ik}}{\gamma} \tag{3.68}$$

Which is the surface Green's function.

3.6.3   One dimensional scattering

If I have two semi-finite one dimensional leads connected to each other by a coupling of $(-\gamma)$ with site energy of (ε_0) as shown in figure(3.6.3). Tackling this simple problem to find the transmission and reflected coefficient of an electron travelling from the left to the right lead is powerful because it seems
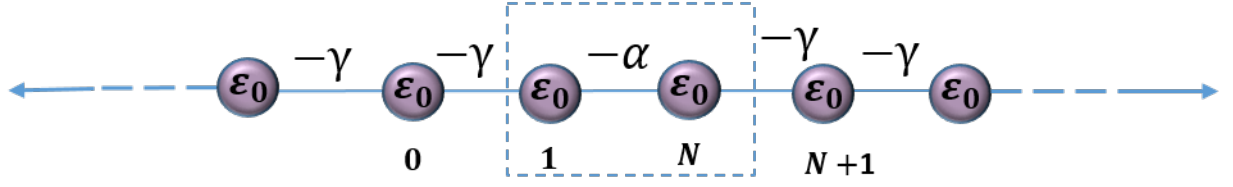
Figure 3.6.3: Tight binding model of a 1-D scattering region attached to a one dimensional lead

intuitively clear that all scattering problems could be reduced to this simple form of a one dimensional system. The Hamiltonian takes the form :

$$
\begin{pmatrix}
\ddots & -\gamma & 0 & 0 & 0 & 0 \\
-\gamma & \varepsilon_0 & -\gamma & 0 & 0 & 0 \\
0 & -\gamma & \varepsilon_0 & \alpha & 0 & 0 \\
0 & 0 & \alpha & \varepsilon_0 & -\gamma & 0 \\
0 & 0 & 0 & -\gamma & \varepsilon_0 & -\gamma \\
0 & 0 & 0 & 0 & -\gamma & \ddots
\end{pmatrix}
=
\begin{pmatrix}
H_L & V_c \\
V_c^\dagger & H_R
\end{pmatrix}
\tag{3.69}
$$

Where H_R and H_L are the Hamiltonians of the semi-infinite leads and V_c is the coupling to connect these leads. Starting from the Green's function of this problem in order to compute the scattering amplitudes which is written as:

$$
G = (E - H)^{-1}
$$

The retarded Green's function has been defined above as equation(3.62)and the semi-infinite Green's function is also defined as equation (3.67). In the case of decoupled leads where $\alpha = 0$ the total Green's function is written as:

$$g = \begin{pmatrix} \frac{-e^{ik}}{\gamma} & 0 \\ 0 & \frac{-e^{ik}}{\gamma} \end{pmatrix} = \begin{pmatrix} g_L & 0 \\ 0 & g_R \end{pmatrix} \tag{3.70}$$

The Green's function for the coupled system can be obtained using the Dyson equation which is:

$$G = (g^{-1} - V)^{-1}$$

clearly:

$$\begin{pmatrix} 0 & V_c \\ V_c^\dagger & 0 \end{pmatrix} = \begin{pmatrix} 0 & -\alpha \\ -\alpha^* & 0 \end{pmatrix} \tag{3.71}$$

Solving Dyson's equation leads to the Green's function of this system which is:

$$G = \frac{1}{\gamma^2 e^{-2ik} - \alpha^2} \begin{pmatrix} \gamma e^{-ik} & -\alpha \\ -\alpha & \gamma e^{-ik} \end{pmatrix} \tag{3.72}$$

After finding the Green's function for this system, the scattering coefficients are obtained by using the Fisher-Lee relation to link the scattering amplitudes of this problem to the Green's function of the same problem. The Fisher-Lee

45

relation is:

$$r = i\hbar v G_{0,0} - 1 \tag{3.73}$$

$$t = i\hbar v G_{0,N+1} e^{ik} \tag{3.74}$$

These coefficients correspond to a particle travelling from the left, the same procedure could done in order to compute these coefficients for a particle travelling from the right.

$$T = |t|^2 \tag{3.75}$$

$$R = |r|^2 \tag{3.76}$$

Finally, now obtain the full scattering matrix in order to calculate the zero bias conductance from Landauer formula equation.

3.6.4 Transport through an arbitrary scattering region

Consider a nano-scale system with a scattering region of sites (1) to (N)connected to one dimensional electrodes from both sides. Each atom in the lead has on-site energy (ε_0) with a coupling of $(-\gamma)$.

The wave functions for this system are:

$$\psi_j = e^{ikj} + re^{-ikj} \tag{3.77}$$
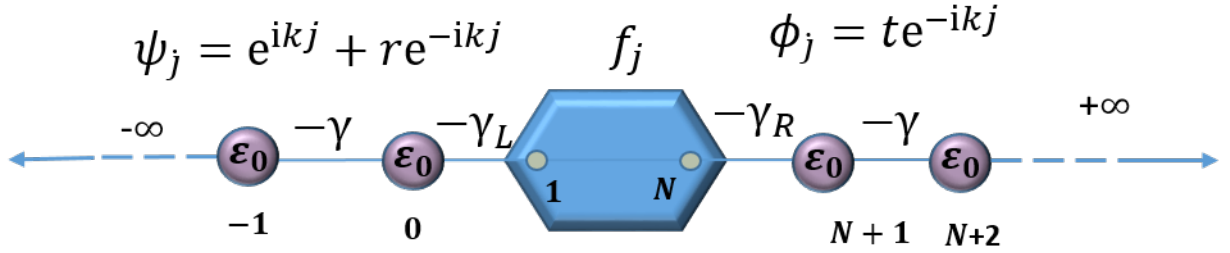
Figure 3.6.4: Tight binding model of 1-D scattering region attached to one dimentional lead

representing the left side.

$$\phi_j = te^{ikj} \tag{3.78}$$

representing the right side.

$$f_j \tag{3.79}$$

representing the scattering region. The Schrodinger equation in these regions could be written as respectively: for $j \leq -1$

$$\varepsilon_0 \psi_j - \gamma \psi_{j-1} - \gamma \psi_{j+1} = E\psi_j \tag{3.80}$$

When j=0

$$\varepsilon_0 \psi_0 - \gamma \psi_{-1} - \gamma_l f_1 = E\psi_0 \tag{3.81}$$

For scattering region:

When j=1

$$\Sigma_{l=1}^{N} H_{1l} f_l - \gamma_l \psi_0 = E f_1 \qquad (3.82)$$

for $2 \leq j \leq N-1$

$$\Sigma_{l=1}^{N} H_{jl} f_l = E f_j \qquad (3.83)$$

for j=N

$$\Sigma_{l=1}^{N} H_{Nl} f_l - \gamma_R \phi_{N+1} = E f_N \qquad (3.84)$$

for j=N+1

$$\varepsilon_0 \phi_{N+1} - \gamma \phi_{N+2} - \gamma_R f_N = E \phi_{N+1} \qquad (3.85)$$

For $j \geq N+2$

$$\varepsilon_0 \gamma \phi_j - \gamma \phi_{j-1} - \gamma \phi_{j+1} = E \phi_j \qquad (3.86)$$

When j=0 in equation(3.81) and (3.82):

$$\gamma_L f_1 = \gamma \psi_1 \qquad (3.87)$$

When j=N+1 in equation(3.87) and (3.86):

$$\gamma_R f_N = \gamma \phi_N \qquad (3.88)$$

finding ψ_0 and ϕ_{N+1}:

48

$$\psi_0 = \frac{\gamma_L}{\gamma_0} e^{ik} f_1 - (2i)(sink)e^{ik} \tag{3.89}$$

$$\phi_{N+1} = \frac{\gamma_R}{\gamma}(e^{ik})f_N \tag{3.90}$$

then: $|\psi\rangle = \Sigma|f\rangle + |S\rangle$

Where Σ_R and Σ_L are the self energy to the left and right lead.

$$\begin{pmatrix} -\gamma_L \psi_0 \\ -\gamma_R \phi_{N+1} \end{pmatrix} = \begin{pmatrix} \Sigma_L f_1 \\ \Sigma_R f_N \end{pmatrix} + \begin{pmatrix} 2\gamma_L i e^{ik} sink \\ 0 \end{pmatrix} \tag{3.91}$$

solve that to get:

$$|\psi\rangle = \Sigma g|\psi\rangle + |S\rangle \tag{3.92}$$

$$|\psi\rangle = (I - \Sigma g)^{-1}|S\rangle \tag{3.93}$$

$$\begin{pmatrix} -\gamma_L \psi_0 \\ -\gamma_R \phi_{N+1} \end{pmatrix} = \frac{1}{det} \begin{pmatrix} 1 - \Sigma_R g_{NN} & \Sigma_L g_{1N} \\ -\gamma_R g_{N1} & 1 - \Sigma_L g_{11} \end{pmatrix} \begin{pmatrix} S_L \\ 0 \end{pmatrix} \tag{3.94}$$

Therefore the transmission (t) could be obtained as:

$$t = \frac{\gamma_L \gamma_R}{\gamma} e^{ik} e^{-ikN} (2isink)(\frac{g_{N1}}{det}) \tag{3.95}$$

49

where the determinant is $det = 1 - \Sigma_R\, g_{NN} - \Sigma_L\, g_{11} + \Sigma_L \Sigma_R (g_{11} g_{NN} - g_{1N} g_{N1})$

The transmission probability is $T(E) = |t|^2$ which could be written as:

$$T(E) = 4\left(\frac{\gamma_R^2 sink}{\gamma}\right)\left(\frac{\gamma_L^2 sink}{\gamma}\right)\left|\frac{g_{N1}}{det}\right|^2 \qquad (3.96)$$

$$T(E) = 4\Gamma_R\Gamma_L\left|\frac{g_{N1}}{det}\right|^2 \qquad (3.97)$$

This is the most general equation to calculate the transmission probability for any scattering region connected with same electrodes.

Bibliography

[1] José M Soler, Emilio Artacho, Julian D Gale, Alberto García, Javier Junquera, Pablo Ordejón, and Daniel Sánchez-Portal. The siesta method for ab initio order-n materials simulation. *Journal of Physics: Condensed Matter*, 14(11):2745, 2002.

[2] Robert G Parr. Density functional theory of atoms and molecules. In *Horizons of Quantum Chemistry*, pages 5–15. Springer, 1980.

[3] EKU Gross and RM Dreizler. Density functional theory: an approach to the quantum many-body problem, 1990.

[4] W Kohn and LJ Sham. doi: 10.1103/physrev. 140. a1133. *Phys. Rev. A*, 140:113, 1965.

[5] P Hohenberg and W Kohn. Inhomogeneous electron gas phys. rev. 136. *B864*, 1964.

[6] Nathan Argaman and Guy Makov. Density functional theory: An introduction. *American Journal of Physics*, 68(1):69–79, 2000.

[7] Richard M Martin and Richard Milton Martin. *Electronic structure: basic theory and practical methods*. Cambridge university press, 2004.

[8] Walter Kohn, Axel D Becke, and Robert G Parr. Density functional theory of electronic structure. *The Journal of Physical Chemistry*, 100(31):12974–12980, 1996.

[9] Max Born and Robert Oppenheimer. Zur quantentheorie der molekeln. *Annalen der physik*, 389(20):457–484, 1927.

[10] Albert Bartók-Pártay. *The Gaussian Approximation Potential: an interatomic potential derived from first principles quantum mechanics*. Springer Science & Business Media, 2010.

[11] Viraht Sahni. The hohenberg-kohn theorems and kohn-sham density functional theory. In *Quantal Density Functional Theory*, pages 99–123. Springer, 2004.

[12] Walter Kohn. Nobel lecture: Electronic structure of matterâĂŤwave

functions and density functionals. *Reviews of Modern Physics*, 71(5):1253, 1999.

[13] Weitao Yang. Direct calculation of electron density in density-functional theory. *Physical Review Letters*, 66(11):1438, 1991.

[14] Reiner M Dreizler and Eberhard KU Gross. *Density functional theory: an approach to the quantum many-body problem.* Springer Science & Business Media, 2012.

[15] Walter Kohn and Lu Jeu Sham. Self-consistent equations including exchange and correlation effects. *Physical review*, 140(4A):A1133, 1965.

[16] Gregory Breit and Eugene Wigner. Capture of slow neutrons. *Physical review*, 49(7):519, 1936.

[17] San-Huang Ke, Weitao Yang, and Harold U Baranger. Quantum-interference-controlled molecular electronics. *Nano letters*, 8(10):3257–3261, 2008.

[18] Robert Stadler. Quantum interference effects in electron transport through nitrobenzene with pyridil anchor groups. *Physical Review B*, 80(12):125401, 2009.

[19] TA Papadopoulos, IM Grace, and CJ Lambert. Control of electron transport through fano resonances in molecular wires. *Physical review b*, 74(19):193306, 2006.

[20] CJ Lambert. Basic concepts of quantum interference and electron transport in single-molecule electronics. *Chemical Society Reviews*, 44(4):875–888, 2015.

[21] Scheer Elke and Cuevas Juan Carlos. *Molecular electronics: an introduction to theory and experiment*, volume 15. World Scientific, 2017.

[22] Rolf Landauer. Spatial variation of currents and fields due to localized scatterers in metallic conduction. *IBM Journal of Research and Development*, 1(3):223–231, 1957.

[23] Rolf Landauer. Electrical transport in open and closed systems. *Zeitschrift für Physik B Condensed Matter*, 68(2-3):217–228, 1987.

[24] NR Claughton, M Leadbeater, and CJ Lambert. Theory of andreev resonances in quantum dots. *Journal of Physics: Condensed Matter*, 7(46):8757, 1995.

Chapter 4

Breakdown of Curly Arrow Rules in Anthraquinone

In this chapter, I determine the validity of curly arrow rules in fully conjugated anthracene and dihydroxyanthracene, cross-conjugated anthraquinone and broken conjugated dihydroanthracene attached to graphene through pi-pi stacking and further test the rule for molecules attached to gold electrodes with thiol and Au-C anchors. I find that this rule breaks down in molecular junctions formed by cross-conjugated anthraquinone. Curly arrow rules predict destructive QI for a *meta* connected anthraquinone core, whereas my calculation predicts constructive QI. This behaviour is independent of the choice of electrode material or anchor groups. The results presented in this chapter were published in: J. Alqahtani, H. Sadeghi, S. Sangtarash and C. Lambert, "Breakdown of Curly Arrow Rules in Anthraquinone", *Angewandte Chemie*, vol. 130, no. 46, pp. 15285-15289, 2018. Available: 10.1002/ange.201807257.

4.1 Introduction

Understanding and controlling quantum interference (QI) in single molecules is fundamental to the development of QI-based single-molecule electronics. Over the past decade, simple rules such as counting rules, curly arrow rules, circuit rules and more recently magic ratio rules have been developed to predict QI patterns in polycyclic aromatic hydrocarbons. These rules have been successful in explaining observed electronic transport properties of molecular junctions and provide helpful design tools for predicting properties of molecules before their synthesis. Curly arrow rules are widely used by chemists, material scientists and physicists to predict destructive QI. Here I examine the validity of curly arrow rules in fully conjugated anthracene and dihydroxyanthracene, cross-conjugated anthraquinone and broken conjugated dihydroanthracene attached to graphene or gold electrodes through pi-pi stacking or thiol and Au-C anchors. For the first time, I demonstrate that curly arrow rules break down in molecular junctions formed by cross-conjugated anthraquinone. In contrast with the destructive QI predicted by curly arrow rules for a meta connected anthraquinone core, I demonstrate that QI is constructive. This behavior is independent of the choice of electrode material or anchor groups. This is significant, because by changing the redox state of meta connected dihydroxyanthracene to form meta connected anthraquinone, the conductance of the junction increases by couple of orders of magnitude due to the cross over form constructive to destructive QI. This opens new avenues for realization of quantum interference based single molecule switches.

Single molecule electronics has recently witnessed significant progress[1]. Much attention has been drawn to phase coherent quantum interference (QI)[2], which plays an essential role in electronic transport through single molecules[3]. Simple design rules such as counting rules[4], curly arrow rules[5][6], quantum circuit rules[7] and more recently magic ratio rules[8]have been

developed to predict the effect of interference patterns in polycyclic aromatic hydrocarbons (PAHs). When a molecule is connected to metallic electrodes with different connectivities, electrons traversing multiple paths interfere constructively or destructively[9]. This constructive (destructive) QI leads to a high (low) conductance. The above rules are helpful in identifying if destructive or constructive QI is expected for a given connectivity. In addition, magic ratio rules provide information about ratios of conductances belonging to different constructive connectivities. These simple rules provide basic understanding of a molecular scale junctions and can qualitatively explain various experiments[5][8][10].

Over the past decades, curly arrow rules (CARs) have been used to predict destructive QI in molecules[5]. Curly arrows predict the movement of pairs of electrons[6]. When an electron is placed on a site in a PAH, the charges should be balanced. A bond is broken if electrons are removed from it; otherwise a bond is formed if electrons are placed between two atoms. This process is illustrated by curly arrows. When an electron path was formed by moving pairs of electrons (using curly arrows) between two injection and collection connectivities, constructive QI is expected. Otherwise, if such a path was not found, destructive QI is predicted[5][6]. For example for a *para* connected anthracene (AC1 in figure 4.1a), the arrows shows the path that the electron could take to travel through the molecule[5]. In contrast, in *meta* connected anthracene (AC2 in figure 4.1b), a loop is formed and the electron entered to the molecule cannot exit[5]. In this case, the CAR predicts destructive QI. Indeed these predictions for anthracene have been observed experimentally[11]. In anthraquinone, when curly arrows are drawn, due to the presence of oxygen, there is no path between both *para* and *meta* connectivities and therefore, CARs predict destructive QI for both *meta* and *para* connectivities (AQ1 and AQ2 in figure 4.1c,d). However, this is not supported with our first principles calculations.
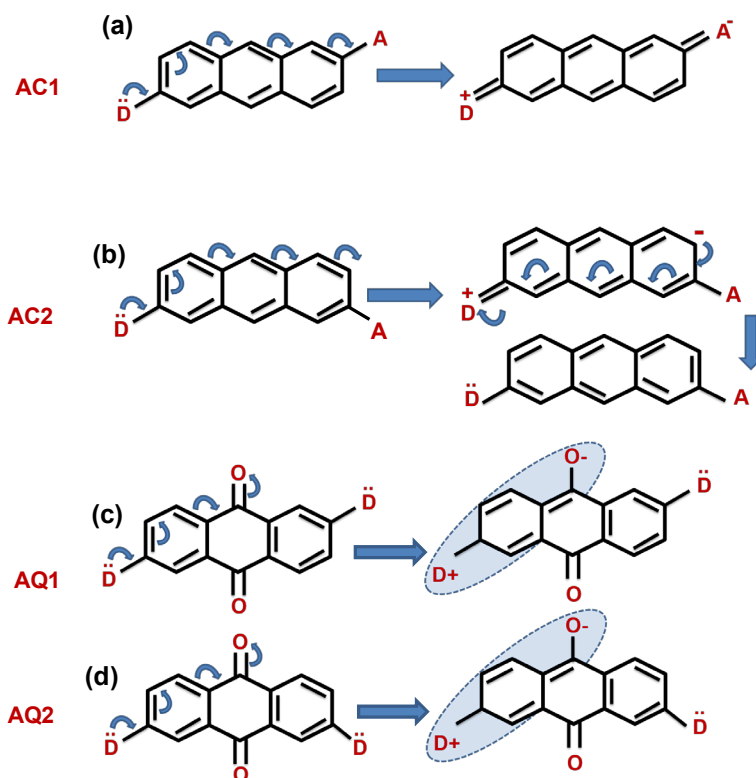
Figure 4.1. The curly arrow rule (CAR). (a) *para* **and (b)** *meta* **connected conjugated anthracene labelled by AC1 and AC2, respectively. (c)** *para* **and (d)** *meta* **connected cross conjugated anthraquinone labelled by AQ1 and AQ2, respectively.**

In this communication, I show that the curly arrow rule breaks down. I examine the validity of CARs using anthraquinone based molecular junctions. In contrast with curly arrow rules which predict destructive QI for both *para* (fig. 4.1c) and *meta* (fig.4.1d) connected anthraquinone, I demonstrate destructive QI for *para* connected anthraquinone (fig. 4.1c), but constructive QI for *meta* connectivity. This is independent of the choice of anchor group or electrodes material. In contrast to conjugated anthracene, anthraquinone is a cross-conjugated molecule. If each oxygen in anthraquinone was replaced by two hydrogens, a broken conjugated dihydroanthracene is obtained. In what follows, I also investigate the quantum interference effect in these three types of molecules. I study the cross-conjugated anthraquinone molecular junctions (AQ1 and AQ2 in fig. 4.2) and compare it with its conjugated counterpart anthracene (AC1 and AC2 in fig.4.2) and

dihydroxyanthracene (QC1 and QC2 in fig. 4.2) and broken conjugated dihydroanthracene (AH)[12] (fig.4.17). Molecular junctions are formed by attaching these molecules to gold electrodes via thiol[13](fig. 4.2b) and direct Au-C[14] (fig. 4.2a) bonds and to graphene electrodes through pi-pi stacking with pyrene anchors[15](fig. 4.2c). I have constructed 22 different molecular junctions by combining ACs, AQs, QCs and AHs with 2 electrodes and 3 anchors.
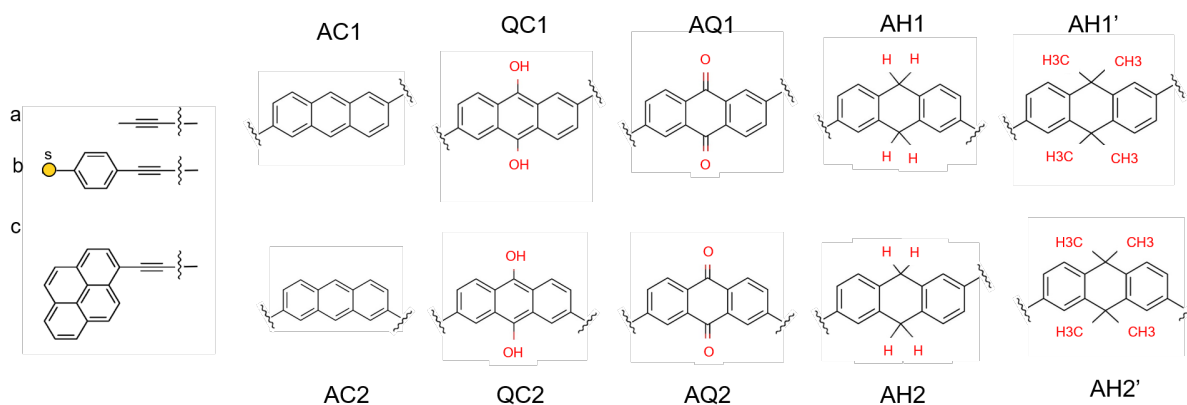
Figure 4.2. The structure of three systems with three central cores (AC, QC, AQ, AH and AH') via different connectivities. (a) A direct C-C bond with gold. (b) Thiol anchor with gold. (c) Pyrene with graphene.

4.2 Result and discussion

In order to investigate the electronic properties of the junctions, I used the DFT code SIESTA to obtain the optimized geometry adopting the generalised gradient approximation (GGA) and PBE functional for the exchange and correlation. We also chose a double-ζ plus polarized (DZP) basis set. The geometry of each structure was relaxed to a force tolerance of 20 meV/Å. A real-space grid was defined with an equivalent energy cutoff of 150 Ry. To calculate electronic properties of the molecules in the junction, from the converged DFT calculation, I extracted the resulting mean-field Hamiltonian and overlap matrices and used them to compute the electrical properties of the devices with transport code Gollum[16] to calculate the transmission coefficient $T(E)$ of electrons with energy E passing from one electrode to the other. The conductance is proportional to $T(E)$

via Landauer formula $G=G_0T(E_F)$ where G_0 is conductance quantum, and E_F is the Fermi energy of electrode.

(a)

(b)

(c)
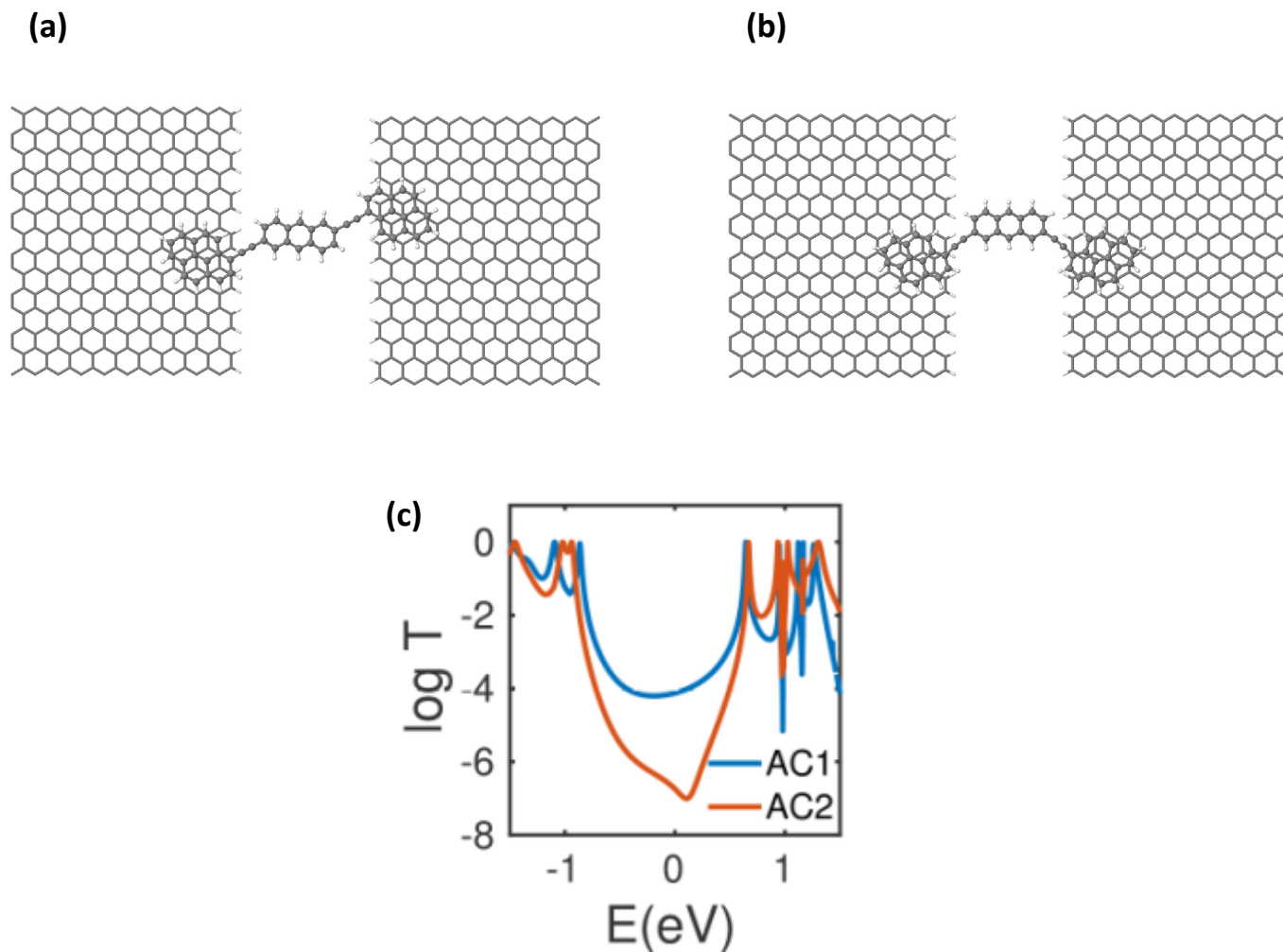
Figure 4.3. Transmission coefficients for electrons passing through the junctions with graphene electrodes via pyrene anchor groups. (a,b) example of junctions formed by AC cores connected to the anchors from *para and meta*. Transmission coefficients for (c) AC1 and AC2. The features around *E=1eV* are mainly due to the changes in the number of open channels in graphene electrodes.

Figure 4.3 shows the calculated transmission coefficient for junctions with graphene electrodes. Figures 4.3a,b show examples of the junctions formed using graphene electrodes via para and meta connectivity, Figures 4.5a,b where AQ's are connected from different connection points to

two pyrene electrodes through acetylene linkers. Pyrene anchors are connected to the electrodes (figure 4.3a,b) ,figure(4.4a,b) and figure(4.5 a,b) through pi-pi interaction with the pi system of graphene.

(a)

(b)

(c)
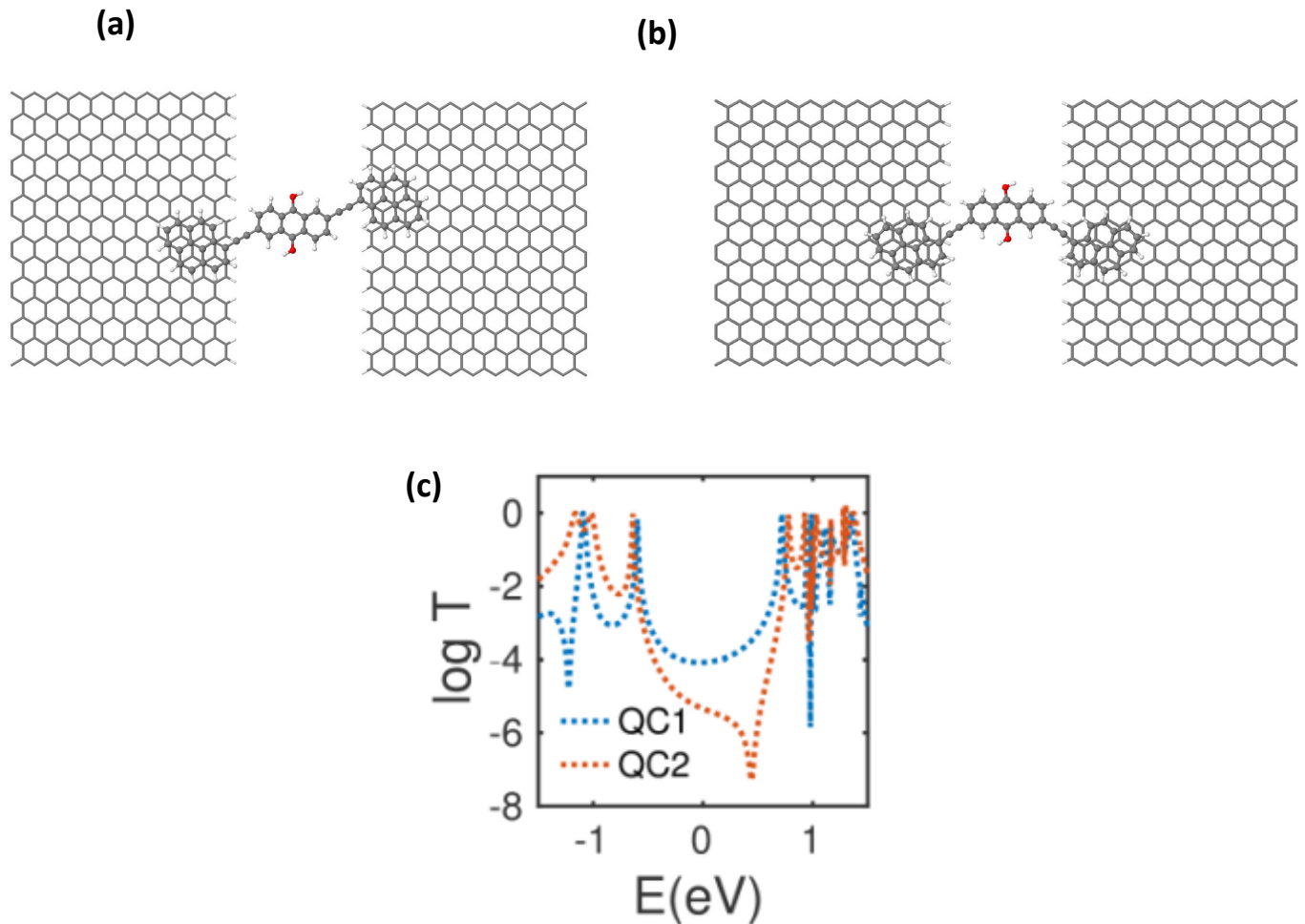
Figure 4.4. Transmission coefficients for electrons passing through the junctions with graphene electrodes via pyrene anchor groups. (a,b) example of junctions formed by QC cores connected to the anchors from *para and meta*. Transmission coefficients for (c) QC1 and QC2. The features around *E=1eV* are mainly due to the changes in the number of open channels in graphene electrodes.

Figure 4.3c shows the transmission coefficient for graphene junctions formed by AC cores. In agreement with previous theoretical[11][17]and experimental studies[11][18][19], the conductance of *para* connected AC1 (fig. 4.2) shows high conductance due to a constructive QI whereas a low conductance is obtained in AC2 due to a destructive QI (fig. 4.3c). Note that since

the junction, including leads and molecule is formed from carbon and hydrogen, a uniform charge distribution is expected. Therefore, the DFT Fermi energy lies close to the middle of the HOMO-LUMO gap. Similar behaviour is obtained in the graphene/QC's/graphene molecular junction (fig. 4.4)
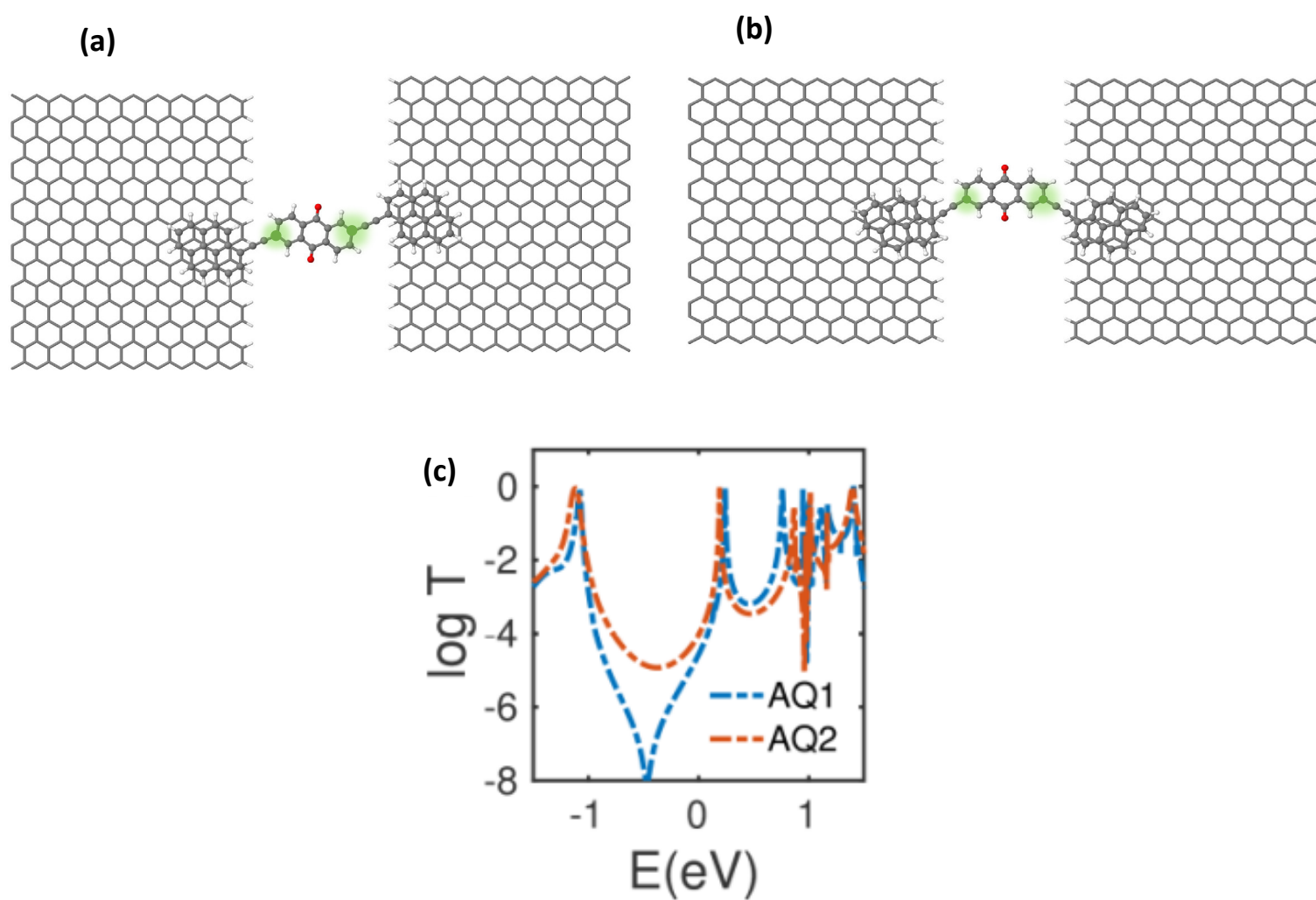
Figure 4.5. Transmission coefficients for electrons passing through the junctions with graphene electrodes via pyrene anchor groups. (a,b) example of junctions formed by AQ cores connected to the anchors from *pa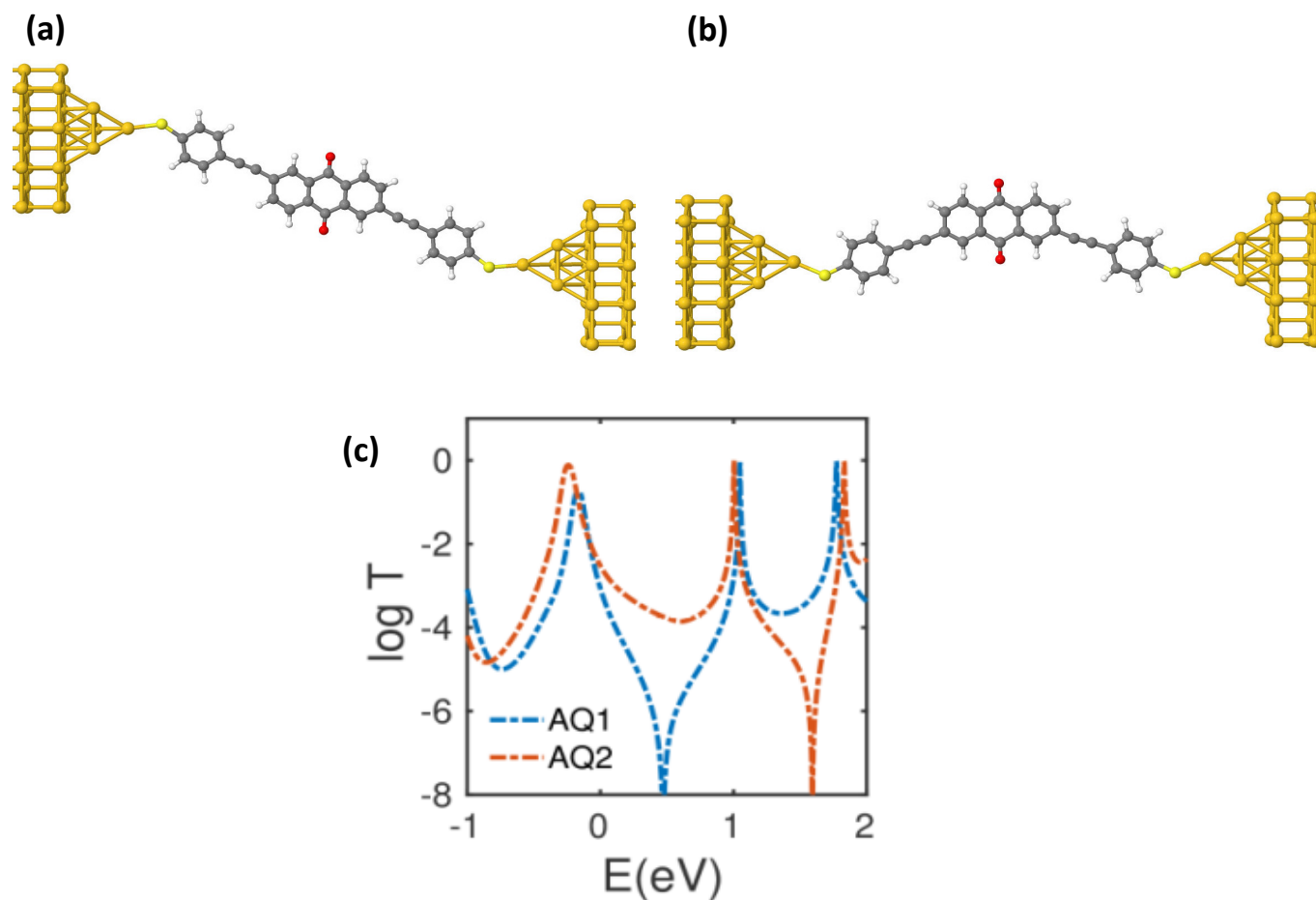ra and meta*. Transmission coefficients for (c) AQ1 and AQ2. The features around *E=1eV* are mainly due to the changes in the number of open channels in graphene electrodes.

The transmission spectrum of QC's is slightly shifted to the right (negative gate) compared to *T(E)* of AC's. This is due to a weak electrostatic gating effect of the oxygen atoms in QC's. In

Both AC and QC molecular junctions, the conjugation is not broken and curly arrow rules works perfectly.

In contrast, in the junctions formed by AQ molecules, *meta* connected AQ2 shows a high conductance and constructive QI (blue curve in fig 4.5.c) whereas *para* connected AQ1 exhibits destructive QI with a low conductance (red curve in fig. 4.5c).
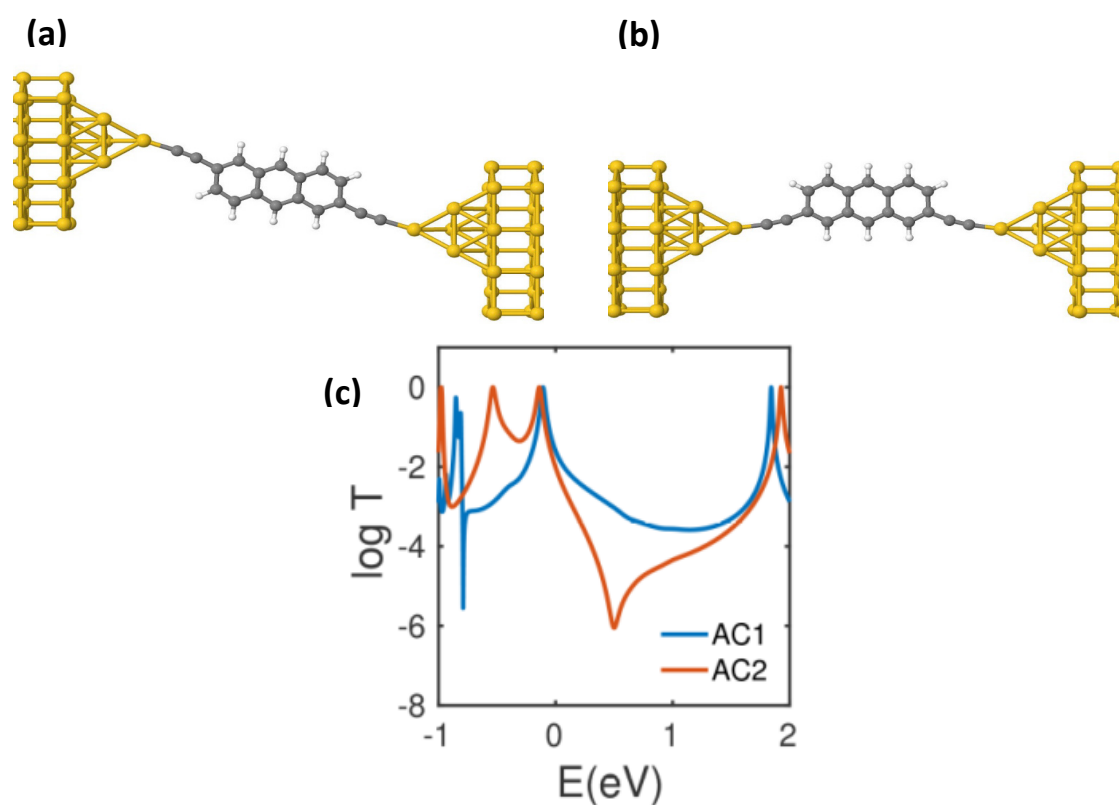
Figure 4.6. Transmission coefficients for electrons passing through the junctions with gold electrode through direct Au-C bond with acetylene linker. (a,b) example of junctions formed by AC cores connected to the anchors from *para* connectivity. Transmission coefficients for (c) AC1 and AC2.

This is opposite to the prediction using curly arrow rules, because when electrons are injected from the left green site in (fig 4.5a,b) there is no electron path to the green sites (fig. 4.5a,b) using curly arrow rules. Therefore, destructive QI is predicted from CARs, which is not supported with our calculation shown in (fig 4.5c) where AQ2 exhibits constructive QI. Similarly, the *meta*-connected AQ2 shows constructive QI with high conductance, which is not consistent with predictions from curly arrow rules. This demonstrates that curly arrow rule breaks down in the *meta* connected anthraquinone.

To demonstrate that this is a generic feature of anthraquinone-based molecular junctions, I study electron transport properties of the junctions formed from gold electrodes using either thiol or direct Au-C anchor groups connected to AC, QC and AQ with *meta* or *para* connectivities.
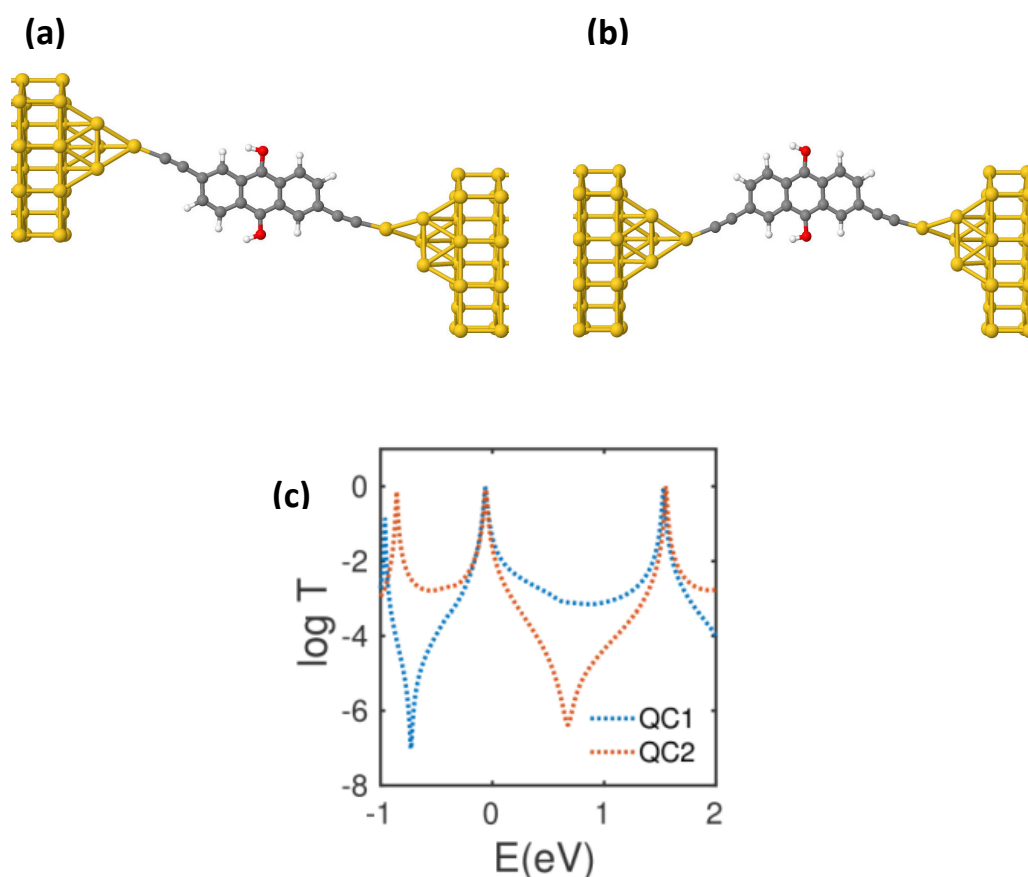
Figure 4.7. Transmission coefficients for electrons passing through the junctions with gold electrode through direct Au-C bond with acetylene linker. (a,b) example of junctions formed by QC cores connected to the anchors from *para* connectivity. Transmission coefficients for (c) QC1 and QC2

(Figs 4.6, 4.7,4.8) shows the transmission coefficient through the gold electrodes via direct Au-C coupling with acetylene linkers in the case of AC, QC and AQ. Junctions formed with AC1 and QC1 molecular cores show constructive QI whereas those formed by AC2 and QC2 molecular core shows destructive QI (figs. 4.6c,4.7c).

The DFT Fermi energy lies in the tail of HOMO resonance in agreement with previous report [38]for molecular junctions formed through direct Au-C bond. Clearly, the destructive QI dip in QC2 has shifted to the right compared to AC2 due to the electrostatic gating effect of the oxygen atoms.
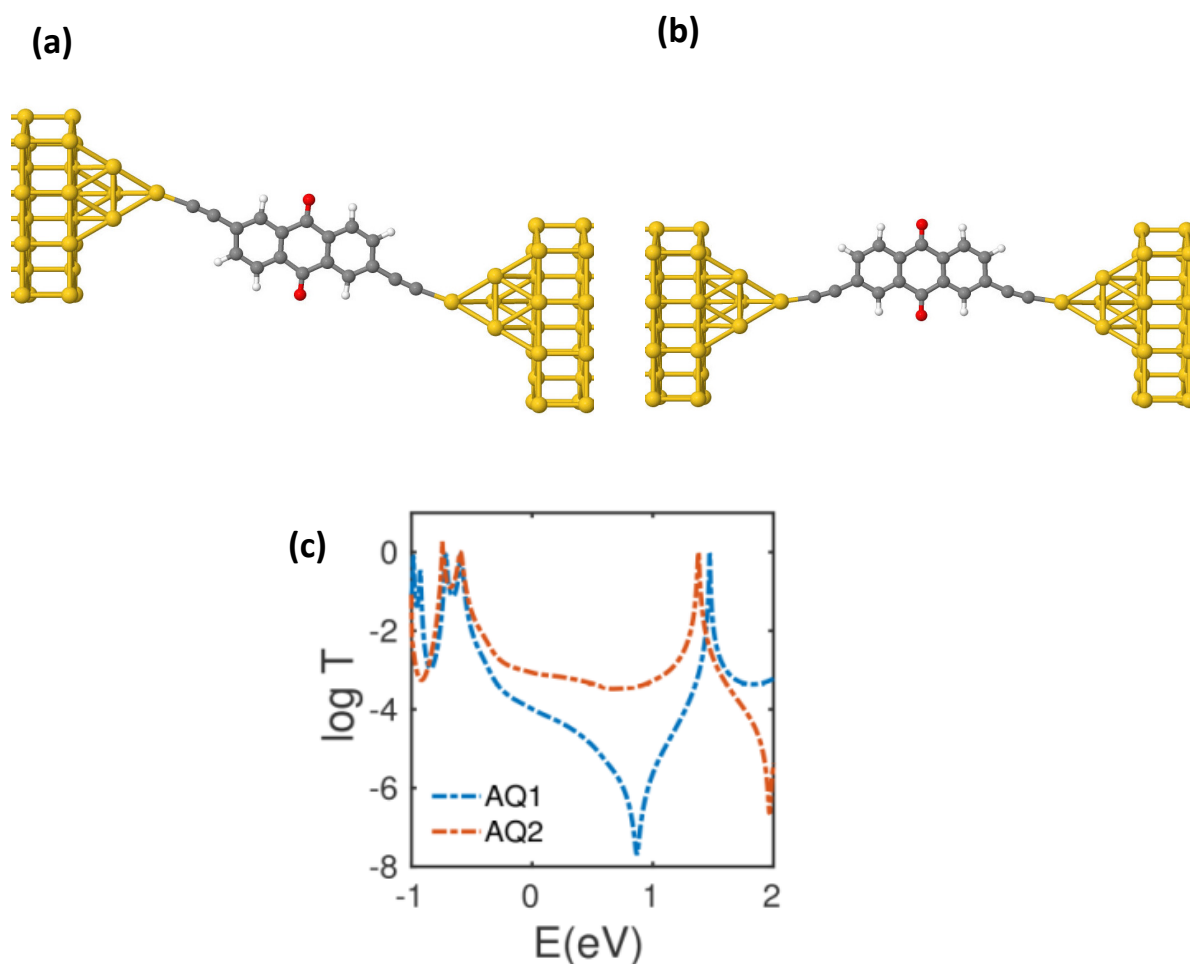
Figure 4.8. Transmission coefficients for electrons passing through the junctions with gold electrode through direct Au-C bond with acetylene linker. (a,b) example of junctions formed by AQ cores connected to the anchors from *para* connectivity. Transmission coefficients for (c) AQ1 and AQ2.

The results for AC and QC are in agreement with predictions from curly arrow rules. However, the CAR again breaks down in the junctions formed by AQ molecular cores (fig. 4.8c), in agreement with our result obtained in graphene junctions (fig. 4.5). It is worth mentioning that although the transport is still HOMO dominated in the gold/AQ/gold junctions, the Fermi energy is closer to the middle of HOMO-LUMO gap.
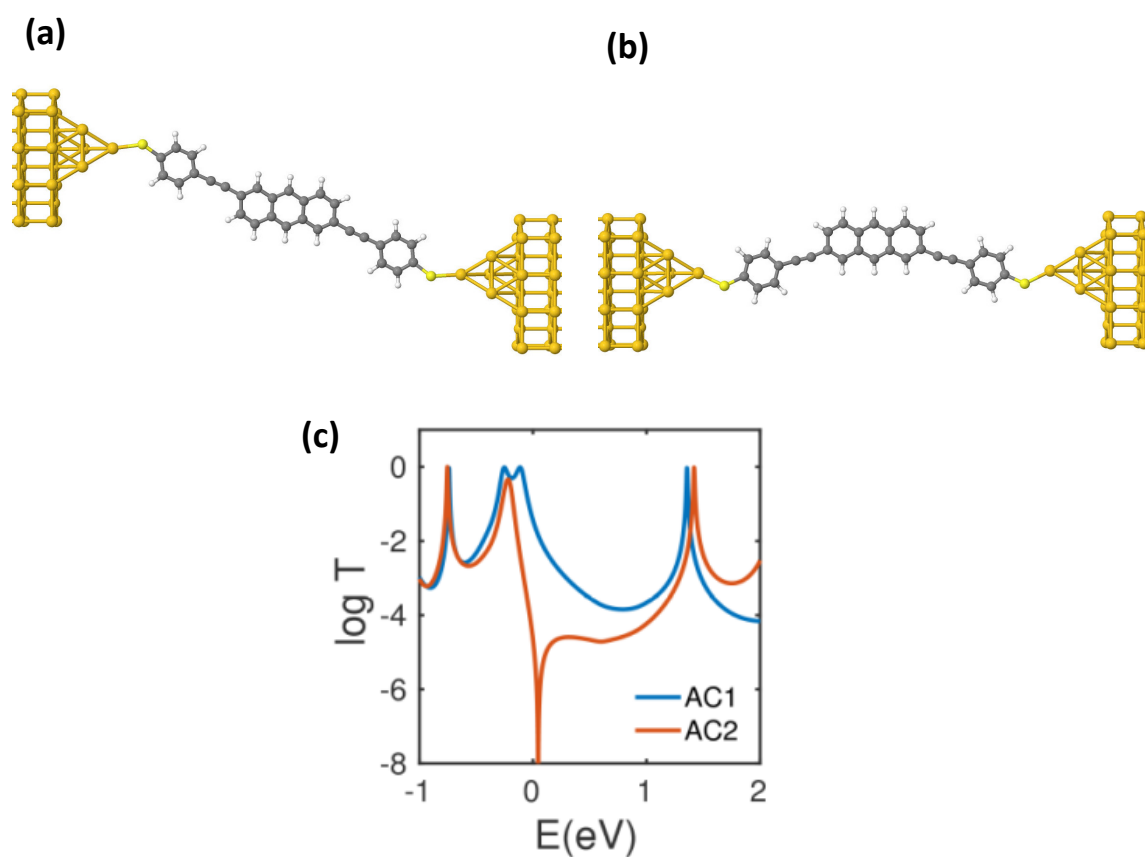
Figure 4.9. Transmission coefficients for electrons passing through the junctions with gold electrode with gold electrode connected to thiol anchor (a,b) example of junctions formed by AC cores connected to the anchors from *para* connectivity. Transmission coefficients for (c) AC1 and AC2.

I now consider a third system, where the three central cores are attached to gold electrodes through thiol anchors (Figs 4.9, 4.10 and 4.11) shows the transmission coefficient obtained for these junctions. Clearly, the result is in excellent agreement with junctions formed from gold electrodes with Au-C direct anchoring (fig. 4.6, 4.7 and 4.8) and graphene electrodes (fig. 4.3, 4.4 and 4.5).

Again, the conductance of the molecular junctions formed by both AC and QC molecular cores shows constructive and destructive interference for *para* and *meta* connectivities, respectively (figs. 4.9c, 4.10c) in contrast to the gold/AQ/gold junctions where opposite behaviour is obtained (fig. 4.11c).
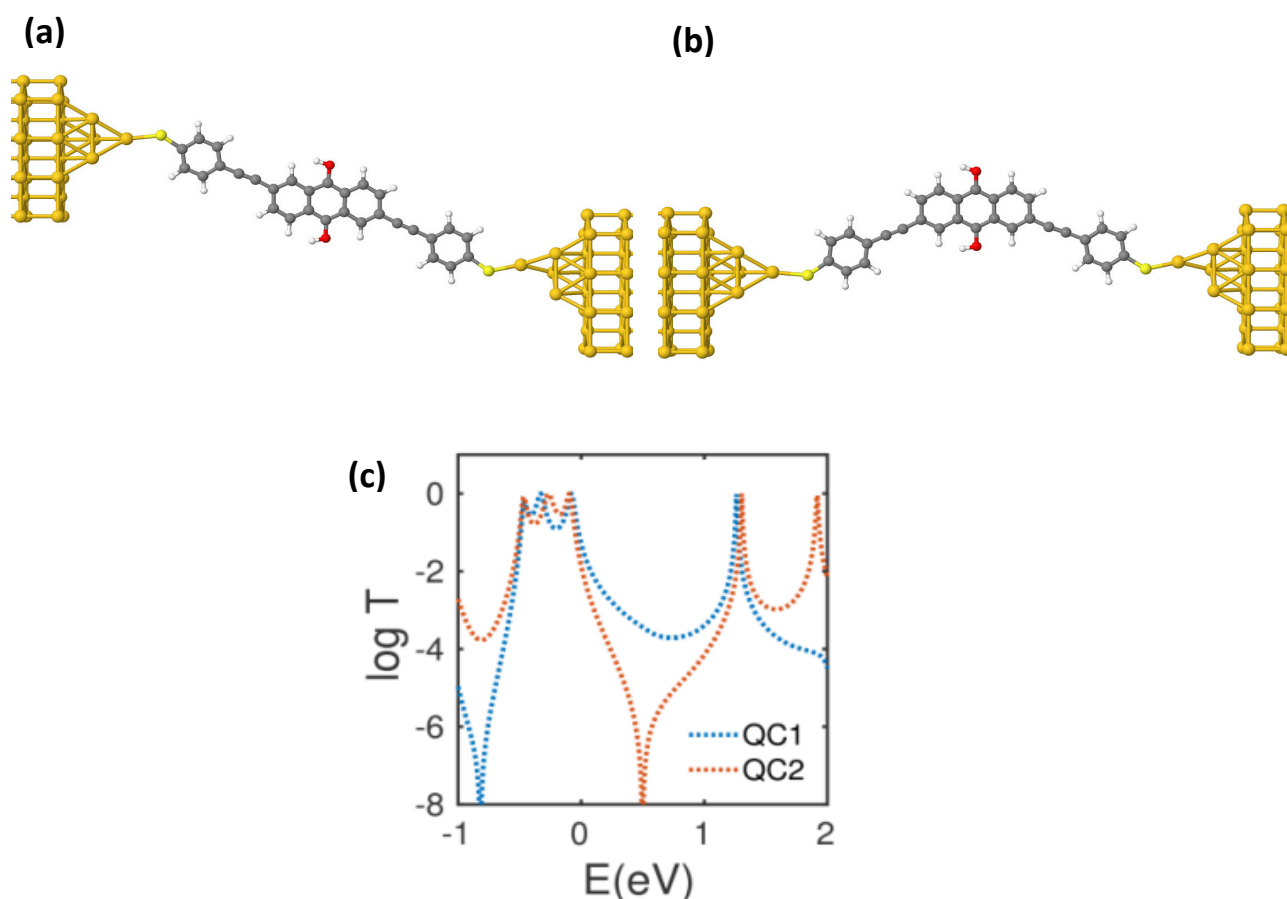
Figure 4.10. Transmission coefficients for electrons passing through the junctions with gold electrode through direct Au-C bond with acetylene linker. (a,b) example of junctions formed by QC cores connected to the anchors from *para* connectivity. Transmission coefficients for (c) QC1 and QC2.

Figure 4.11. Transmission coefficients for electrons passing through the junctions with gold electrode through direct Au-C bond with acetylene linker. (a,b) example of junctions formed by AQ cores connected to the anchors from *para* connectivity. Transmission coefficients for (c) AQ1 and AQ2.

In order to understand the difference between the transmission coefficients of AQ and QC cores, I examined the evolution of the transmission coefficient starting from QC2 and then

increasing the distances d between the hydrogens and oxygens of the two carbonyl groups in a series of steps. Fig. 4.12 shows that as d increases, the HOMO of QC2 evolves into the LUMO of AQ2 (see also figs 4.13 and 4.14), which pushes the anti-resonance from the HOMO-LUMO gap of QC2 into the LUMO-LUMO+1 gap of AQ2.
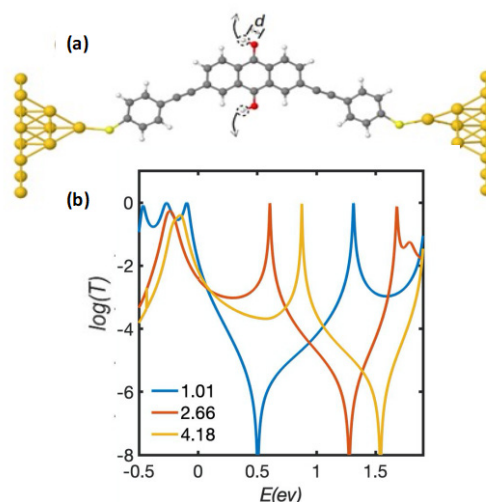
\Figure 4.12. Transmission coefficients for the QC2 junctions with gold electrode connected to thiol anchor (a). The hydrogen connected to the oxygens are initially placed at their equilibrium distance (d = 1.01 angstroms) from their neighbouring oxygen. Then the distance between the hydrogens and oxygens in the two carbonyl groups is increased in a series of steps, indicated by the legend.
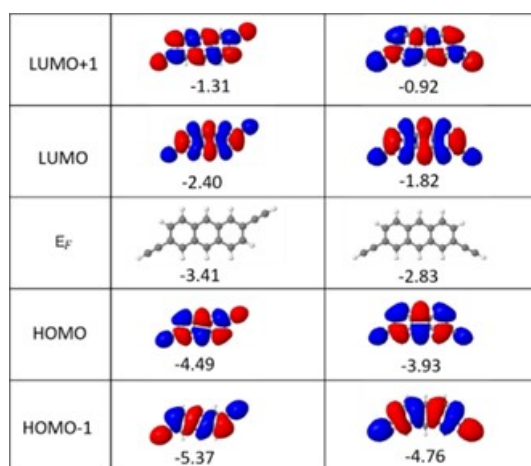
Figure 4.13. The wave functions of HOMO-2, HOMO-1, HOMO, LUMO, LUMO+1 and LUMO+2 levels in AC1 and AC2.
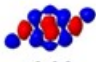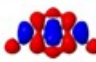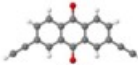
Figure 4.14. The wave functions of HOMO-2, HOMO-1, HOMO, LUMO, LUMO+1 and LUMO+2 levels in AQ1 and AQ2.
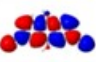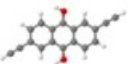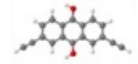
Figure 4.15. The wave functions of HOMO-2, HOMO-1, HOMO, LUMO, LUMO+1 and LUMO+2 levels in QC1 and QC2

When comparing the anti-resonance in the para-connected AQ1 with those of the meta-connected AC2 and QC2, it is helpful to note that in addition to the electrostatic gating effect by oxygen, the character of the frontier orbitals changes, such that (see figure 4.17) the HOMO and LUMO of QC resembles the LUMO and LUMO+1 of AQ. The effect of this, is most clearly illustrated in figures (4.6, 4.7and 4.8), where the meta-connected AQ2 possesses an anti-resonance in the gap between the LUMO and LUMO+1 (at 1.5eV). This anti-resonance evolves into the anti-resonance between the HOMO and LUMO of QC2.

.
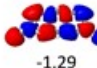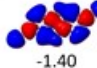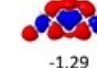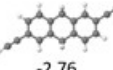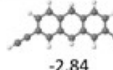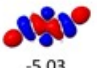
Figure 4.16. The wave functions of HOMO-2, HOMO-1, HOMO, LUMO, LUMO+1 and LUMO+2 levels in AH1 and AH2
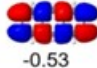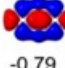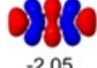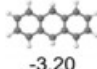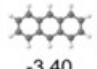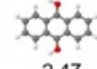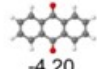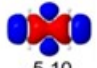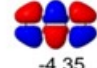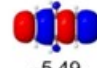
Figure 4.17. The wave functions of HOMO-2, HOMO-1, HOMO, LUMO, LUMO+1 and LUMO+2 levels in the isolated system.

71

This surprising behaviour in the AQ2 based junctions is also present in a simple tight-binding model of p orbitals within the molecules, in which the AC or AQ cores are connected to two 1D leads through a weak coupling. Figure 4.18 shows the calculate transmission coefficient $T(E)$ for both *meta* and *para* connected junctions. Figure 4.18a shows $T(E)$ for anthracene junctions with all on-site energies $\varepsilon_0=0$ and hopping integrals $\gamma= -1$.
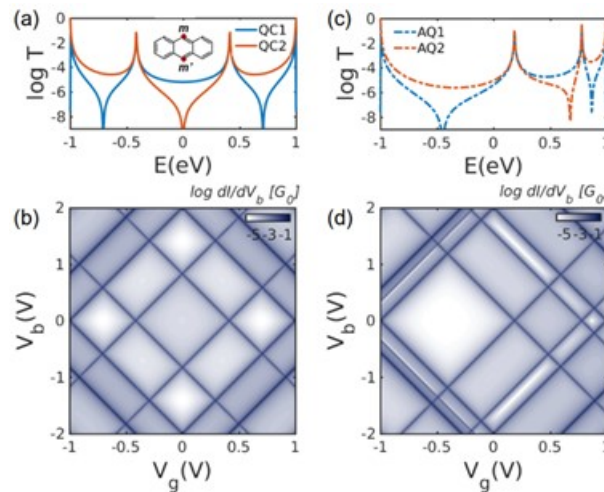
Figure 4.18. Simple tight-binding model. (a) The transmission coefficient for QC1 (blue line) and QC2 (red line). Inset (a) lattice structure considered in TB model. All on-site energies and couplings in a are $\varepsilon_0=0$ and $\gamma=-1$, respectively, (b) differential conductance of QC1 versus bias V_b and gate V_g voltages (c) the transmission coefficient for AQ1 (blue line) and AQ2 (red line) where all on-site energies and couplings in a are $\varepsilon_0=0$ and $\gamma=-1$, respectively; except on-site energies at sites m and m' ($\varepsilon_m=\varepsilon_{m'}=-1.5\gamma$) and (b) differential conductance of AQ1 versus bias V_b and gate V_g voltages.

Clearly, constructive QI is obtained in the conjugated QC1 (AC1) junction compared to QC2 (AC2). When (m and m' in the inset of figure 4.18a) hydrogen atoms in anthracene are replaced by oxygen, the on-site energies are increased due to electrostatic gating induced by oxygen atoms. This is captured by a minimal tight-binding model of cross-conjugated AQ junctions, where I only change the on-site energies at sites m and m' (see inset of fig. 4.18a) to $\varepsilon_m=\varepsilon_{m'}=-1.5\gamma$. This is because, in the cross-conjugated structure, the site energy of carbon attached to an oxygen is increased. As shown by the resulting transmission coefficients in figure (4.18c), this leads to

destructive QI for *para* connectivity and constructive QI for *meta* connectivity, in agreement with the $T(E)$ of figure (4.11c), calculated by DFT.

I also calculated the current through the junctions versus different bias Vb and gate Vg voltages. By differentiating the current with respect to the bias voltage, I obtain the differential conductance $G = dI/dV_b$. In this model, I assume that the main bias potential drops at the interface between the leads and molecules and the gate voltage potential profile is uniform over the junctions.
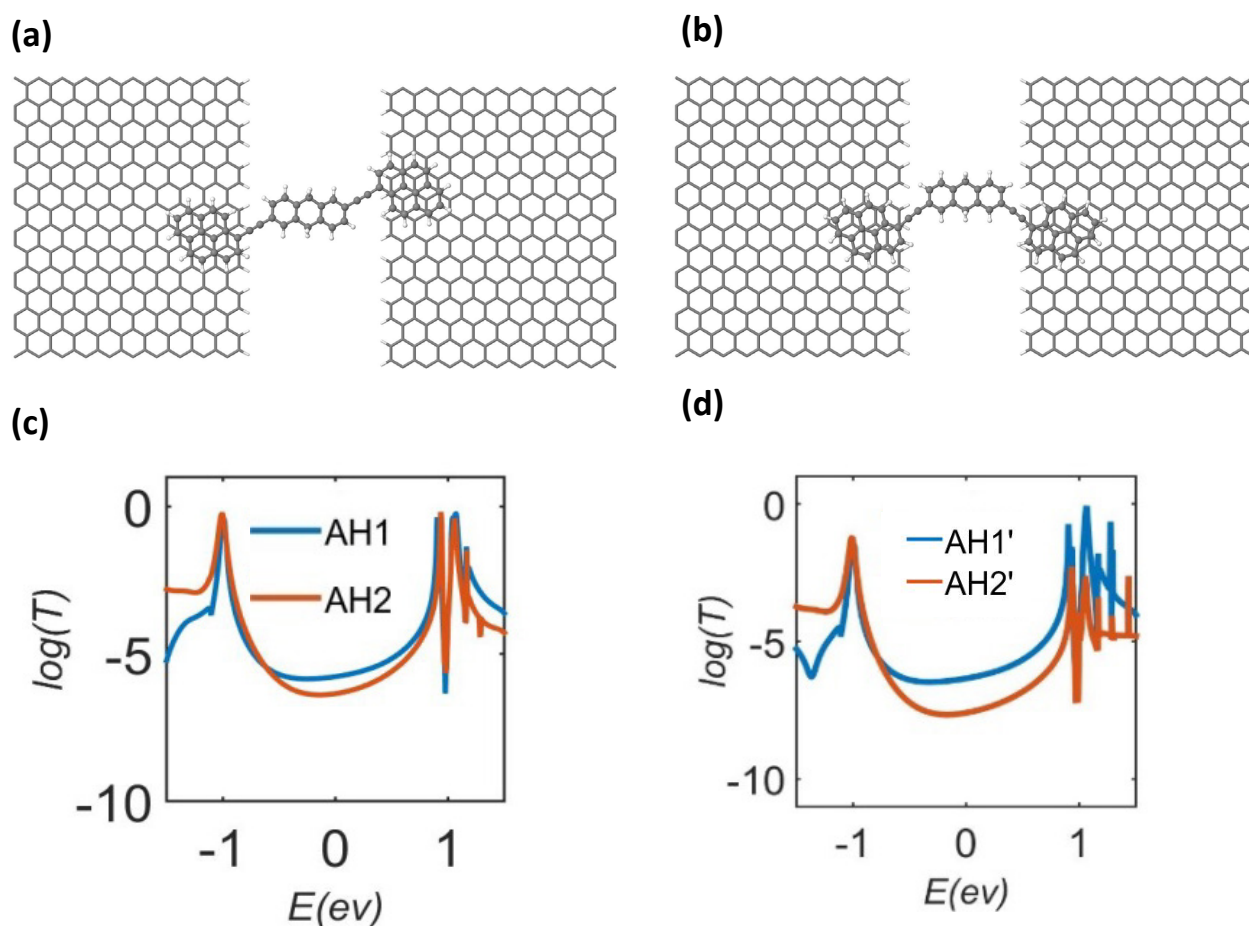
Figure 4.19. The transmission coefficient for the broken conjugation dihydroanthracene (AH) when connected to graphene. (a) para connectivity (b)meta connectivity (c) for the dihydroanthracene (AH) (d) when the H of each carbonyl group is replaced by CH₃.

Figure (4.18b,d) shows the calculated differential conductance for QC1 (AC1) and AQ1 junctions, respectively. The higher and lower conductance are illustrated by dark blue and white colours in figures (4.18b,d). By changing the redox state of QC1 to form AQ1, the conductance of the junction decreases by a couple of orders of magnitude due to the cross over form destructive (the diamond involving $V_b=0V$ and $V_g=0V$ in figure 4.18b) to constructive QI (the diamond involving $V_b=0V$ and $V_g=0V$ in figure 13d). This opens new avenues for realization of quantum interference based single molecule switches.
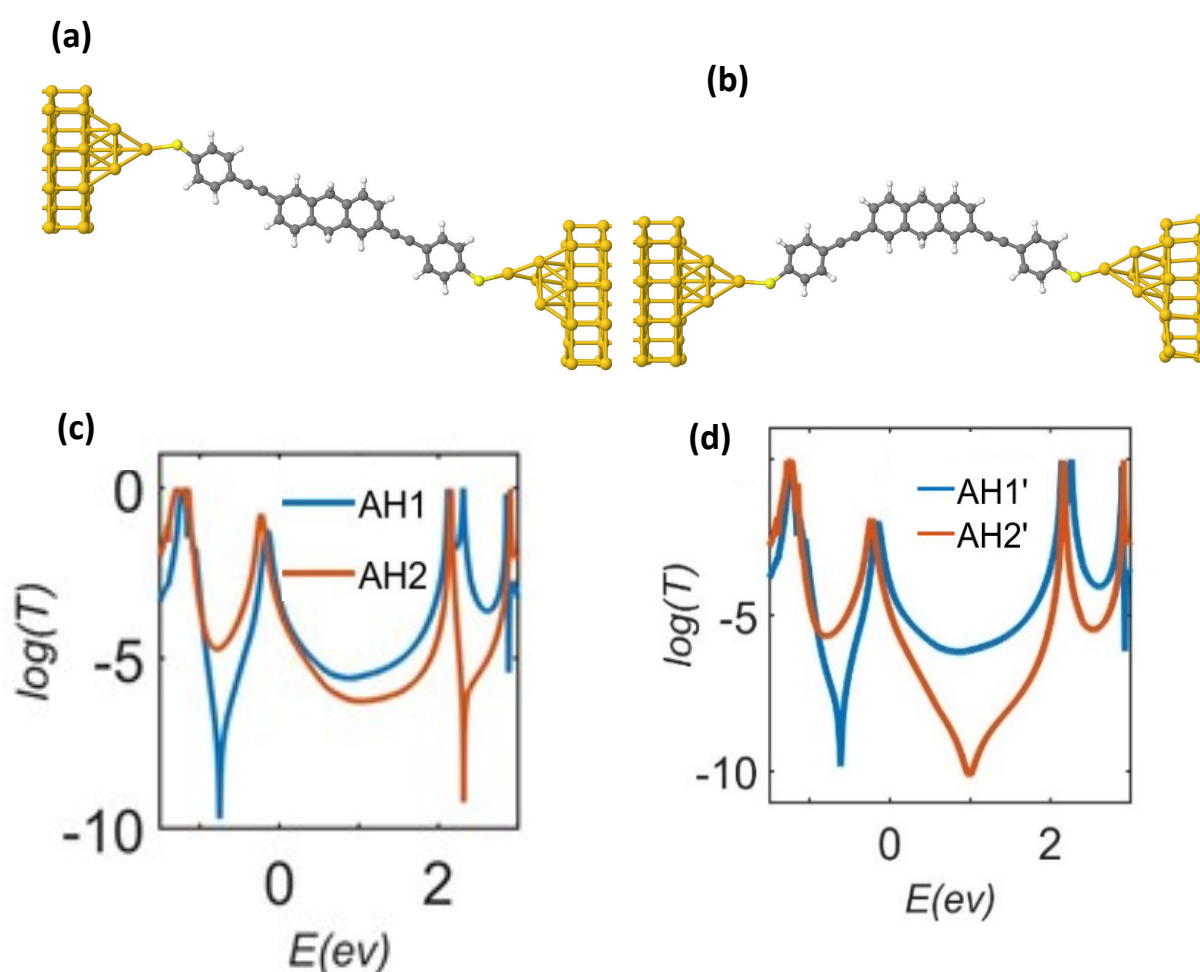
Figure 4.20. The transmission coefficient for the broken conjugation when connected to gold electrode via Au-C bonds. (a) via para connectivity (b)meta connectivity (c) for the dihydroanthracene (AH) (d) when the H of each carbonyl group is replaced by CH$_3$

In order to understand how interference patterns are affected by replacing oxygen atoms in AQ with two hydrogens to form broken conjugated dihydroanthracene (AH), I calculate the transmission coefficients for two *para* and *meta* connectivities attached to graphene or gold electrodes through either pi-pi stacking or using thiol or direct Au-C anchors.

Figure 4.19c,4.20c and 4.21c shows the transmission coefficient for these junctions. There is no signature of a strong destructive interference dip in these junctions in contrast with the destructive QI predicted by CARs. The transmission is slightly lower for *meta* connected junctions compared to *para* ones around DFT Fermi energy.
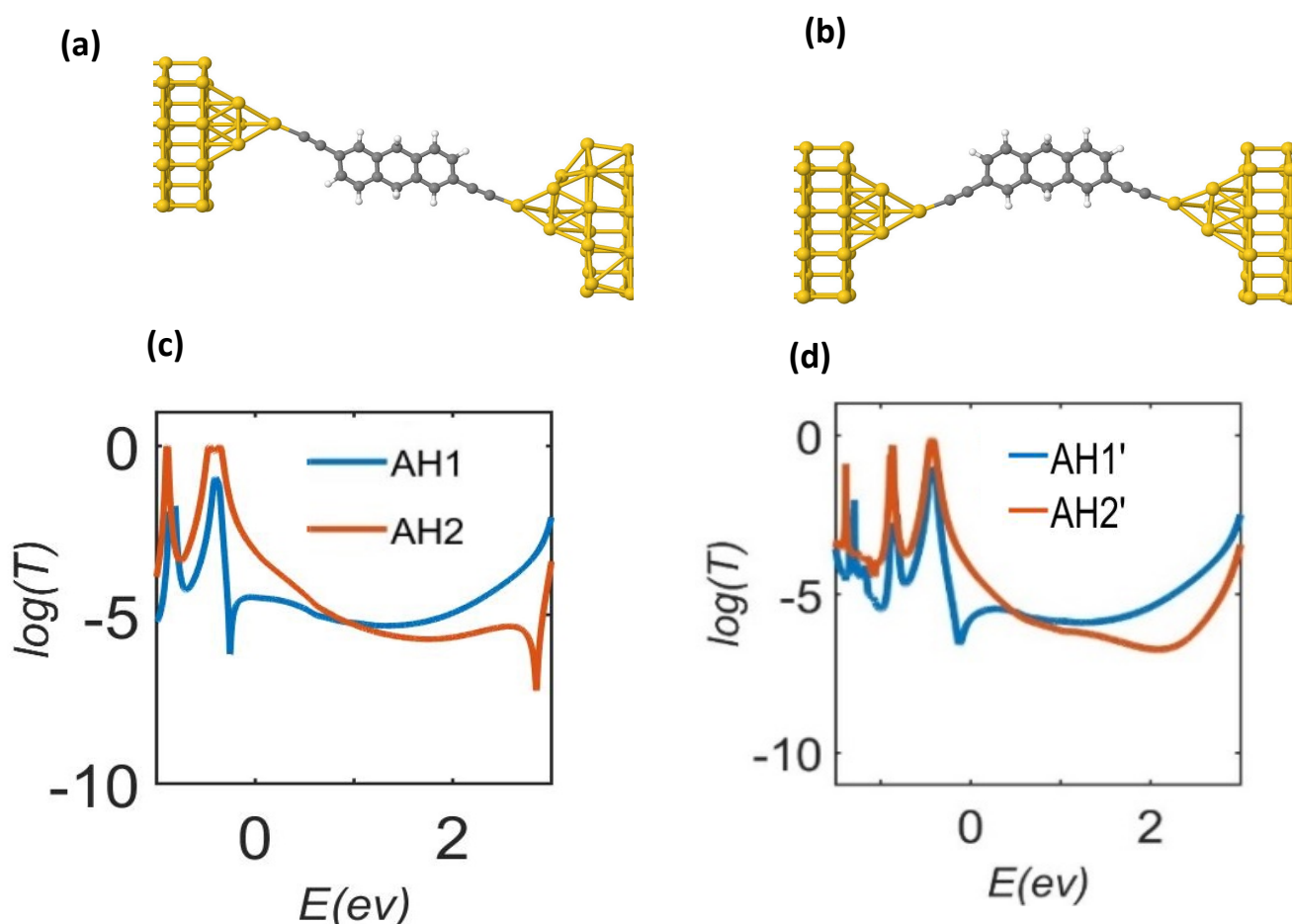
Figure 4.21. The transmission coefficient for the broken conjugation when connected to gold electrode via thiol (a) para connectivity (b)meta connectivity (c) for the dihydroanthracene (AH) (d) when the H of each carbonyl group is replaced by CH$_3$.

Replacing hydrogens with methyl groups does not change the overall trends although the magnitude of differences between *meta* and *para* connectivities is generally more pronounced (figs. 4.19d,4.20d and 4.21d).
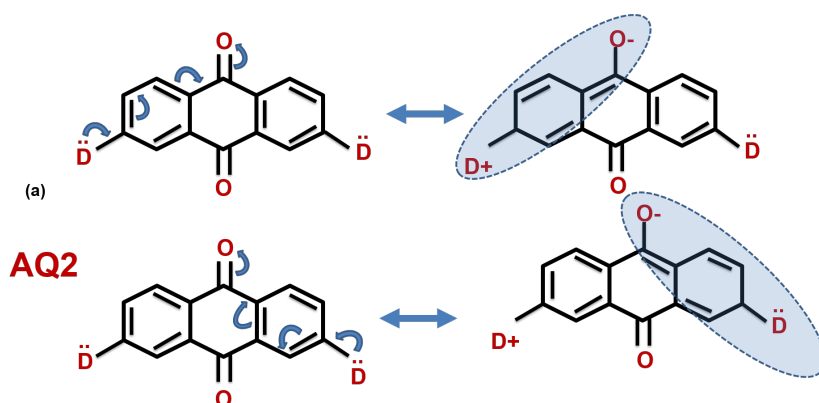
Figure 4.22. The modified curly arrow rule (CAR). (a) *meta* connected cross conjugated anthraquinone labelled byAQ2.

Figure(4.22) suggests that it should be possible to form a transport path through π-system from one electrode to the other, as indicated in figure (4.22). Essentially, if it is possible to form two equivalent pathways from different donors to same oxygen, this will lead to constructive interference, whereas this approach in not allowed in the case of para connectivity in which destructive interference is occurred.

4.3 Conclusions

In summary, I demonstrated that the charge transport of anthraquinone and its derivatives in different conjugation systems. DFT calculation reveals that a curly arrow rule is broken in the case of the cross conjugated molecule (anthraquinone). Confirmation that this rule is still broken when trying various of anchor groups with two different kinds of electrodes, shows that

this behaviour is a generic feature for anthraquinone. This behaviour originates from the evolution of the HOMO of dihydroxyanthracene into the LUMO of anthraquinone when removing of the hydrogen atoms from the OH groups of dihydroxyanthracene. The conductance of the junction increases by a couple of orders of magnitude due to the transition from constructive to destructive QI. This opens new avenues for realization of QI-based single-molecule switches. Curly arrow rules predict destructive QI for a *meta* connected anthraquinone core, whereas the first principle material specific calculation predicts constructive QI. This behaviour is independent of choice of electrode material or anchor groups and arises from the evolution of the HOMO of dihydroxyanthracene into the LUMO of anthraquinone upon removal of the Hs from the pendant OH groups of dihydroxyanthracene. This pushes the anti-resonance from the HOMO-LUMO gap of *meta*-connected dihydroxyanthracene into the LUMO-LUMO+1 gap of *meta*-connected anthraquinone. In addition, I find that the destructive interference predicted by curly arrow rules in broken conjugated dihydroanthracene is not apparent in DFT-based transport calculations. Although, curly arrow rules are widely used by chemists, material scientists and engineers and have been successful in predicting destructive QI in many molecular junctions, it is not valid in cross-conjugated anthraquinone with *meta* connectivities to electrodes

Bibliography:

[1]   S. V. Aradhya and L. Venkataraman, "Single-molecule junctions beyond electronic transport," *Nat. Nanotechnol.*, vol. 8, no. 6, pp. 399–410, 2013.

[2]   R. Baer and D. Neuhauser, "Phase coherent electronics: A molecular switch based on quantum interference," *J. Am. Chem. Soc.*, vol. 124, no. 16, pp. 4200–4201, 2002.

[3]   G. C. Solomon *et al.*, "Quantum interference in acyclic systems: Conductance of cross-conjugated molecules," *J. Am. Chem. Soc.*, vol. 130, no. 51, pp. 17301–17308, 2008.

[4]   T. Markussen, R. Stadler, and K. S. Thygesen, "The relation between structure and quantum interference in single molecule junctions," *Nano Lett.*, vol. 10, no. 10, pp. 4260–4265, 2010.

5]   2016 TA Su, M Neupane, ML Steigerwald, L Venkataraman… - Nature Reviews Materials, "Chemical principles of single-molecule electronics," *Nat. Rev. Mater.*, vol. 1, no. 3, p. 16002, 2016.

[6]   W. O. Kermack and R. Robinson, "LI. - An explanation of the property of induced polarity of atoms and an interpretation of the theory of partial valencies on an electronic basis," *J. Chem. Soc. Trans.*, vol. 121, pp. 427–440, 1922.

[7]   B. Sc and M. Sc, "QUANTUM THEORY OF ELECTRON TRANSPORT THROUGH PHOTO-SYTHETIC PORPHYRINS July 2017," no. July, 2017.

[8]   S. Sangtarash *et al.*, "Searching the Hearts of Graphene-like Molecules for Simplicity, Sensitivity, and Logic," *J. Am. Chem. Soc.*, vol. 137, no. 35, pp. 11425–11431, 2015.

[9]   H. Sadeghi, "Theory of electron, phonon and spin transport in nanoscale quantum devices," *Nanotechnology*, vol. 29, no. 37, 2018.

[10]   X. Liu *et al.*, "Gating of Quantum Interference in Molecular Junctions by Heteroatom Substitution," *Angew. Chemie - Int. Ed.*, vol. 56, no. 1, pp. 173–176, 2017.

[11]   C. M. Guédon, H. Valkenier, T. Markussen, K. S. Thygesen, J. C. Hummelen, and S. J. van der Molen, "Observation of quantum interference in molecular charge transport," *Nat. Nanotechnol.*, vol. 7, no. 5, pp. 305–309, 2012.

[12]   M. L. Perrin *et al.*, "Large negative differential conductance in single-molecule break junctions," *Nat. Nanotechnol.*, vol. 9, no. 10, pp. 830–834, 2014.

[13]   P. Moreno-García *et al.*, "Single-molecule conductance of functionalized oligoynes:

Length dependence and junction evolution," *J. Am. Chem. Soc.*, vol. 135, no. 33, pp. 12228–12240, 2013.

[14] Z. L. Cheng *et al.*, "In situ formation of highly conducting covalent Au-C contacts for single-molecule junctions," *Nat. Nanotechnol.*, vol. 6, no. 6, pp. 353–357, 2011.

[15] H. Sadeghi, S. Sangtarash, and C. Lambert, "Robust Molecular Anchoring to Graphene Electrodes," *Nano Lett.*, vol. 17, no. 8, pp. 4611–4618, 2017.

[16] J. Ferrer *et al.*, "GOLLUM: A next-generation simulation tool for electron, thermal and spin transport," *New J. Phys.*, vol. 16, 2014.

[17] T. Markussen, J. Schiötz, and K. S. Thygesen, "Electrochemical control of quantum interference in anthraquinone-based molecular switches," *J. Chem. Phys.*, vol. 132, no. 22, 2010.

[18] H. Valkenier, C. M. Guédon, T. Markussen, K. S. Thygesen, S. J. van der Molen, and J. C. Hummelen, "Cross-conjugation and quantum interference: a general correlation?," *Phys. Chem. Chem. Phys.*, vol. 16, no. 2, pp. 653–662, 2014.

[19] D. Fracasso, H. Valkenier, J. C. Hummelen, G. C. Solomon, and R. C. Chiechi, "Evidence for quantum interference in sams of arylethynylene thiolates in tunneling junctions with eutectic Ga-In (EGaIn) top-contacts," *J. Am. Chem. Soc.*, vol. 133, no. 24, pp. 9556–9563, 2011.

Chapter 5

Charge Transport in Photo-switchable Dimethyldihydropyrene Derivatives

5.1 Introduction

This chapter provides a detailed understanding of the electronic and transport properties of the photo-switchable dimethyldihydropyrene and its derivatives. Since, the conductance of a single molecule is sensitive to the change of the molecule structure, which in this case can be induced by light, it is crucial to understand how this behaviour is influenced by molecular orbitals. In this chapter, a theoretical model is proposed to extract additional information about the change in the electrical conductance and a tight binding model is developed to describe how the switch takes place. This model suggests that the low and high conductance of DHP in connectivity of (5,12)ON ,(2,9)ON and CPD in connectivity of (5,12)OFF , (2,9)OFF respectively are found to be a consequence of an energy level crossing between the HOMO-1 and HOMO , which occurs as the molecule, makes the transition between open and closed states.

The field of molecular electronics has received a significant attention over the past decades[1][2][3][4]. Molecular switches have been studied extensively due to their ability to switch between two states under external stimuli such as an electrical field or light[5][6][7][8]. This switchable behaviour is attractive in the field of electronics devices, and its applications. However, many challenges are still present on the road to improving functions towards useful electronic applications. Photochromic molecules, have been widely investigated in single-molecule junctions, such as dimethyldihydropyrene (DHP)/cyclophanediene (CPD) [9], [10], [10]–[14]. These molecules undergo changes in conductance and structure due to the significant effect on charge transport when irradiated. A variety of photo-switchable molecules have been widely used, due to their ability to be reversibly switched either photo chemically or thermally between two different conducting and non-conducting states [15][7] [16][5]. Various previous experimental works have investigated the properties of such photochromic molecules[17][18][19] [20].
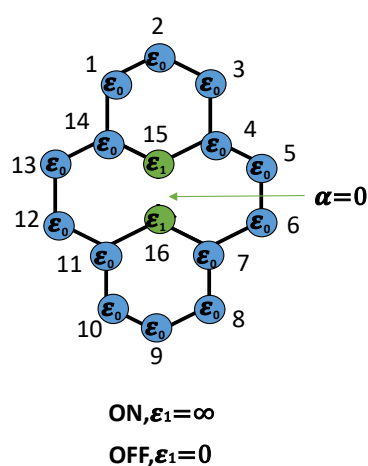
Figure. 5.1 Tight binding model of the switch. A numbering system for the core correspond to the connectivity (2,9) and connectivity (5,12) for ON state when $\varepsilon_1=\infty$ and OFF state when $\varepsilon_1=0$

To understand the origin of switching behaviour of DHP with connectivity of (5,12) and (2,9) as one changes from the open to the closed to the open structure, I shall first introduce a tight binding model, which allow us to follow the transition smoothly from one state to the other. Fig 5.1 shows the cores of DHP (corresponding to the 'on' state of the switch) and CDP (corresponding to the 'off' state of the switch). When the pyridyl anchors (not shown) are connected by single or triple bonds to the cores in (5,12) and (2,9). The notation used to refer to these molecules is summarised in Table 5.1. To model the evolution between the 'ON' state and 'OFF' state, we start from the simplest tight-binding model of a pyrene core, with 14 p_z orbitals labelled 1 to 14, in which each orbital is assigned a site energy of zero and a nearest neighbour hopping integral of -1.

Then to model the core, in which there are no p_z orbitals on atoms 15 and 16, we set their site energies to $\varepsilon_1=\infty$. (Note that when $\varepsilon_1 = \infty$ all properties of this model are independent of the bond α between sites 15 and 16.) To model the OFF state of the core, the hopping integral α connecting sites 15 and 16 is set to zero and the site energies of sites 15 and 16 are set to zero.

connectivity	State of switch
(5,12)	ON, $\varepsilon_1=\infty$
(5,12)	OFF, $\varepsilon_1=0$
(2,9)	ON, $\varepsilon_1=\infty$
(2,9)	OFF, $\varepsilon_1=0$

Table 5.1. Notation used to refer to different molecules and the values of the tight binding parameter ε_1 used to model the ON and OFF states.

Figure (5.2) shows how the frontier orbitals of this tight binding model evolve as a function of ε_1, starting with the 'parent' molecule at $\varepsilon_1 = 0$ and evolving to the frontier orbitals of the 'daughter' at large ε_1. Due to the asymmetric nature of the parental HOMO and LUMO about a line passing through sites 15 and 16, the perturbation due to ε_1 on sites 15 and 16 does not couple to the HOMO and LUMO.
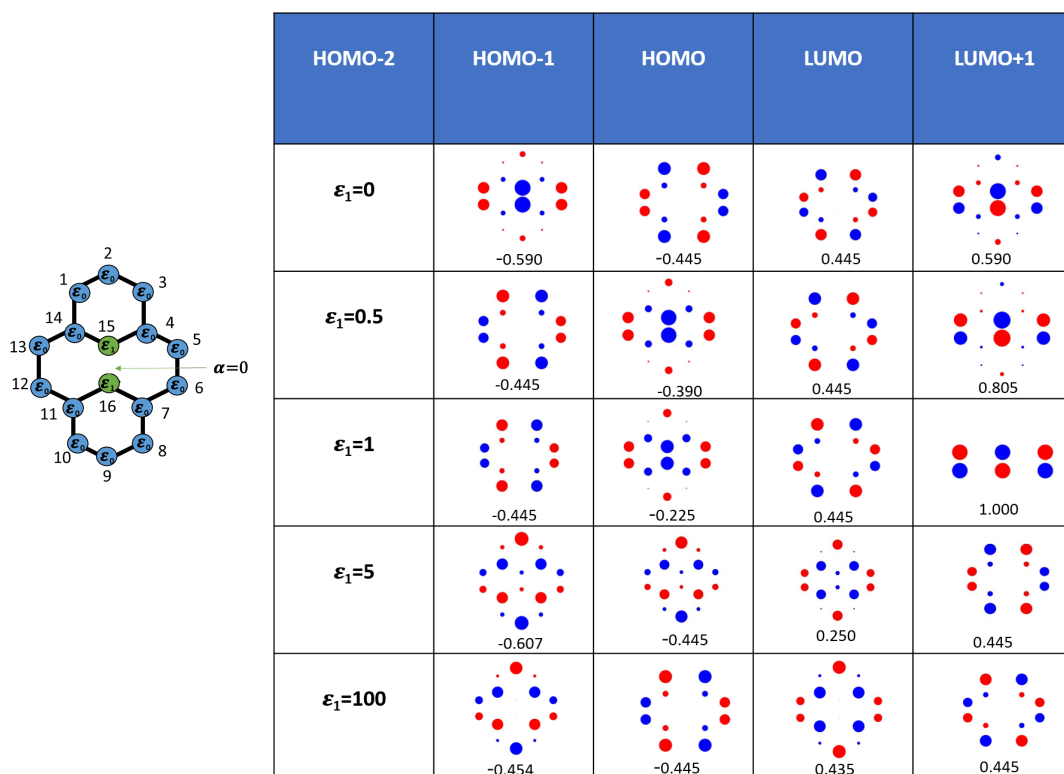
Figure 5.2. Frontier orbitals of the tight binding model for various values

Figure (5.3) shows the corresponding transmission coefficients obtained when one-dimensional tight binding chains are weakly coupled to sites (5,12) or (2,9). For the (5,12) connectivity, the transmission resonances associated with the parental HOMO and LUMO are indicated by vertical dashed lines. As noted above, since these molecular orbitals have no weight on sites 15 and 16, they are insensitive to the value of ε_1. On the other hand, as shown in figure (5. 2), the parental LUMO+1, HOMO-1 and HOMO-2 have a non-zero

weight on sites 15 and 16 and therefore as ε_1 increases from zero, the energies of these

orbitals increase. As indicated by the black arrows, this causes the parental HOMO-1 to cross

the parental HOMO and evolve into the HOMO of the daughter, eventually becoming

degenerate with the parental LUMO. At the same time, as indicated by the red arrows, the

parental HOMO-2 increases in energy and eventually becomes degenerate with the parental

HOMO. This degeneracy occurs, because for $\varepsilon_1 = \infty$ the daughter molecule is equivalent to

a ring of 14 sites with periodic boundary conditions, whose energy levels are given by $E =$

$-2\cos\frac{2\pi n}{14}$, $n = 0, \pm 1, \pm 3, \pm 4, \pm 5, \pm 7, \pm 8, 9$. Figure (5.3) (lower panels) shows that the

same behaviour of the HOMO-2, HOMO-1 and LUMO+1 also occurs for (2,9) connectivity.

However, in this case, the HOMO and LUMO are 'silent.' In they do not couple to the

external leads and do not create a resonance in the transmission coefficient.
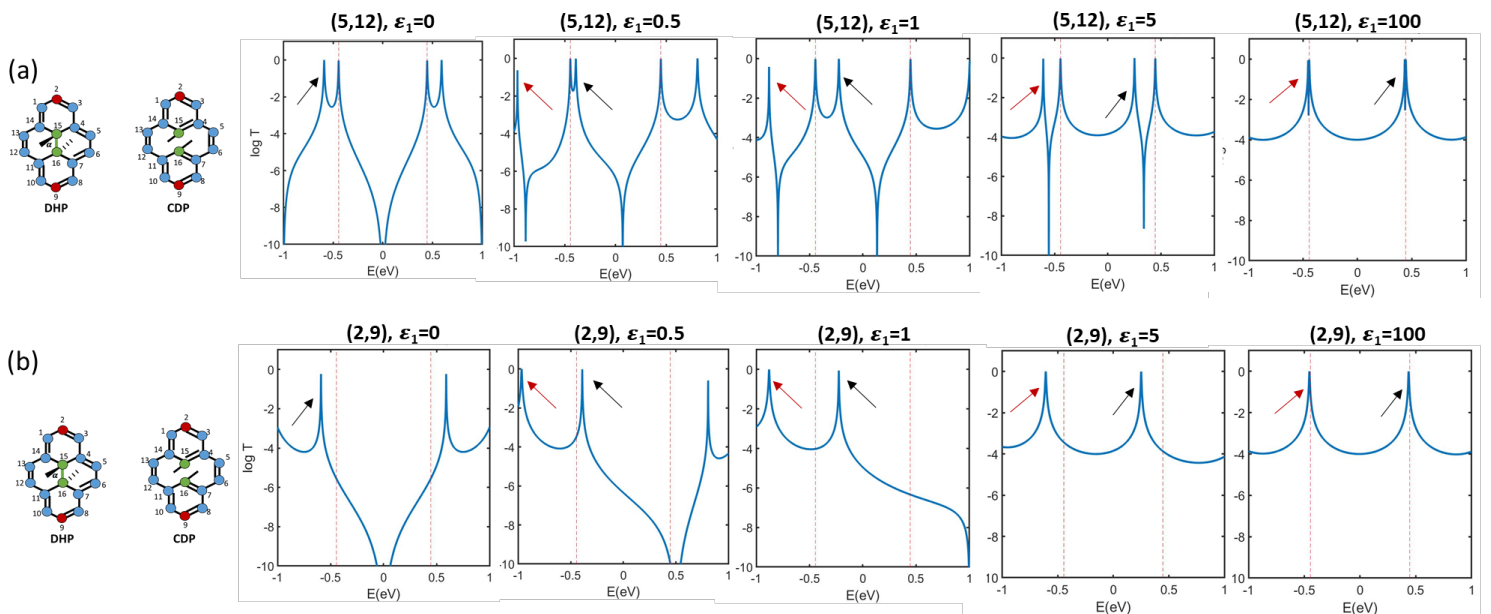
Figure (5.3) Evolution of the (5,12) and (2,9) transmission coefficients as ϵ_1 increased from zero to 100, where the latter value is in effect infinity, since no significant change is found for higher values of ϵ_1.

The magic ratio rule based on the magic numbers(M_{ij}) in figure (5.4), which predict electrical conductance corresponding to different connectivities of polyaromatic hydrocarbons (PAHs), in the co-tunnelling regime. When a single molecule is weakly connected to the electrodes via sites (i) and(j), electrons passing through the molecule from one electrode to the other.

To obtain the table of magic numbers (also known as a M-table) shown in figure 5.4, first construct a connectivity table for the core molecule by placing a (1) when two sites are connected and zero otherwise. Then the M-table is obtained by taking the inverse of the connectivity table and multiplying by the determinant. The transmission of the core is connectivity dependent and can be calculated from the magic number associated with each connectivity. This rule states that the conductance ratio of two molecules is equal to the square of the ratio of their magic integers [21].

Interestingly, at $\varepsilon_1 = 0$, the transmission coefficients of the parents, for both connectivities, exhibit destructive quantum interference (DQI) at the gap centre. This is predicted from the 'magic number table' for the parental core, shown in figure (5.4), which contains zeros at elements $M_{5,12}$ and $M_{2,9}$.

$M_{i,j}$	2	4	6	8	10	12	14	16
1	-1	1	-1	1	-1	1	-1	0
3	-1	-1	1	-1	1	-1	1	0
5	0	0	-2	1	-1	0	0	1
7	0	0	0	-1	1	0	0	-1
9	0	0	0	-1	-1	0	0	1
11	0	0	0	1	-1	0	0	-1
13	0	0	0	-1	1	-2	0	1
15	1	-1	1	0	0	1	-1	-1

Figure 5.4 An example of the bipartite pyrene lattice together with its M-Table

5.2 Results and Discussion

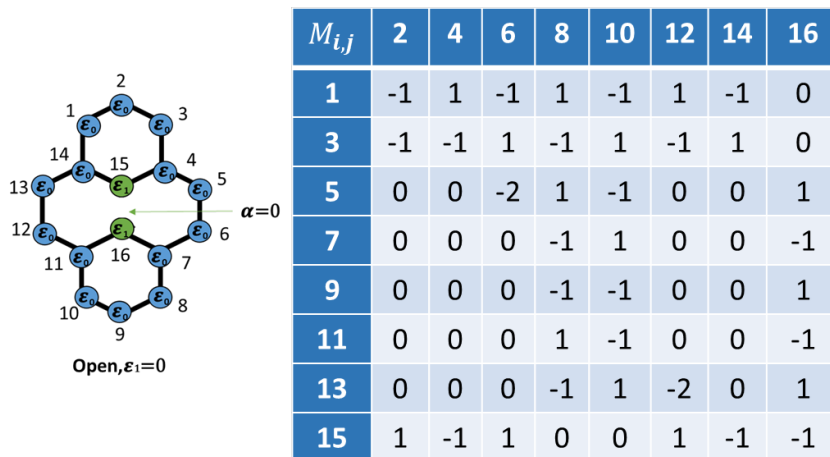To demonstrate how the swap occurs in the symmetry between the molecular orbital of HOMO and HOMO-1 taken place, I used DFT to optimize the geometry and he ground state Hamiltonian with overlap matrix elements of each structure combined with the quantum transport code Gollum to compute the transmission coeffienet of the system. Siesta employs psudo-potential to account for the core electrons and linear combination of atomic orbital to construct the valence states. The generalized gradient approximation (GGA) of the exchange and correlation functional is used with the parameterization (PBE), a double-ζ plus polarized (DZP) basis set and a real-space grid was defined with an equivalent energy cutoff of 150 Ry. The geometry of each structure was relaxed to a force tolerance of 20 meV/Å. The above analysis leads us to identify a new concept for molecular switching, based on changing the relative symmetry of the HOMO and LUMO due to level crossing during the switch transition. When this symmetry change takes place, quantum interference within the HOMO-LUMO gap changes from being destructive to constructive, leading to a large change in electrical conductance.

This level crossing is a consequence of the different symmetries of frontier orbitals For example, as shown in figure(5.2), when atoms 15 and 16 are perturbed by$\varepsilon_1 = 0.5$, the HOMO is found to cross the HOMO-1 , because the perturbation affects differently the HOMO and HOMO-1. In the case of open state when $\varepsilon_1 = 0$, it is noted that HOMO-1 is symmetric which means it is going to be affected by the perturbation ε_1 significantly more than the antisymmetric HOMO figure (5.2). Which means this switch is governed by this change in the molecular orbitals.

More importantly, a simple model of tight binding could explain the difference in transmission coefficient between the ON and OFF states. In which this difference is independent of the connectivities between (5,12), (2,9)for the ON state, and (5,12) (2,9) for the OFF state and only

depends on the behaviour of molecular orbital states in these molecules. To understand the significance of switching the relative symmetries of the HOMO and LUMO, a molecular orbital rule has been used to investigate the transport properties for both connectivities.

To confirm the above behaviour, I have carried out detailed DFT modelling of these molecules the properties of these molecules was examined using DFT. I investigated the switchable molecule dimethyldihydropyrene(DHP) ON state /cyclophanediene (CPD) (OFF state) with their distinguishable conducting features with two connectivities (2,9) and (5,12) when the only difference between the two connectivities is in the attachment of a series of alkyls as pendant group. These pendant groups do not expect to be chemically reactive, but only change the geometry.
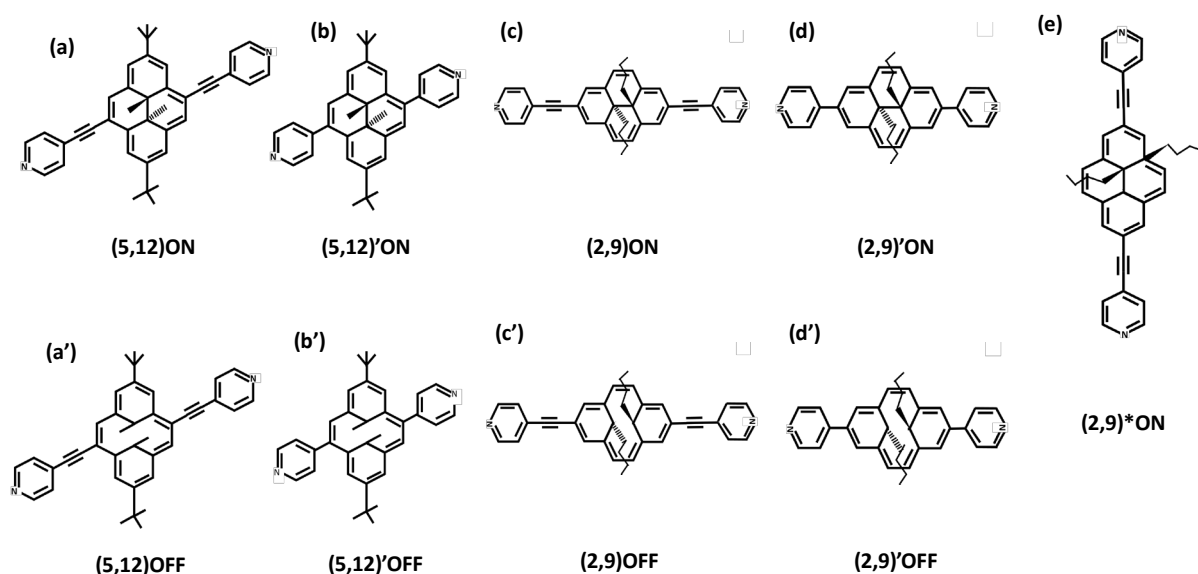
Figure 5.5. The structure of five systems with two connectivities connected to pyridine anchor group for all structures(a) (5,12) ON state with acetylene spacer(b) ON state (5,12)' without acetylene spacer (c) (2,9) ON state with acetylene spacer. (d) (2,9)' ON state without acetylene spacer. When (a') (b') (c') (d') same systems with OFF states. (e)ON state (2,9)* with same connectivity as (c)but with different connection in the internal part of the core with chain of CH3.

In fact, these calculations are computed with these molecules when they linked to bipyridine as anchor groups in the presence of the acetylene spacer in one case and in the absence of that space in another case for both connectivities as shown in figure (5.5). These molecules covalently bond to gold electrodes to provide robust connection to the molecular junction[22]

Switching properties of dimethyldihydropyrene derivatives, were first reported by Boekelheide et al , who demonstrated that they can be opened to the colourless cyclophanediene (CPD)OFF under irradiation by visible light[18]and then switched back to (DHP)ON when subjected the heat or UV light. Recent theoretical studies have shown that these molecules possess robust photo-switchable behaviour when embedded between two gold electrodes[23], [24][25][26]. One positive advantage of this behaviour is that it leads to a dramatic change in the conductance, which make these molecules good candidates to design effective electronic devices. Until recently, there has been no reliable investigation showing how effectively molecular orbitals can play a role to switch between the two states. Our aim now is to elucidate the appearance of these states using DFT to support the above TB calculation, in order to provide a microscopic explanation of this feature. Here, Dimethyldihydropyrene with connectivity (5,12) and (2,9) and its derivatives studied when they contacted to a gold electrodes via bipyridine as anchor group either directly or via an acetylene spacer in which bipyridine enables stable junction and better junction formation [27][28]. This study is to assess the influence of the acetylene spacers to know the impact of removing this spacer on

the conductance in both connectivities. Which have a significant effect on the photo-switch function of these molecules.

Fig. 5.6. DFT-based transmission calculations. (a) The molecular junction containing (5,12) ON with acetylene (b) (5,12)OFF with acetylene (b) Transmission as a function of energy for the ON (blue) the OFF molecule (red).

To analyse the switch mechanism, the electronic transport of the ON states for a various switchable molecule (5,12) and (2,9) were calculated with the corresponding OFF states of same connectivity as shown in figure (5.1). Then plotted the calculated transmission function of the (5,12) and (2,9) ON states and their OFF states in figures (5.6 and 5.7).

A higher transmission probability was found for (5,12) and (2,9) in ON state compared to (5,12) and (2,9) in OFF state by about two orders of magnitude. This result is confirmed experimentally for the case of (5,12)ON and OFF state in the literature[10].

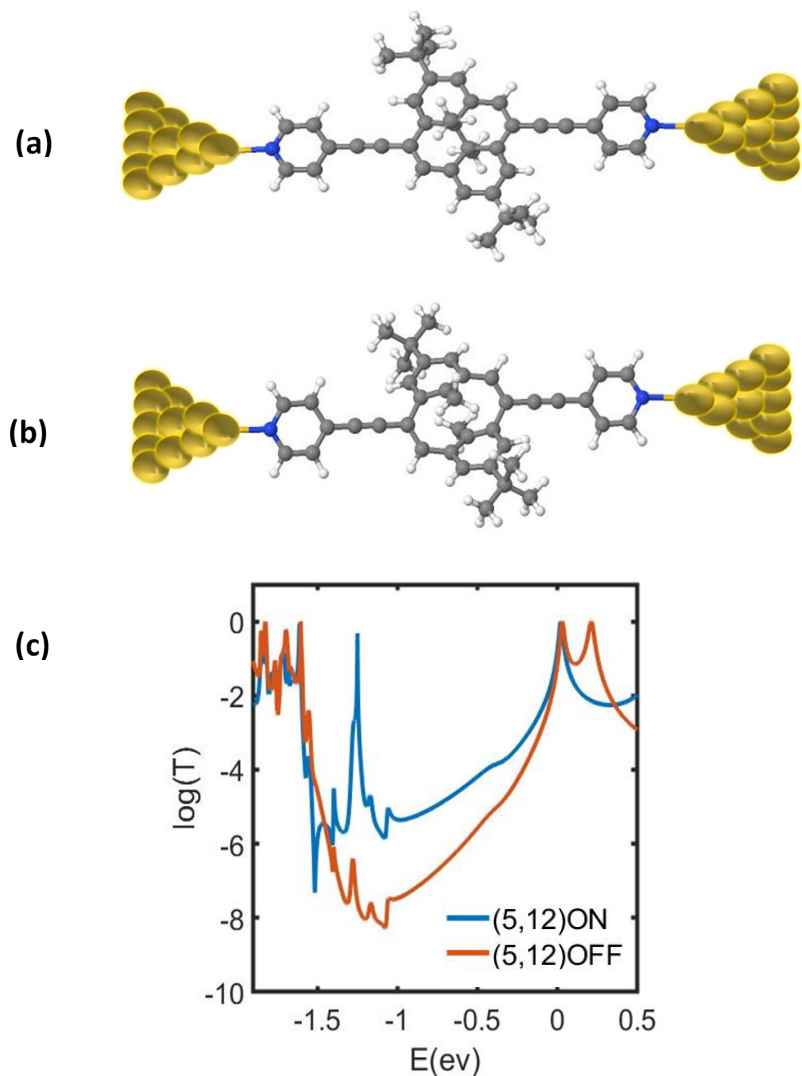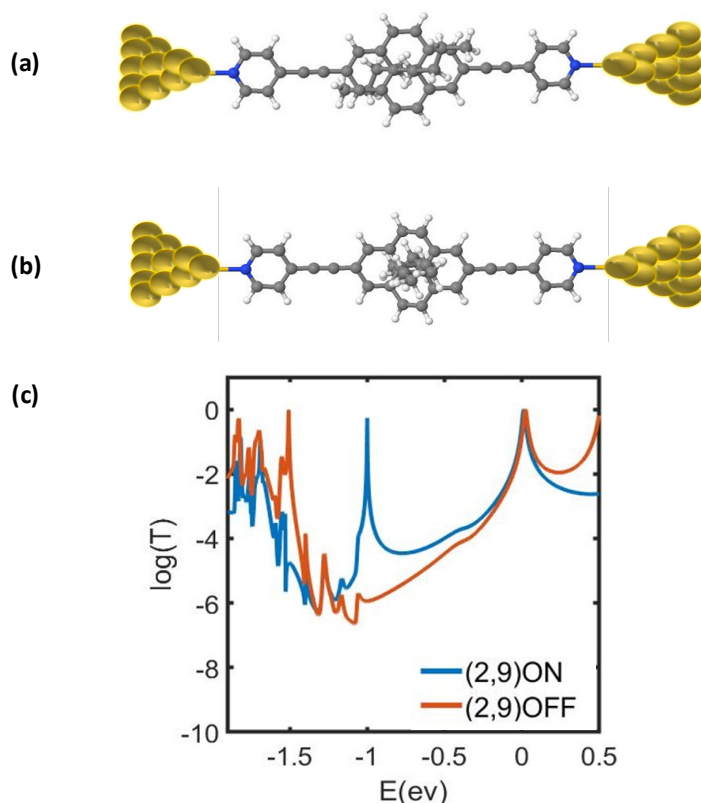**Fig. 5.7. DFT-based transmission calculations. (a) The molecular junction containing (2,9) ON with acetylene (b) (2,9)OFF with acetylene (c) Transmission as a function of energy for the ON (blue) the OFF molecule (red).**

This finding can be explained due to the extended pi-conjugation across the whole junction in (5,12) ON, whereas some of the conjugation is broken in the case of (5,12) OFF.

In the following, two different pi-conjugated molecules were evaluated (2,9) ON and (2,9) OFF with same anchor when the spacer is included figure (5.7a) and (5.7b). As I introduce the spacer, this makes the conjugation extended all over the junction, when both molecules are ON and OFF. The transport through the ON state is dominated by a fully conjugated system, whereas some of conjugation are missing in the OFF state. The calculated transmission

function for the (2,9)ON and (2,9)OFF using DFT is presented in Figure (5.7c), which shows a higher value of transmission coefficient for the ON case compare to the OFF, as expected with smaller HOHO-LUMO gap in both (5,12)ON and (2,9)ON. To examine the possibility of these molecules to switch or not, in the case where the acetylene is presented in both states.

I have applied electric field, which cause molecules to respond and make some changes in the configuration in order to induce the cleavage and thereby switch the state. An external electric field is applied correspond to different electric fields, ranging from 0.1 to 1 V/A^0 to the isolated molecules (5,12) ON and (5,12) OFF along the transport direction (z).
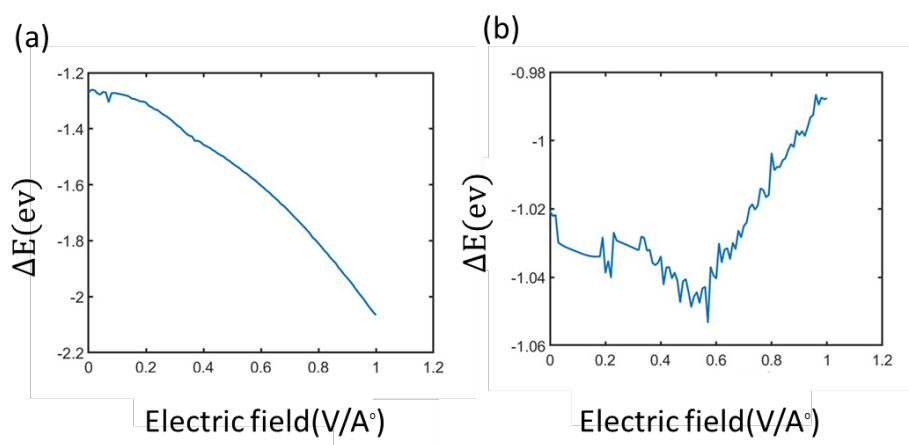
5.8. The resulting energy difference between ON and OFF states (ΔE) vs Electric field in (5, 12) connectivity when (a) the acetylene is presented (b) acetylene not presented.

I calculate the total energy for (5,12) ON and (5,12) OFF when the acetylene spacer is included and take the difference between them which is (ΔE) in the presence of the electric field using different values of electric field as in figure (5.8a). Subsequently, this calculation indicates that switch behaviour is not possible. I attributed the failure in switching the closed state due to the presence of spacer, which play an essential role in this behaviour. Acetylene make the π orbitals extended all over the junction and make it harder to switch between two states. Therefore, I

have removed the spacer acetylene to study how important does the absence of this space play a role to affect the conductance. Also, test whether or not these molecules with different connectivities (2,9) and (5,12) in this geometry are possible to be open. The absence of this space introduces a ring rotation for the pyridine relative to the π system of the core as shown in figure (5.9-10).
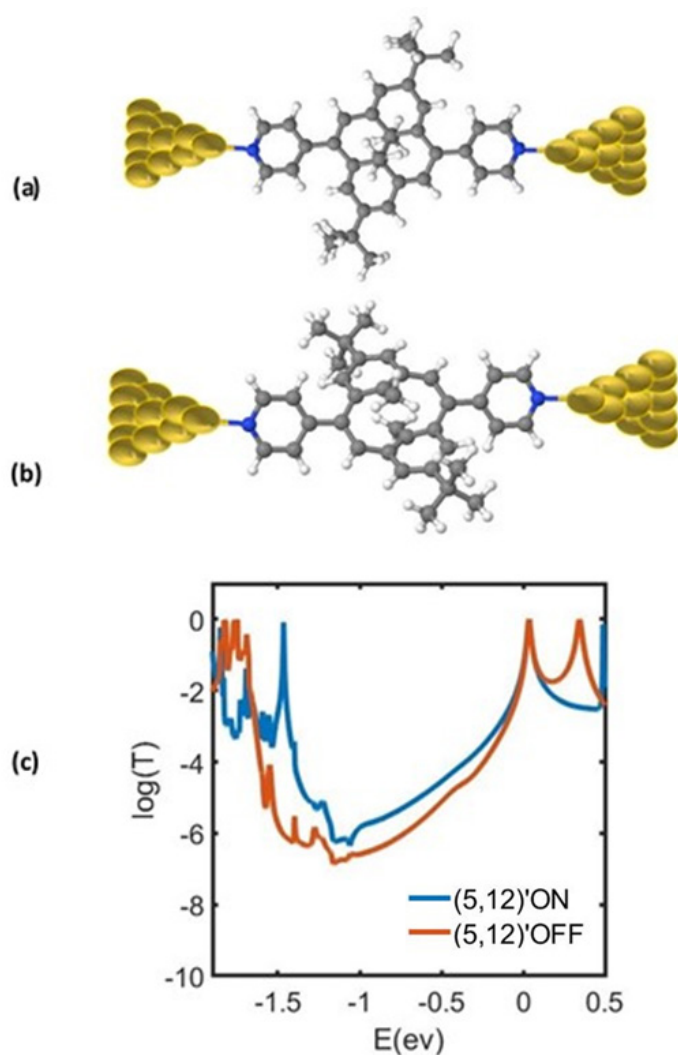

Fig. 5.9. DFT-based transmission calculations. (a) The molecular junction containing (5,12)'ON without acetylene (b) (5,12)'OFF without acetylene (c) Transmission as a function of energy for the ON (blue) and the OFF molecule (red).

Toward this goal, I constructed these molecules without the acetylene spacer as shown in figures (5.4 b, b, d, d'). In contrast, attaching the (5,12)'ON and (5,12)'OFF to the bipyridine without the acetylene spacer figure (5.9). Obviously, this caused a decrease in the difference between the ON and OFF state in which this difference is less than one order of magnitude, where this was not the case in the present of the spacer. This result demonstrated that a change in π-conjugation could affect the conductance of the molecule in the absence of the acetylene spacer due to π-system of ON state orthogonal to π-system in the spacer with dihedral angle which is the angle formed by the planes of the pyridine and Dimethyldihydropyrene derivatives $\phi= (41.1^0,-42.3^0)$for right and left side respectively compare to the presence of acetylene with $\phi= (-3.7^0,5.8^0)$ in closed system. In the OFF system I found that $\phi = (-13.5^0,2^0)$ compare to $\phi = (-32.1^0,25.3^0)$ when the acetylene not present in OFF system.
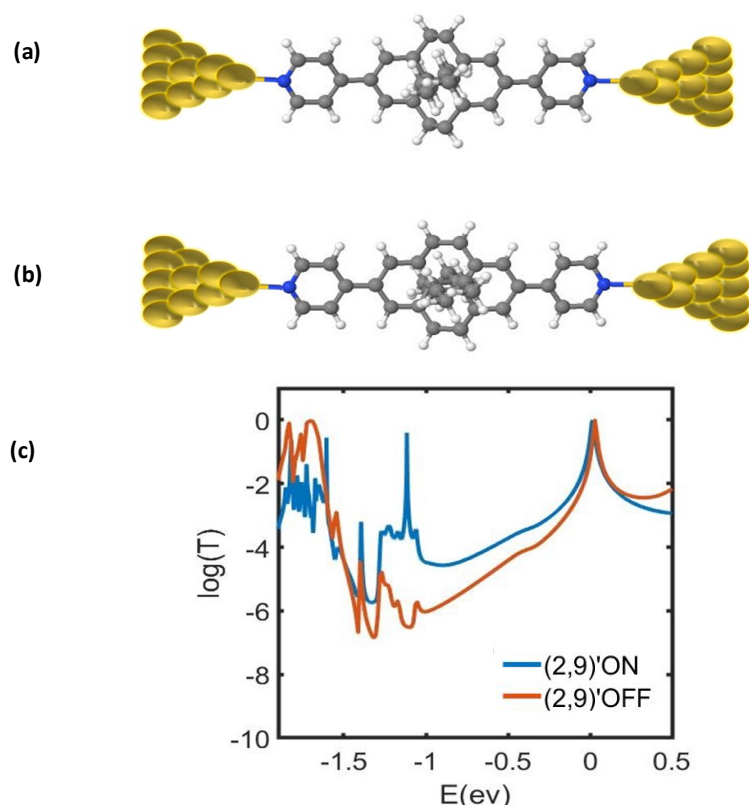

Fig. 5.10. DFT-based transmission calculations. (a) The molecular junction containing (2,9)'ON without acetylene (b) (2,9)'OFF without acetylene (c) Transmission as a function of energy for the ON (blue) and the OFF molecule (red).

A second approach in addition to the previous molecules are systems with bridging to bipyridine from both sides without the acetylene linker in ON system (2,9)' and (2,9)'OFF. On the contrary, the acetylene spacer unlike the (5,12)'ON and (5,12)'OFF has not affected the difference of transmission coefficient between (2,9)'ON and its OFF state as in figure (5.10). In addition, transmission curve for (2,9)'ON is almost same as (2,9) ON in the absence of the spacer as shown in figure (5.11). In terms of dihedral angle which is the angle formed by the planes of the pyridine and Dimethyldihydropyrene derivatives in (2,9) for the ON system when acetylene is included= $(2.5^0, 2.6^0)$ compare to $\phi = (12.1.5^0, 13.6^0)$ when acetylene is absent. Whereas (2,9) OFF is $\phi = (1.7^0, 2.2^0)$ in contrary to $\phi = (-23.7^0, 28.2^0)$ in (2,9)'OFF when acetylene not included.

Fig. 5.11. DFT-based transmission calculations. Transmission as a function of energy for the closed (5,12)'ON (blue) (2,9)'ON (yellow)and the (5,12)'OFF in (red), (2,9)'OFF (purple) in solid lines. The dashed lines represent the same molecules in the present of the acetylene spacer.

Thereby, these results indicate that the difference between ON and OFF is enhanced by the absence of the acetylene for (5,12) connectivity compare to (2,9) ON and OFF as shows in

figure (5.11). The apparent difference in the transmission curve has been attributed to the spacer acetylene, which leads to shrink in the HOMO-LUMO gap when acetylene is presented.

To enable a more precise comparison between the (5,12)and (2,9) in ON state to (5,12)and (2,9)OFF state, I have calculated the transmission spectra when acetylene is presented and with exactly same internal core in these different connectivities, in order to gain a deeper insight about the switching effect and the connectivities dependence. Figure (5.12) shows that the difference in the transmission coefficient was found to be sensitive to the connectivity especially for the OFF state and this is supported as well by the tight binding model as in figure(5.3).
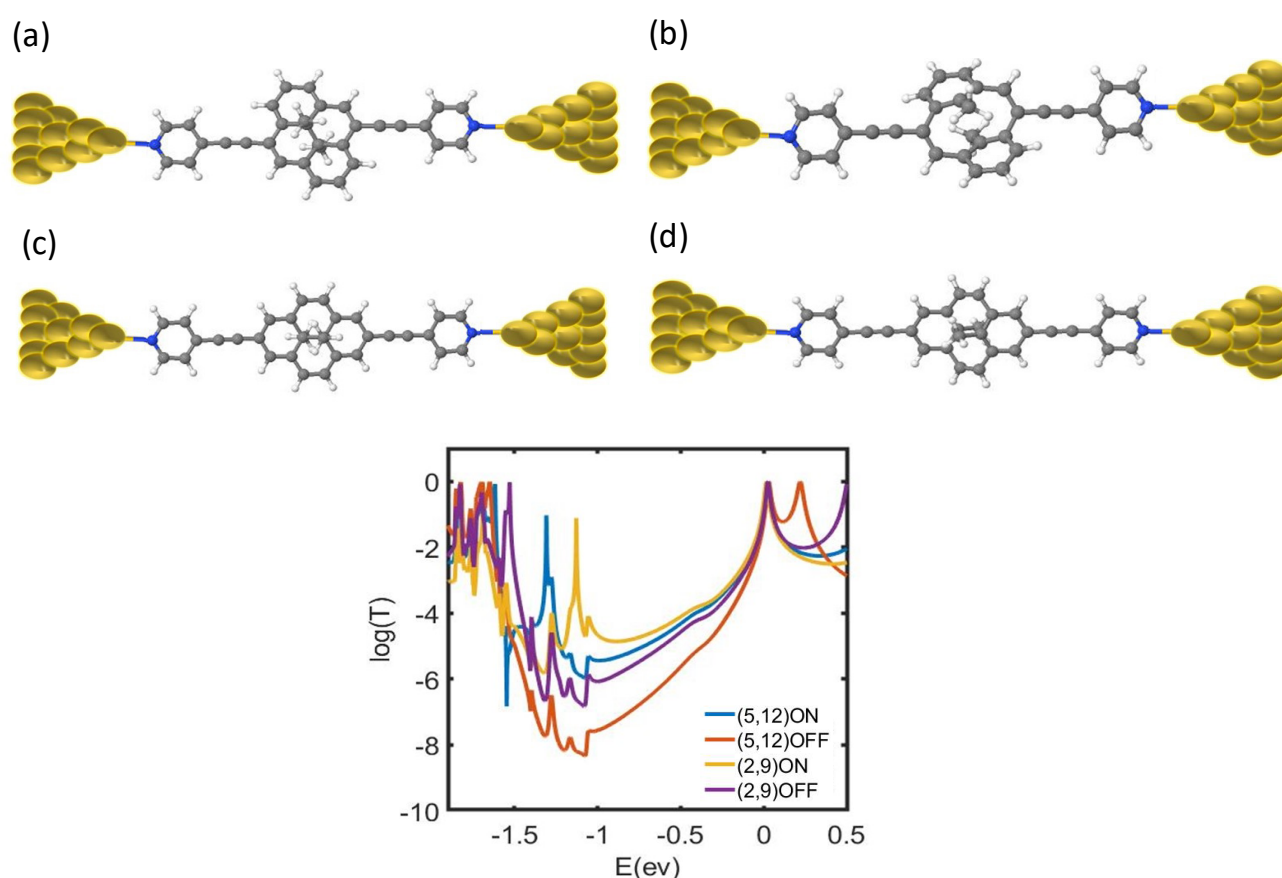
Fig. 5.12. DFT-based transmission calculations. Transmission as a function of energy for (a) (5,12)ON(blue) ,(b) (5,12)OFF in (red), (c)(2,9)ON(yellow)and(d) (2,9)OFF(purple) when having same internal part in the core and remove alkyls from the sides of (5,12).
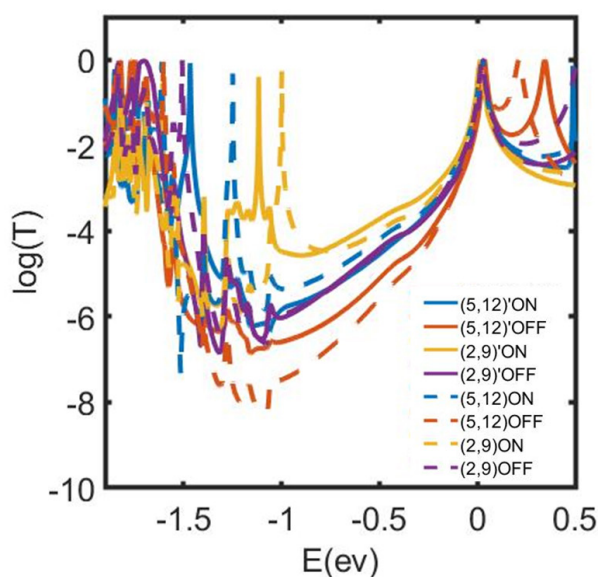
Fig. 5.13. DFT-based transmission calculations. Transmission as a function of energy for the closed (2,9)*ON (blue) (2,9)ON (red).

In addition, the transmission coefficient was calculated for (2,9)* ON in same position (2,9) but with different connection in the internal part of the core with chain of CH3. It is expected that this molecule yields the same transmission as the previous (2,9) ON due to the weak effect of CH3. It is worth noting that methyl groups usually have a weak effect on the conductance, but this is not the case here as shown in figure (5.13). To test the effect of methyl group, another electron transport calculation was performed on (2,9)*ON after removing this group and replacing it by hydrogens. It should be noted that the transmission is significantly increased

compare to the case when the methyl group presents. This higher transmission coefficient arises

due to the presence of this group and prove the significant role of this group in figure (5.14).

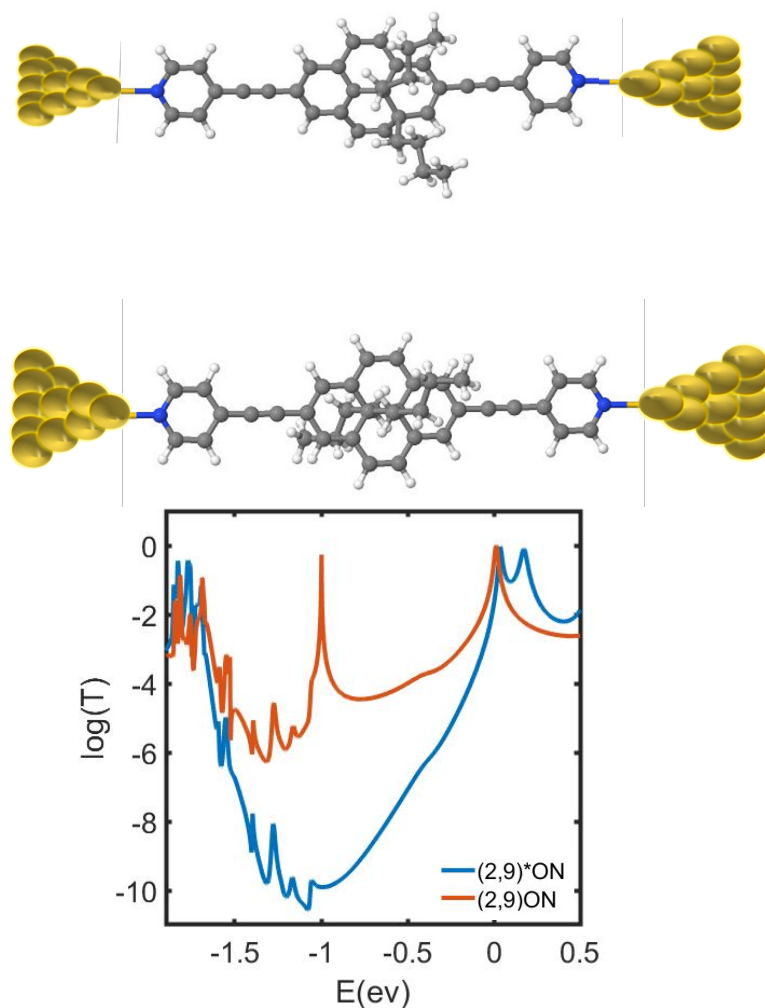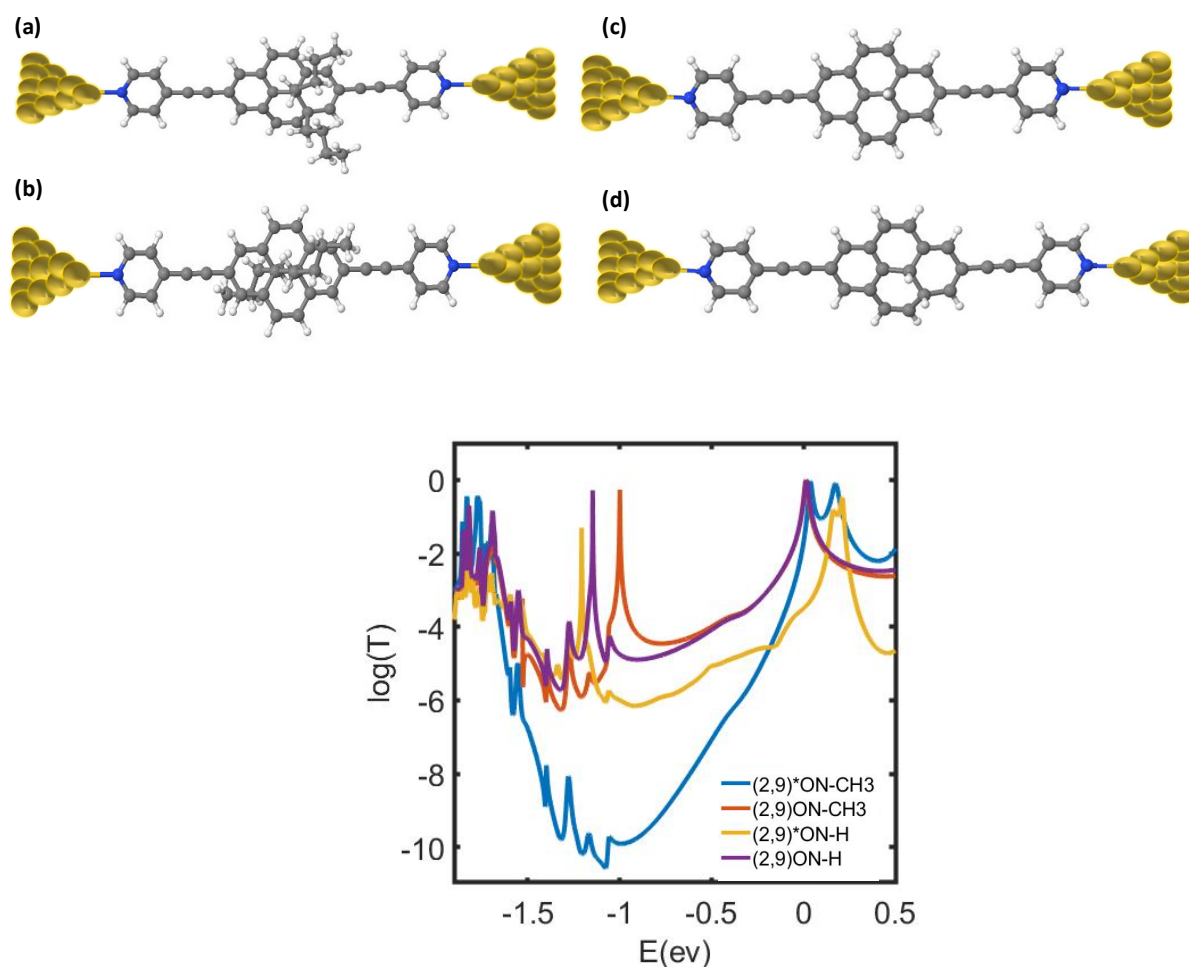**Fig. 5.14. DFT-based transmission calculations. Transmission as a function of energy for the closed (2,9)*ON with CH3 (blue) (2,9)ON with CH3 (red), whereas (2,9)*ON with H is (yellow) and (2,9)ON with H is (purple).**

This switch behaviour is verified not only by TB calculations, but also by DFT. For ON states

both DFT and TB exhibit a constructive interference with high conductance, which means the

DFT results agreed well with the simple concept that was captured by the tight binding model.

In the OFF state, both calculations are also similar, showing that a destructive interference in

the case of TB whereas DFT shows a lower constructive interference compare to the ON state.

This more pronounced DQI behaviour in the TB model is due to the neglect of σ-orbital

contributions in the transport calculation. Inspection of the molecular orbitals in (5,12) ON and (2,9) ON shows that almost all orbitals are well extended across the backbone in figure (5.15), except the L+1 in the triple case is localized compare to the single case figures (5.16).

Fig. 5.15. Molecular orbitals when the acetylene spacer presents in (5,12) ON, (2,9) ON and their OFF states.

Fig. 5.16. Molecular orbitals when the acetylene spacer is absent in (5,12)ON , (2,9)ON and their OFF states

Moreover, in the H-2 for the (5,12) ON, the weight is localized in the pyridines from both sides, whereas with the triple bond it is concentrated in one side only. It 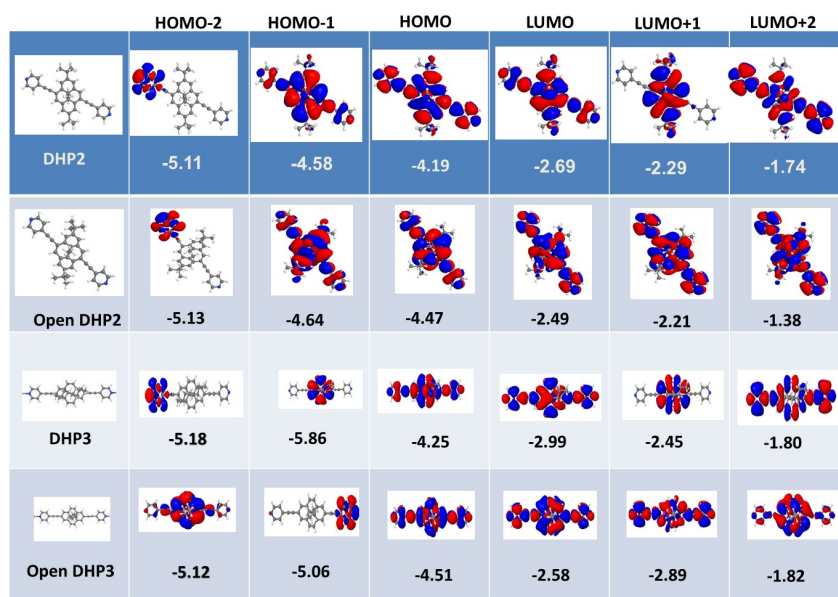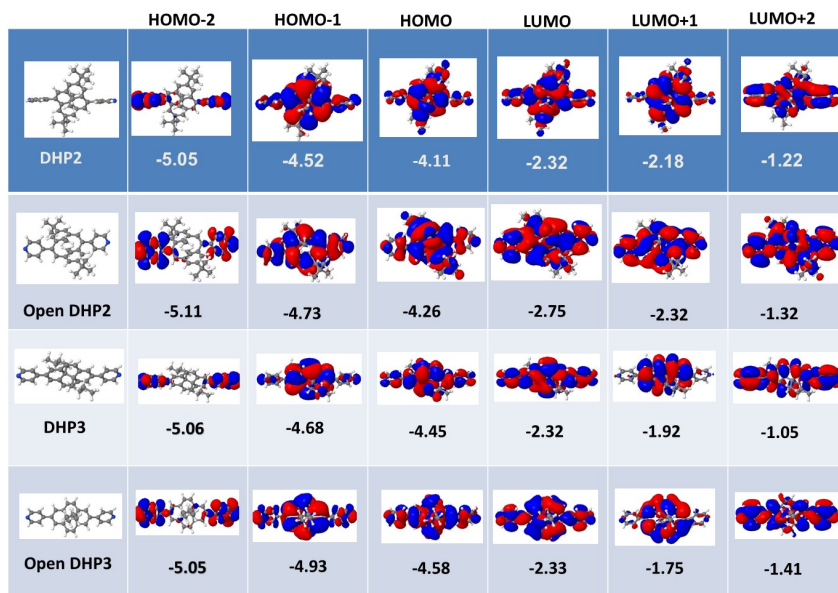is worth mentioning that the pyridine ring is highly twisted due to the absence of the spacer in (5,12) ON compare to (2,9) ON. This effect means that the (2,9) ON transmission coefficient as a function of energy has a smaller difference when spacer is present and without it.

Molecule in (5,12)	Dihedral angle	Molecule in (2,9)	Dihedral angle
DHP2	$\phi = (-3.7^0, 5.8^0)$	DHP3	$\phi = (2.5^0, 2.6^0)$
DHP2'	$\phi = (41.1.5^0, -42.3^0)$	DHP3'	$\phi = (-12.1^0, 13.6^0)$
CPD2	$\phi = (-13.2^0, 2^0)$	CPD3	$\phi = (1.7^0, 2.2^0)$
CPD2'	$\phi = (-32.1^0, 25.3^0)$	CPD3'	$\phi = (-23.7^0, 28.2^0)$

Figure (5.17) shows different dihedral angle formed by the planes of the pyridine and Dimethyldihydropyrene derivatives in the case of single and triple bond in (5,12), (2,9) ON and (5,12),(2,9)OFF

Furthermore, the relaxed configuration in (2,9) ON when the spacer presents and without it shows a slight change in the geometry compare to the geometry change of (5,12) ON in the present of the spacer, which is significantly affected when the acetylene not presented. These changes reflect in the molecular orbitals of the core and the pyridine. Thus, the transmission curve shows in both cases of (2,9) ON and (2,9)'ON for single and triple bonds almost the same value compare to the effect in (5,12) ON and (5,12)'ON for single and triple bond.

5.3 Conclusions

In summary, a study in dimethyldihydropyrene (DHP)ON state and cyclophanediene (CPD) OFF state in different connectivities. It highlights the role of perturbation theory in these switchable molecules when a swap occurs in the symmetry between the molecular orbital of HOMO and HOMO-1 taken place. Moreover, this switch from OFF state to ON state does not create new orbitals; it is merely a change of the molecular orbital ordering.

I performed a theoretical study for ON state and OFF state in different connectivities. I presented a detailed calculation analysis of the conducting (5,12) and (2,9) when it switched to the non-conducting state with same connectivities. A direct correlation of electronic structure and transport properties of ON and OFF molecules was found by using perturbation theory, in which this perturbation can be captured in a simple tight binding model of the switch behaviour. This perturbation causes a swap between the molecular orbitals in HOMO-1 and HOMO switching them from asymmetric and symmetry in open state to symmetric and asymmetric ON state. Furthermore, the influence of the acetylene spacer, can promote the conductance difference in (5,12) but not in (2,9).

Bibliography

[1]   2016 TA Su, M Neupane, ML Steigerwald, L Venkataraman… - Nature Reviews Materials, "Chemical principles of single-molecule electronics," *Nat. Rev. Mater.*, vol. 1, no. 3, p. 16002, 2016.

[2]   N. Xin *et al.*, "Concepts in the design and engineering of single-molecule electronic devices," *Nat. Rev. Phys.*, vol. 1, no. 3, pp. 211–230, 2019.

[3]   M. Ratner, "A brief history of molecular electronics," *Nat. Nanotechnol.*, vol. 8, no. 6, pp. 378–381, 2013.

[4]   S. V. Aradhya and L. Venkataraman, "Single-molecule junctions beyond electronic transport," *Nat. Nanotechnol.*, vol. 8, no. 6, pp. 399–410, 2013.

[5]   Z. Liu, S. Ren, and X. Guo, "Switching Effects in Molecular Electronic Devices," *Top. Curr. Chem.*, vol. 375, no. 3, pp. 1–33, 2017.

[6]   J. L. Zhang *et al.*, "Towards single molecule switches," *Chem. Soc. Rev.*, vol. 44, no. 10, pp. 2998–3022, 2015.

[7]   S. Jan Van Der Molen and P. Liljeroth, "Charge transport through molecular switches," *J. Phys. Condens. Matter*, vol. 22, no. 13, 2010.

[8]   M. A. Ratner *et al.*, "Organic-based molecular switches for molecular electronics," *J. Am. Chem. Soc.*, vol. 8, no. 3, pp. 4003–4014, 2014.

[9]   Y. Tsuji and R. Hoffmann, "Frontier orbital control of molecular conductance and its switching," *Angew. Chemie - Int. Ed.*, vol. 53, no. 16, pp. 4093–4097, 2014.

[10]   D. Roldan *et al.*, "Charge transport in photoswitchable dimethyldihydropyrene-type single-molecule junctions," *J. Am. Chem. Soc.*, vol. 135, no. 16, pp. 5974–5977, 2013.

[11]   S. G. Robinson, "The Synthesis of Oligothiophene Functionalized Dimethyldihydropyrenes and their Electrical and Photochromic Properties," 2008.

[12]   S. Muratsugu and H. Nishihara, "π-Conjugation modification of photochromic and redox-active dimethyldihydropyrene by phenyl- and ethynyl-terpyridines and Ru(bis-terpyridine) complexes," *New J. Chem.*, vol. 38, no. 12, pp. 6114–6124, 2014.

[13]   W. Hu, G. P. Zhang, S. Duan, Q. Fu, and Y. Luo, "Molecular design to enhance the

thermal stability of a photo switchable molecular junction based on dimethyldihydropyrene and cyclophanediene isomerization," *J. Phys. Chem. C*, vol. 119, no. 21, pp. 11468–11474, 2015.

[14]   G. P. Zhang *et al.*, "Optimizing the conductance switching performance in photoswitchable dimethyldihydropyrene/cyclophanediene single-molecule junctions," *Phys. E Low-Dimensional Syst. Nanostructures*, vol. 109, no. December 2018, pp. 1–5, 2019.

[15]   M. Alemani, M. V. Peters, S. Hecht, K. H. Rieder, F. Moresco, and L. Grill, "Electric field-induced isomerization of azobenzene by STM," *J. Am. Chem. Soc.*, vol. 128, no. 45, pp. 14446–14447, 2006.

[16]   L. Sun, Y. A. Diaz-Fernandez, T. A. Gschneidtner, F. Westerlund, S. Lara-Avila, and K. Moth-Poulsen, "Single-molecule electronics: From chemical design to functional devices," *Chem. Soc. Rev.*, vol. 43, no. 21, pp. 7378–7411, 2014.

[17]   K. Matsuda, H. Yamaguchi, T. Sakano, M. Ikeda, N. Tanifuji, and M. Irie, "Conductance photoswitching of diarylethene-gold nanoparticle network induced by photochromic reaction," *J. Phys. Chem. C*, vol. 112, no. 43, pp. 17005–17010, 2008.

[18]   S. J. Van Der Molen *et al.*, "Light-controlled conductance switching of ordered metal-molecule-metal devices," *Nano Lett.*, vol. 9, no. 1, pp. 76–80, 2009.

[19]   W. Haiss *et al.*, "Redox State Dependence of Single Molecule Conductivity," *J. Am. Chem. Soc.*, vol. 125, no. 50, pp. 15294–15295, 2003.

[20]   V. Ferri *et al.*, "Light-powered electrical switch based on cargo-lifting azobenzene monolayers," *Angew. Chemie - Int. Ed.*, vol. 47, no. 18, pp. 3407–3409, 2008.

[21]   Y. Geng *et al.*, "Magic Ratios for Connectivity-Driven Electrical Conductance of

Graphene-like Molecules," *J. Am. Chem. Soc.*, vol. 137, no. 13, pp. 4469–4476, 2015

[22] M. L. Perrin *et al.*, "Mechanically controlled binary conductance switching of a single-molecule junction," *Nano Lett.*, vol. 14, no. 1, pp. 1–7, 2016.

[23] S. Muratsugu, S. Kume, and H. Nishihara, "Redox-assisted ring closing reaction of the photogenerated cyclophanediene form of bis(ferrocenyl)dimethyldihydropyrene with interferrocene electronic communication switching," *J. Am. Chem. Soc.*, vol. 130, no. 23, pp. 7204–7205, 2008.

[24] M. Alemani *et al.*, "Phase coherent electronics: A molecular switch based on quantum interference," *J. Am. Chem. Soc.*, vol. 8, no. 5, pp. 1–10, 2014.

[25] P. A. Liddell *et al.*, "Photonic Switching of Photoinduced Electron Transfer in a Dihydropyrene-Porphyrin-Fullerene Molecular Triad," *J. Am. Chem. Soc.*, vol. 126, no. 15, pp. 4803–4811, 2004.

[26] S. Muratsugu, M. A. Kishida, R. Sakamoto, and H. Nishihara, "Comparative study of photochromic ferrocene-conjugated dimethyldihydropyrene derivatives," *Chem. - A Eur. J.*, vol. 19, no. 51, pp. 17314–17327, 2013.

[27] W. Hong *et al.*, "Single molecular conductance of tolanes: Experimental and theoretical study on the junction evolution dependent on the anchoring group," *J. Am. Chem. Soc.*, vol. 134, no. 4, pp. 2292–2304, 2012.

[28] X. Zhao, G. Kastlunger, and R. Stadler, "Quantum interference in coherent tunneling through branched molecular junctions containing ferrocene centers," *Phys. Rev. B*, vol. 96, no. 8, pp. 1–12, 2017.

Chapter 6

6.1 Conclusion

In conclusion, this thesis theoretically investigates transport properties at the nanoscale, by using DFT, Green's function methods and tight binding methods, as discussed in chapters 2 and 3, respectively.

Chapter 4 presents studies of the charge transport of anthraquinone and its derivatives in different conjugation systems. DFT calculation reveals that a curly arrow rule is broken in the case of the cross conjugated molecule (anthraquinone). Confirmation that this rule is still broken when trying various of anchor groups with two different kinds of electrodes. These calculations shows that this behaviour is a general behaviour for anthraquinone. This feature originates from the evolution of the HOMO of dihydroxyanthracene into the LUMO of anthraquinone when removing of the hydrogen atoms from the hydroxyl groups of dihydroxyanthracene. The conductance of the junction increases by a couple of orders of magnitude due to the transition from constructive to destructive QI. This opens new avenues for realization of QI-based single-molecule switches. Curly arrow rules break down in molecular junctions formed by cross-conjugated anthraquinone. Whereas Curly arrow rules predict destructive QI for a meta connected anthraquinone core, we obtained a constructive QI. This behaviour is independent of choice of electrode material or anchor groups and arises from the evolution of the HOMO of dihydroxyanthracene into the LUMO of anthraquinone upon removal of the Hs from the pendant OH groups of dihydroxyanthracene. In addition, my result does not confirm the validity of the curly arrow rules in broken conjugated dihydroanthracene, where a strong destructive QI dip was not obtained.

Finally, chapter 5 shows a theatrical study in dimethyldihydropyrene (DHP)ON and cyclophanediene (CPD) OFF in different connectivities(5,12) and (2,9). I demonstrated the role of perturbation theory in theses switchable molecules when a swab occurs in the symmetry between the molecular orbital of HOMO and HOMO-1 taken place. Moreover, this switch from ON state to OFF state does not create new orbitals; it is only a change of the molecular orbital ordering.

In summary, I performed a study for two connectivities (5,12) and (2,9)ON states compare to (5,12) and (2,9)OFF states with different connectivities. I presented a detailed calculation analysis of the conducting (5,12) and (2,9) when it switched to the non-conducting state. Introducing a perturbation in (2,9) and (5,12) OFF states cause a swap between the molecular orbitals in HOMO-1 and HOMO and can be exhibited in simple tight binding model. I found that the difference in conductance between the two states ON and OFF can be promoted by using the acetylene spacer in the case of the connectivity of |(5,12) but not in (2,9)

6.2 Future Works

In chapter 4, I studied the connectivity dependence of quantum transport through anthraquinone and anthracene cores, connected to both graphene and gold electrodes. For the future, it would be of interest to explore the connectivity dependence of phonon transport [1][2], since the control of heat through solids and solid-molecule interfaces is of interest for thermal management of nanoscale devices and for increasing the performance of thermoelectric materials. It would also be of interest to explore the use of alternative electrode materials for molecular electronics, including superconducting electrodes [3][4]. The latter would be particularly interesting, because the interplay between superconducting quantum interference effects and quantum interference within molecules is a largely unexplored area of research. Quantum interference can also be controlled by introducing

pendant redox units [5], charge transfer complexes [5] and heteroatoms [6][7]and therefore detailed studies of the connectivity dependence of such effects in the presence of five-membered rings would be of interest. In addition, many other aspects in this field deserve further attention, including spin transport in dihydroxyanthracene on the removal one hydrogen in the presence of gold and graphene electrodes. In chapter 5, I focussed on the connectivity dependence of electrical conductance and the tuning of quantum interference via the symmetry of frontier orbitals, which underpins the switching behaviour of the photo-switchable dimethyldihydropyrene and its derivatives.

Bibliography

[1]   A. Kambili, G. Fagas, V. I. Fal, and C. J. Lambert, "Phonon-mediated thermal conductance of mesoscopic wires with rough edges," vol. 60, no. 23, pp. 593–596, 1999.

[2]   G. Fagas *et al.*, "Lattice dynamics of a disordered solid-solid interface," vol. 60, no. 9, pp. 6459–6464, 1999.

[3]   C. J. Lambert, V. C. Hui, S. J. Robinson, V. C. Hui, C. J. Lambert, and C. J. Lambert, "Andreev Scattering , Universal Conductance Fluctuations and Phase Periodic Transport Andreev Scattering , Universal Conductance Fluctuations and Phase Periodic Transport .," 1993.

[4]   C. J. Lambert, R. Raimondi, V. Sweeney, and A. F. Volkov, "Boundary conditions for quasiclassical equations in the theory of superconductivity," vol. 55, no. 9, pp. 6015–6021, 1997.

[5]   E. Article *et al.*, "Chemical Science Charge transfer complexation boosts molecular conductance through Fermi level pinning †," pp. 2396–2403, 2019.

[6]   X. Liu *et al.*, "Gating of Quantum Interference in Molecular Junctions by Heteroatom

Substitution," *Angew. Chemie - Int. Ed.*, vol. 56, no. 1, pp. 173–176, 2017.

[7]   S. Sangtarash, H. Sadeghi, and C. J. Lambert, "Exploring quantum interference in heteroatom-substituted graphene-like molecules," *Nanoscale*, vol. 8, no. 27, pp. 13199–13205, 2016.